Ecology and Development Series No. 18, 2004

Ayodele Ebenezer Ajayi

Surface runoff and infiltration processes in the Volta Basin, West Africa: Observation and modeling

Cuvillier Verlag Göttingen

Dedication

To Bishop (Dr.) David Oyeniyi Oyedepo
for showing me the path to greatness

and

to Mr. Mayowa Oyedeji (ACA)
for encouraging me against the odds

ABSTRACT

This study presents the results from field observations and subsequent development and solution of a process-based, two-dimensional numerical model capturing surface runoff processes in the Volta Basin, West Africa. The developed model summarizes the interactions between temporally varying rainfall intensity and interactive infiltration processes in soils with spatially varied soil physical and hydraulic characteristics. Varied catchment geometry, microtopographic (vegetated and soil surface) forms, slope length and angle were also examined. The model also incorporates the rainfall interception by mixed vegetation.

The interactive infiltration process is modeled with the Philip two-term equation (PTT), while ponding time is approximated with the time compression algorithm. Interception by vegetation is estimated with the modified Gash model, while the friction effect of vegetation on surface overland flow is quantified. The developed surface flow equations were solved with a second-order Leapfrog explicit finite difference scheme, with centered time and space derivatives. This scheme was modified to accommodate the peculiar nature of surface runoff on a complex microtopographical plane. The model reliably reproduces the results from experimental field data on the basis of parameterized effective soil hydraulic parameters and passed severe numerical tests for hydrodynamic equations.

The analyses of results from both field observations and numerical simulations shows that the dominant runoff generation mechanism in the study area is the infiltration excess (Hortonian) process. A consistent trend of exponential reduction runoff coefficient and runoff discharge per unit area with increasing slope length was observed. The results also showed that both temporal and spatial variability induced factors determine runoff response to rainfall events. Spatial variability in infiltration opportunities, which varies with slope length, and the distribution pattern of saturated conductivity, leading to differences in temporal dynamics of transmission losses potential during runoff routing downslope; moderated by surface roughness and vegetation (Microtopography), which determines surface depression shapes and networks, results in the consistent differences in runoff response. Temporal patterns of rainfall intensity, particularly the distribution in terms of number of pulses, the duration of pulses, total event time, length of time for recession, also affect runoff response. Initial moisture status of the soil may also significantly increase runoff volume. However, a classical demarcation of the prevalent factor at any instant could be defined.Variability in temporal factors dominates the response to high intensity events, while spatial variability in the distribution pattern of soil-related factors i.e., hydraulic properties dominate the response to low intensity events. The prevalence of temporal factors in the basin is traceable to the high intensity tropical storms, which often do not allow the spatial factors to become fully manifest.

The developed model will be useful in studying surface runoff, water erosion, and nutrient dynamics under complex microtopographic conditions, spatially varying soil hydraulic characteristics and temporally dynamic rainfall intensity occurring in many tropical catchments. It also provides practical tool for facilitating decision processes in soil management techniques aimed at managing surface runoff and soil erosion.

Oberflächenabfluss und Infiltrationsprozess im Volta-Becken: Beobachtungen und Modellierung

KURZFASSUNG

Diese Studie präsentiert die Ergebnisse aus Felduntersuchungen sowie die Entwicklung und Lösung eines prozessbasierten, zweidimensionalen numerischen Modells, das den Prozess des Oberflächenabflusses im Voltabecken, Westafrika, darstellt. Das Modell erfasst die Wechselwirkung zwischen zeitlich variierender Niederschlagsintensität und Versickerungsprozessen in Böden mit räumlich variierenden physikalischen und hydraulischen Eigenschaften. Eine unterschiedliche Oberflächengestalt des Wassereinzugsgebiets, verschiedene mikrotopographische Formen (mit und ohne Vegetationsbedeckung), Hanglängen und –neigungen wurden ebenfalls untersucht. Das Modell berücksichtigt auch die Interzeption des Niederschlags durch die Vegetation.

Der interaktive Infiltrationsprozess ist mit der ‚Philip two-term' Gleichung (PTT) gekoppelt, während die Wasserakkumulation (ponding) mit dem Algorithmus der Zeitkompression (Zeitverdichtung) ermittelt wird. Die Interzeption durch den Niederschlag wird mit dem modifizierten Gash Modell bestimmt, der Reibungseffekt der Vegetation durch einen entwickelten Vegetationsfaktor. Die Gleichung wurde mit dem bekannten Schema 2. Ordnung, Leapfrog Explizit-Finite-Unterschiede (FDM) mit zentrierten zeitlichen und räumlichen Differentialquotienten gelöst. Dieses Schema wurde modifiziert, um die besondere Natur des Oberflächenabflusses auf einer komplexen mikrotopographischen Ebene zu erfassen. Das Modell reproduziert zuverlässig die Ergebnisse der Feldversuche auf der Basis von parametisierten wirksamen bodenhydraulischen Parametern und bestand die strengen numerischen Tests für die hydrodynamischen Gleichungen.

Die Analysen sowohl der Felddaten als auch der numerischen Simulationen weisen den Prozess des Infiltrationsüberschusses als den am stärksten bestimmenden Mechanismus bei der Erzeugung von Oberflächenabfluss im Voltabecken nach. Ein durchgängiger Trend hinsichtlich der exponentiellen Reduktion des Abflusskoeffizienten und der Menge des Oberflächenabflusses wurde mit zunehmender Hanglänge beobachtet. Die Ergebnisse zeigen weiterhin, dass die sowohl durch zeitliche als auch räumliche Variabilität bedingten Faktoren die Reaktion des Abflusses auf das Niederschlagsereignis bestimmen. Eine klassische Abgrenzung des zum jeweiligen Zeitpunkt vorherrschenden Faktors konnte jedoch definiert werden. Zeitliche Muster der Niederschlagsintensität, insbesondere die Verteilung hinsichtlich Anzahl und Dauer der Impulse, Gesamtlänge des Ereignisses, Rezession und durchschnittliche Intensitätswerte kombiniert mit der zeitlichen Variation der Wasserbewegung hangabwärts bestimmen weitgehend die Reaktion auf Niederschlagsereignisse von hoher Intensität. Die räumliche Variabilität der bodenabhängigen Faktoren, z. B. hydraulische Eigenschaften und Hanglänge, beeinflusst Ereignisse von geringer Niederschlagsintensität. Das Vorherrschen der zeitlichen Faktoren im Voltabecken kann auf die Niederschlagsereignisse von hoher Intensität, gleichbedeutend mit tropischen Stürmen, zurückgeführt werden, die oft die Manifestierung der räumlichen Faktoren verhindern. Ein weiterer Bodenfaktor, der die Reaktion beeinflusste, ist der anfängliche Bodenfeuchtigkeitsstatus. Dieser Einfluss wird jedoch ebenfalls begrenzt, da er schnell

durch die hohe Niederschlagsintensität überlagert wird. Bei Ereignissen von geringer Niederschlagsintensität könnte eine hohe anfängliche Bodenfeuchte die Abflussmenge signifikant erhöhen.

Das entwickelte Modell wird hilfreich sein bei Untersuchungen über Oberflächenabfluss, Erosion durch Wasser sowie Nährstoffdynamik unter komplexen mikrotopographischen Bedingungen, mit räumlich variierenden bodenhydraulischen Eigenschaften und bei zeitlich dynamischer Niederschlagsintensität, wie sie in vielen tropischen Wassereinzugsgebieten vorkommen. Es stellt auch ein nützliches Instrument für die Unterstützung von Entscheidungsprozessen im Zusammenhang mit Bodenbewirtschaftungstechniken zur Kontrolle von Oberflächenabfluss und Bodenerosion zur Verfügung.

TABLE OF CONTENTS

LIST OF SYMBOLS AND ABBREVIATIONS

Symbol	Description	Dimension	Applied unit
U	flow velocity in the x-direction	$L\ T^{-1}$	cms^{-1}
V	flow velocity in the y-direction, m/s	$L\ T^{-1}$	cms^{-1}
S_{ox}	ground slope in the x-direction	$L\ L^{-1}$	°
S_{oy}	ground slope in the y-direction	$L\ L^{-1}$	°
S_{fx}	friction slope in the x-direction	$L\ L^{-1}$	
S_{fy}	friction slope in the y-direction	$L\ L^{-1}$	
q_x	uh-x-momentum	$L^2\ T^{-1}$	cm^2s^{-1}
q_y	vh y-momentum	$L^2\ T^{-1}$	cm^2s^{-1}
H	height/depth of flow (m)	L	cm
i, j	Timesteps; i = first and j = last time steps	T	S
q_{xb}	value of q_x at boundaries;	$L^2\ T^{-1}$	cm^2s^{-1}
q_{yb}	value of q_y at boundaries;	$L^2\ T^{-1}$	cm^2s^{-1}
h_b	value of h at boundaries	L	cm
$\overline{q_x}$	filtered variable (q_x)	$L^2\ T^{-1}$	cm^2s^{-1}
$\overline{q_y}$	filtered variable (q_y)	$L^2\ T^{-1}$	cm^2s^{-1}
$\overline{h}$	filtered variable (h)	L	cm
F_{xx}	flux of x-momentum in x-direction;	-	-
F_{xy}	flux of x-momentum in y-direction;	-	-
G_{xy}	flux of y-momentum in x-direction		-
G_{yy}	flux of y-momentum in y-direction	-	-
Q_x	flux of height in x-direction	L	cm
Q_y	flux of height in y-direction	L	cm
F_{xxb}	F_{xx} at boundaries	-	-
F_{xyb}	F_{xy} at boundaries	-	-
G_{xyb}	G_{xy} at boundaries		-
G_{yyb}	G_{yy} at boundaries	-	-
h_0	initial constant height	L	cm
h_m	microtopography height	L	cm
npy	no of point on y axis	-	-
npx	no of point on x axis	-	-
CFL	Courant–Friedrichs–Lewy parameter	-	-
g^{n-1}	Flow generic variable	$L^2\ T^{-1}$	cm^2s^{-1}
a	time filtering coefficient	-	-
Dt	time step length	T	sec
Ds	grid length ($dx=dy=Ds$)	L	cm
k_{diff}	artificial diffusion coefficient	-	-
G	Gravitational acceleration	$L^2\ T^{-1}$	$m^2\ s^{-1}$
F_{rsu}	flux for the friction slope in the x-direction	L	
F_{rsv}	flux for the friction slope in y-direction	L	
$S_e(y)$	effective saturation /reduced water content	$L^{-3}\ L^{-3}$	$m^{-3}\ m^3$
q_r	residual volumetric water contents	$L^{-3}\ L^{-3}$	$m^{-3}\ m^3$
q_s	saturated volumetric water contents	$L^{-3}\ L^{-3}$	$m^{-3}\ m^3$
V_{obs}	observed runoff volume	L^3	Liter

Symbol	Description	Dimension	Applied unit
V_{sim}	simulated runoff volume	L^3	Liters
C_e	coefficient of efficiency	%	%
Q_i	observed runoff discharge at time i	$L^3 T^{-1}$	Liter s^{-1}
$\bar{Q}$	mean runoff rate of the particular rainfall-runoff event	$L^3 T^{-1}$	Liter s^{-1}
$\hat{Q}_i$	runoff discharge predicted by the model at time I	$L^3 T^{-1}$	Liter s^{-1}
N	number of time step in the computation	-	-
G	gravitational acceleration, 9.81	$L T^{-2}$	ms^{-2}
F	Darcy–Weisbach friction factor	-	-
R_e	Reynolds-number	-	-
K_o	resistance parameter, which relates to the ground surface characteristics.	-	-
ν	kinematic viscosity of water = 10^{-6}	$M L^{-1} T^{-1}$	ms^{-1}
N	Manning's roughness coefficient	-	-
k	Dimensionless extinction coefficient	-	-
$R(t)_{ri}$	interception-reduced rainfall intensity	$L T^{-1}$	mm hr^{-1}
I(t)	instantaneous infiltration rate [m/s]	$L T^{-1}$	mm s^{-1}
S	Sorptivity [$m/s^{½}$]	$L T^{-1/2}$	mm $s^{-1/2}$
C	effective hydraulic conductivity [m/s]	$L T^{-1}$	mm hr^{-1}
FEM	Finite Element Method	-	-
FDM	Finite Difference Method	-	-
FVM	Finite Volume Method	-	-
A_1 B_1, A_2 & B_2	Long Plots (LP)	L	m
A_3 & B_3	Medium plot (MP)	L	m
A_4 & B_4	Short Plot (SP)	L	m
RQ	Runoff Coefficient	$L^{-3} L^{-3}$	%
UD	Runoff Discharge per unit area	$L^{-3} m^{-2}$	Lit m^{-2}

1 GENERAL INTRODUCTION

1.1 Surface runoff, infiltration process and rainfall partitioning in the tropics

Surface runoff (flux at a point in space), often used interchangeably with the term overland flow (a spatially distributed phenomenon), resulting from the rainfall-runoff transformation process plays a significant part in the hydrological cycle (process) in West Africa as in many other tropical regions. It is recognized as an essential component of most erosion and catchment water balance models (van Dijk, 2002) and is a critical factor controlling rill erosion and gully development (Hudson, 1995).

Overland flow significantly influences the amount of water available in the rivers, streams and ponds, and determines the size and shape of flood peaks (Troch et al., 1994), and, when properly managed, could be converted into valuable water resources for agricultural production in floodplain farming. This could be very useful in most sub-Saharan African countries, facing a consistent trend of declining or fluctuating annual rainfall totals, which is affecting food production under rainfed agriculture (Joel et al., 2002; Le Barbé and Lebel, 1997; Rockström and Valentin, 1997; FAO, 1995;).

Surface runoff in the form of long-term water availability and extreme flows are also very important in designing hydraulic structures in civil engineering works (Lidén and Harlin, 2000). It determines the magnitude of sediment transport in water erosion process (Kiepe, 1995; Lane et al., 1997), and resolves the transport and fate of nutrients and agro-chemicals, which reside on the soil surface (Jolánkai and Rast, 1999). Consequently, adequate understanding and knowledge of its dynamics constitute one of the most important and challenging problems in hydrology and are quintessential in understanding several other catchment processes.

Substantial progress has been made in understanding the surface runoff process and its impact on the global water cycle in some parts of the world. However, very little has been done in sub-Saharan Africa countries (van de Giesen et al., 2000), particularly in West Africa, where only few examples exist of detailed hydrological studies that use sub-daily information on small experimental catchments (<10 km2) (Chevallier and Planch, 1993).

There is a general consensus among researchers that the Hortonian or ‘infiltration excess’ runoff mechanism, dominates the generation of runoff in tropical

catchments, while the Dunne's or 'saturation excess' mechanism applies to the flood plains and valley bottoms (Esteves and Lapetite, 2003; Masiyandima et al., 2003; Joel et al., 2002; Peugeot et al., 1997; Dunne, 1978). By definition, Hortonian overland flow occurs at a point on the ground surface when the rate of rainfall exceeds the infiltration capacity of the soil and there is a sufficient gradient to facilitate the flow. This process is well defined and understandable at a point scale, but the model representation of the process is mostly done at a far higher resolution, i.e., the catchment or regional scale when done deterministically (Fiedler, 1997).

Understanding and modeling of surface runoff processes, requires the selection of appropriate spatial and temporal discretization, to reduce scale discrepancies, between observation and application. It is also essential in formulating appropriate hydrological models that can most effectively simulate water balances for large areas with the use of available computer resources. Such models are useful tools in flood forecasting and in improving the atmospheric circulation models (Schmidt et al., 2000). However, most large-scale models cannot incorporate detailed and physically based descriptions of the processes because of unknown boundary conditions, but with appropriate scale definition, this problem can be solved.

Surface runoff process, as can be seen from the two widely accepted concepts, is strongly influenced by the infiltration and percolation characteristics of the soil in a catchment, implying, that surface infiltration or overland flow processes cannot be adequately understood if the infiltration behavior of the soil in the catchment is not properly studied. Infiltration properties among other biophysical factors determine the amount of rainfall that flows on the surface as overland flow. In continental United States, it is generally held that 70% of the annual precipitation infiltrates and the remaining contributes to the stream flow through surface runoff (Chow, 1964). Infiltration process in soil has received more attention in hydrological studies than any other component, and this has led to the development of several conceptual and empirical models to describe the process. Commonly used conceptual infiltration models include models based on the Richards equation, Green-Ampt model, Philip two-term model, Parlange model, etc., while the empirical models include the Kostyakov model, Horton model, Holtan model, Overton model, Soil Conservation Service (SCS) model, Hydrologic Engineering Center (HEC) model among many others (Singh, 1988).

These models have been frequently compared and divergent results on effective models have been reported, depending on experiment locations among other factors. Quite clearly, the classical point scale infiltration theory (e.g., Green-Ampt Smith-Parlange, and the Philip Two Term model (PTT) is often used in physically based hydrologic models (Fiedler and Ramirez, 2000).

1.2 Research goals and objectives

Within the context of the GLOWA Volta Project, (http://www.glowa-volta.de), which was set up to develop a decision support system (DSS), for sustainable water management in the Volta Basin, providing a comprehensive monitoring and simulation framework that will assist decision makers; to evaluate the impact of manageable (irrigation, primary water use, land-use change, power generation, trans-boundary water allocation) and less manageable (climate change, rainfall variability, population pressure) factors on the social, economic, and biological productivity of water resources; the overall goal of this research work is to provide the details about surface runoff formation, transmission and dynamics for the decision support system.

Therefore the objectives are:

1. To establish by the means of field studies, the dominant runoff formation mechanism in the basin;
2. Study the effect of the catchment heterogeneous structure (vegetation, geometric attributes and spatial variation of hydraulic properties) on surface runoff processes;
3. Determine possible influence of observation scale on the processes;
4. Develop a process based model capable of representing the observed surface runoff processes; and consequently
5. Evaluate the influence of temporal factors (varying rainfall intensity, surface runoff routing) on scale effect.

A combination of scaled-plots experiments, detail catchment monitoring and process-based numerical investigations is considered necessary to understand these interactions. It is hypothesized that runoff process responds variably to spatial and temporal variation in catchment hydraulic properties and rainfall properties. The

influence of these parameters varies at each different scale of observation. This will help in identifying critical field parameters for upscaling.

1.3 Justification of the study

From a historical perspective, surface runoff and overland flow is often recognized as one of the key components of the hydrological process. However, it has hardly been studied and quantified over the Volta Basin. Consequently, a knowledge gap still exists concerning the hydrologic behavior of the catchment in spite of the importance of the basin to the hydrology of the West African sub-region. There is also a general desire for efficient regional model of the hydrological processes around the world, which is expected to incorporate runoff process. However, surface runoff is non-linear, making upscaling a difficult task. It is therefore necessary to investigate the runoff process at various scales to achieve this goal. This is challenging but achievable.

This thesis is divided into six chapters. Chapter 2 reviews the state-of-the-knowledge in rainfall partitioning and surface runoff process modeling. Chapter 3 describes the study area in terms of geography. It also explains the construction of the runoff plot and presents the methods for all measurements during the field study. Chapter 4 presents a review of different method of representing surface runoff process. It also present the development of the numerical model used in this study and the model validation methods. Results of the field observation presented in chapter 5, while chapter 6 discuss the result from the model simulation experiments, outlining the effect of various components. A summary of major findings and recommendation are thereafter presented.

2 STATE OF KNOWLEDGE

The surface runoff process is among the most extensively studied in the hydrological system, leading to great progress in the understanding of the processes governing the transformation of rainfall to runoff. Comparatively, there are more documented studies of the process in the temperate climates relative to the tropical zones (van de Giesen et al. 2000; Chevallier and Planchon 1993). Runoff volume, timing, and duration affect water supply, flood propagation and many other hydrological processes in catchments. Surface runoff studies have been approached using different methods that could be broadly classified under three categories:

- Field studies of the hydrologic processes using runoff plots, watershed monitoring under natural rainfall and simulated rainfall conditions;
- Physically based mathematical modeling of surface runoff processes using either field observations, synthetic / hypothetical or simulated data sets or a combination of the different sets of data; and
- Geomorphometric analysis and digital terrain modeling approaches using geometric drainage units and simplified flow equations.

A recent trend in the study of this process is the investigation of the response at various spatial and temporal scales with emphasis on understanding the dynamics of the numerous factors influencing the process at the different scales. This is often captured under the heading:

- Scale issue in infiltration and runoff studies.

The review of literature in this study was conducted to highlight the state-of-the-art within the scope of the research objectives under the various headings. A review of the issues of scale is integrated to match the goal of understanding the scale dependency of the rainfall-runoff response.

2.1 Runoff generation phenomena

As observed by Brown (1995), the earliest process studies in watershed hydrology were motivated by a need to understand, model and predict runoff generation phenomena. This has led to the identification of two major runoff mechanisms amongst several other proposed mechanisms, based largely on field observations in the eastern United States.

Horton (1933) proposed an infiltration capacity-based model (infiltration excess) of runoff generation, which is often referred to as the Horton overland flow. Other processes of runoff generation were later presented, but another widely accepted concept was proposed by Dunne (1970). He outlined the importance of a rising water table in initiating and sustaining surface runoff generation. Thus, Dunne (1978) proposed the soil saturation-based (saturation excess) runoff process otherwise referred to as the Dunne overland flow. A third but less popular runoff generation process is that proposed by Hursh (1936), which enumerates the importance of subsurface flow in the runoff generation process. The various runoff generation schemes and their enabling environmental conditions are illustrated in Figure 2.1.

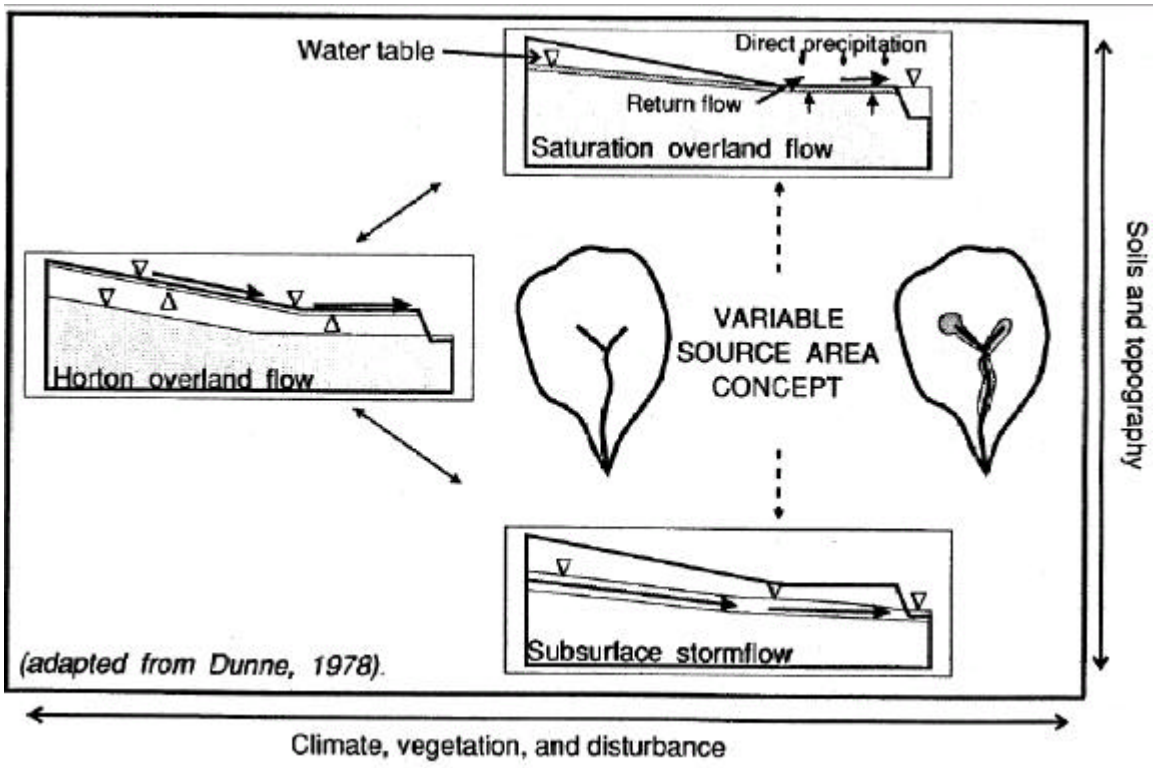

Figure 2.1 Summary of major runoff generation models

2.2 Field studies

The two major runoff mechanisms have been investigated in a number of field experiments. Most of the studies are however linked to the understanding of soil detachment and erosion processes. Some others focus on nutrient dynamics in agricultural field soils and some on more general topics like soil management

techniques (Littleboy et al., 1996). Developments in field investigations of the Hortonian overland flow between the 1930's and late 1970's have been summarized by Dunne (1978).

Runoff studies are carried out with either model - or statistical-design based runoff plots measurements or with catchment observation, and sometimes with the combination of both. One major interest in the study of the runoff processes at field level has been that of determining discharge or yield (volume of water available at the plot or catchment outlet) over a specified period of time in relation to the total rainfall. This fundamental problem in hydrology largely depends on total surface runoff and has been expressed in several temporal scales using the relationship derived from studies on catchments, runoff plot experiments, or river gauging studies combined with different simple empirical formulae or complex models (Ponce and Shetty, 1995; Lal, 1997). Results from most of the studies have shown a good relationship between discharge and plot or catchment area subject to the translocation factors. The effect of some translocation factors which include slope degree, length and orientation on the runoff process and discharge has also been a major area of interest in several field studies. Sharman et al. (1983) and Lal (1997) concluded that, an increasing slope length induces a corresponding increase in runoff volume from plots. This is contrary to the conclusion that runoff volume decreases with increasing slope length made by Poessen et al. (1984). Mah et al. (1992) however opined that, slope length had no significant effect on runoff volume in their plot experiments. These contradictions could possibly emanates from differences in the study areas. Fitzjohn et al. (1998) also investigated the effect of soil moisture content and its spatial variation on runoff yield. They concluded that, runoff yield from the plot increases with increasing soil moisture.

Of particular interest in the present study is the effect of changes in land use pattern on surface runoff, the importance of micro-scale topography (microtopography) sometimes associated with the effect of tillage practice and soil properties in controlling the magnitude and distribution of surface runoff, and the effects of scales of observation on the rainfall-runoff transformation process. The potential disturbance of the hydrologic cycle by changing land use is well documented and is now a major topic of interest in several hydrological forums. Changing land use results in changes in canopy cover, degradation of the vegetative cover, and increased soil disturbance. These were

found to increase surface runoff and soil erosion (Návar and Synnott, 2000). In a study in Argentina, Braud et al. (2001) concluded that it is difficult to relate runoff volume to simple catchment descriptors such as average slope or average vegetation cover. In a simulation of the result using the ANSWER model, it was shown that vegetation significantly affects runoff volumes in small-scale plots when the geology is homogeneous. From the result of field trials under simulated rainfall, Fiedler et al. (2002) analyzed the effect of grazing on overland flow in a semi - arid grassland, and observed that grazing affects the point scale hydraulic conductivity of vegetated soil, resulting in increased runoff discharge. Under the GLOWA - Volta Project, the effect of short-term change in vegetation and land use due to bush burning and cropping patterns and long-term changes due to changing agricultural practices affecting the surface runoff processes would be investigated.

The latest subject of interest in runoff studies is the understanding of the effect of scale observation (both temporal and spatial) on the rainfall-runoff dynamics (Yair and Lavee 1985; Lal 1997; van de Giesen et al., 2000; Joel et al., 2002; Esteves and Lapetite, 2003). Most attempts at understanding this have been made with a combination of both field trials and model simulation results, and this has shown to be very important for the future of runoff studies particularly with the increasing need to develop or improve the efficiency of regional hydrological models. Such improvement will enhance the understanding of water resources dynamics. Effect of scale will be reviewed in detail at a later section of this thesis.

2.3 Study by models

As noted by van Loon (2001), before the computer era (till the early 1970's), the distributed nature of overland flow was a serious impediment, since (mobile) equipment was not available to observe and store the relatively large amount of information. From the 1970's onwards, the relative appreciation of model studies has marginalized the attention for field observations. Investigation of the rainfall-runoff transformation process by modeling technique has been shown to be an excellent tool in the understanding the process at a cost that is very minimal, compared to that for field measurements.

Physically based mathematical models have been applied using both simplified flow equations and more general governing equations. Simplified models are developed from the kinematic wave approximation or the diffusion wave approximation of the unsteady open channel flow equation, otherwise called the full hydrodynamic or shallow water equations (Ponce et al., 1978; Parlange et al., 1981). The diffusion wave model assumes that the inertia terms in the equation of motion are negligible as compared with pressure, friction, and gravity terms, while the kinematic wave approximation assumes that the inertia and pressure terms are negligible compared to the friction and gravity terms; thus the discharge is taken as a single value function of depth. Both approximate models have been solved analytically and numerically using different surface resistance formulas in several studies (Julien and Moglen, 1990; Dunne et al., 1991; Ogden and Julien, 1993; Woolhiser et al., 1996). Although approximate, both the kinematic and diffusion models have given fairly good descriptions of the physical phenomenon in a variety of cases. They are however limited in their abilities to accommodate spatial variation of hillslope attributes, and do not allow the accurate simulation of spatially variable hydraulics (Zhang and Cundy, 1989).

Due to its simplicity and good performance in spite of the identified limitation, the kinematic wave approximation has been used extensively in several modeling studies of the rainfall-runoff process (Singh, 1996). Smith and Hebbert (1983) developed a model based on kinematic wave approximations for both surface and subsurface flows. This model was limited in its ability to handle spatial variability of soil properties, especially along a hillslope gradient. Beven (1982) analyzed subsurface storm flow based on the kinematic wave theory. He remarked that the validity of the model is limited by several limiting assumptions, which include simplified soil hydraulic properties, uniform initial moisture conditions, and constant rainfall used in the study. Julien and Moglen (1990) used the kinematic wave approximation combined with the Manning's resistance formula to study the influence of spatial variability in slope, surface roughness, surface width and excess rainfall on surface runoff characteristics. They reported that the solution of the model using the finite element will permit quantitative evaluations of the effect of spatial variability in terms of physically based dimensionless parameters such as dimensionless discharge and duration. Following the success of Julien and Moglen (1990), van de Giesen et al. (2000) studied

the scale effects on the Hortonian flow in a tropical catchment using analysis based on the kinematic wave approximation. Other studies based on this approximation include the study by de Lima and Singh (2002) that investigated the influence of moving rainstorm patterns on overland flow.

Kinematic wave modeling of overland flow is implemented in a one-dimensional form, thereby limiting the accuracy of its prediction compared with actual field observations. To characterize actual field observations of variable slopes in the kinematic wave models, Kibler and Woolhiser (1970) proposed the kinematic cascade method, where the real surface is approximated using a series of plane surfaces each with different gradients. This attempt was later extended in the work of Borah et al. (1980) using kinematic shock-fitting techniques and it significantly improve the accuracy of the kinematic wave model prediction of overland flow. However, such cascading techniques still do not represent the actual field observation and become complicated as the cascade levels increases, thus introducing shock and discontinuity problems in the numerical solution. In reducing this complication, the two-dimensional modeling technique was pursued by Constantinides and Stephenson (1981). This approach improved the accuracy of predictions from the kinematic wave approximation, but equally complicates the numerical solution process. Other common limitations of the kinematic wave model include the neglect of backwater effect. Backwater effects often characterize large areal catchment with low slopes, causing widespread ponding and slow regional flow dynamics (Wasantha-Lal, 1998; Zhang and Cundy, 1989). The kinematic wave approximation also fails for highly sub-critical flows on flat slopes and when the downstream boundary condition is an important factor (Morris and Woolhiser, 1980).

Diffusion wave models are applicable over a wider range of flow conditions and, therefore may be used for highly sub-critical flows. Hromadka et al. (1987) developed a two-dimensional diffusion wave model assuming constant effective rainfall intensity. Govinradinju et al. (1988) derived an approximate analytical solution to overland flow under a specified net lateral inflow using the diffusion wave approximation. They also provide the complete numerical solutions for the diffusion wave equation. Todini and Venutelli (1991) also developed a two-dimensional diffusion

wave model in which the governing equations were solved with both finite difference and finite element methods.

Although computationally very intensive, clearer understanding of the surface runoff processes is obtained from the solution of the full hydrodynamic equation. A one-dimensional form of the equation was developed by Ligget and Woolhiser (1967), to study overland flow on a plane surface. The study showed the suitability of the hydrodynamic model in simulating overland flow. Other studies based on the one-dimensional form include the studies by Strelkoff (1969) and Akan and Yen (1981).

A pioneering study with the two-dimensional form of the hydrodynamic model is that of Chow and Ben-Zvi (1973), wherein a simple geometry made up of two sloping faces was modeled using a modified Lax-Wendroff finite difference scheme. The scheme allows the inclusion of artificial viscosity terms. Their simulated outflow hydrograph compares well with laboratory measurements. Katopodes and Strelkoff (1979) developed a solution based on the method of characteristics for the two-dimensional form of the hydrodynamic equation. This was used to analyze the two-dimensional dam-break flood wave. The study showed the applicability of the method of characteristics in the solution of the hydrodynamic equation. However, the solution did not account for infiltration, soil surface roughness and variability in slope, since these factors are not tractable in the method of characteristics. The two-dimensional hydrodynamic equation was solved with a Lax-Wendroff scheme to model flood flow resulting from a dam break (Iwasa and Inoue, 1982).

Kawahara and Yokoyama (1980) developed and solved the two-dimensional solution of the hydrodynamic equation using the finite element scheme. This solution, however, failed to represent spatial variability in infiltration and soil surface roughness. A semi-implicit finite scheme that utilizes a space-staggered grid system was employed to solve the shallow water equation in oceans by Casulli (1998). The solution did not account for rainfall and infiltration, but considers the wind stress term effect on moving water. It was tested on a rectangular basin and simulates periodic tidal forcing that represents the boundary conditions.

Higher-order methods are reported to improve the prediction of rapidly varying flow (Wasantha-Lal, 1998). The studies by Garcia and Kahawita (1986) and Zhang and Cundy (1989) were part of the pioneering efforts in the application of higher-

order methods for the solution of hydrodynamic models. Both studies applied the MacCormack method, which is a simple variation of the Lax-Wendroff scheme, for solving the full hydrodynamic model. In the study by Zhang and Cundy (1989), runoff response to a time constant rainfall and infiltration was modeled. This study considered spatially variable hillslope features including surface roughness, infiltration and microtopography. Since only time constant rainfall was used, and the scale of microtopography measurements were coarse, there was not much variation in the output hydrographs from different surfaces. It was also reported that the simulation process becomes unstable at intervals after 500 seconds. Another higher-order method shown to have performed well in solving the hydrodynamic equation is the Leapfrog finite difference scheme. This method was applied in developing a simulation tool for basin irrigation schemes (Playan, 1992) and to investigate the effect of soil surface undulations and variable inflow discharge on the performance of an irrigation event on a level basin with spatially varying infiltration characteristics (Playan et al., 1994). Detail discussion on the application of higher order method is given in the section on model development (4.1) since it was applied in this study.

Conclusively, the problem of determining a solution for fluid flow by modeling is usually divided into two stages. The first of these is concerned with a description of the flow of the fluid in such general terms that this description will hold at each and every point in the domain of the solution at all times. Such a description is said to be generic to the class of flows concerned. The result is either a so - called 'point description' (i.e. the partial differential equation), or an 'interval description' (i.e. the integral equation). The second stage of the problem is concerned with transforming this 'point' or 'interval' descriptor into a representation that is distributed over the entire domain of the solution at all times, such as is, for example, realized by the process of integrating a partial differential equation. The difficulties experienced in integrating over complicated domains has led to the widespread and now almost universal use of numerical methods in which point and integral descriptions are extended to finite spatial descriptions that are maintained over finite time intervals, thus providing solution procedures of finite cardinality (Dibike, 2002). Solving this paradigm has led the development of different methods of defining effective grid points to determine dependent variables. The way in which the computation proceeds from values of

dependent variables at grid points at one time level to their values at the next time level depends on the computational scheme considered (Abbott and Basco, 1989).

2.4 Geomorphometric analysis and digital terrain modeling

The various processes in surface runoff formation and movement have also been studied with the geomorphometric properties of the catchment including local slope angle, convergencies and drain density (Schmidt et al., 2000). A classic example is the TOPMODEL (Beven et al., 1988; Wood et al., 1990), which is a topographically based hydrological model that aims to reproduce the hydrological behavior of the catchment in a semi - distributed way (Campling et al., 2002) and has produced good results in several climate zones. The GUH (geomorphic unit hydrograph) model (Rodriguez-Iturbe and Valdes, 1979) is also based on this method. This model is admired for the scale independence in its methods of solution and it is considered useful in studying microtopography effects. The advent of more precise and high-resolution digital elevation data over the last two decades and the availability of powerful geographical information system (GIS) packages have enhanced the use of this method. Specifically, the application of these techniques has shown that the hillslope - scale observation of runoff production mechanisms is influenced by soil properties, while the basin - scale observation is influenced by basin morphometry. Basin morphometry can be expressed by representative attributes for catchment height distribution (relief indices), length and form of the basin (form indices), and parameters describing the drainage network (Schmidt and Dikau, 1999).

2.5 Infiltration process

Infiltration is a key component that significantly influences the rainfall-runoff process. It must be well understood and represented before a reasonable prediction of overland flow in catchments can be made. Infiltration during a runoff-generating rainfall event is regulated by the hydraulic properties of the various soil layers the antecedent soil moisture conditions. Such hydraulic properties include unsaturated conductivity, saturated conductivity and soil water retention (holding) capacity. These hydraulic properties depend on the granular composition (texture) of the soil and on the spatial arrangement of the particles and voids in the soil (structure). In rainfall-runoff

processes, soil texture is a static property while the soil structure is dynamic. Consequently soil structure may vary in space as well as in time, depending on soil type and soil management (Dunne et al., 1991; Mallants et al., 1996; Stolte et al., 1996)

Spatial and temporal heterogeneity of infiltration and other hydraulic properties have received considerable attention in several hydrological studies. These observed variabilities have been attributed to several factors, prompting investigations into several processes considered to influence the infiltration behavior of soil in spatial and temporal dimensions. In studies relating spatial variability of infiltration properties to changes in soil structure as a result of tillage activities, Sharma et al. (1983) and Cassel and Nelson (1985) found significant differences in bulk density, cone index and soil water characteristics due to tillage, with the greatest spatial variation in the 0-14 cm layer. This changes influence the saturated conductivity and therefore infiltration. However a linear relationship with tillage treatment could not be established. In another study focused on the influence of repeated tillage treatments in the same locality on infiltration and hydraulic conductivity in a relatively homogeneous soil profile; Matula (2003) observed that conventional ploughing techniques (widely practiced in the Volta basin also) did not result in any significant change in hydraulic conductivity values after three years. However, reduced till treatment and no-till treatment results in significant decrease in the infiltration rate after three years. Hydraulic conductivity value decreased approximately three times for reduced till and six times for no-till treatment. It was concluded that such decrease associated with the treatment on soil could lead to negative results in surface soil hydrology and agriculture. This result from the increase in surface runoff, decrease in water storage and yield, increase in the compaction of soil surface layer and increased soil erosion. In another study on tillage and crop effects on ponded and tension infiltration rates in a 'Kenyon' loam, it was observed that the effect of tillage and crop rotation on infiltration patterns is not consistent. This observation was attributed to possible intra-season dynamics of the soil surface seal. The study also showed that temporal changes in infiltration were greater than tillage or rotation differences. It was, therefore, concluded that, evaluating the effect of management practice on soil hydraulic properties require several well-documented measurements (Logsdon et al., 1993).

In several catchments of the Volta basin, there is general trend of change of vegetation types (e.g., from woodland to cashew plantation or grassland). It was thus of interest to review the effect of land use change on soil hydraulic properties. In a study characterizing and comparing hydraulic properties of fine-textured soils on native grassland, a recently tilled cropland, and a re-established grassland, Schwartz et al. (2003) observed that long-term structural development on native grasslands was principally confined to effective pore radii greater than 300 μm, suggesting that land-use practices had a greater effect on water movement than on the soil series. This indicates that the modifying effects of tillage, reconsolidation, and pore structure evolution on hydraulic properties are important processes governing water movement in fine-textured soils. Mapa et al. (1986) showed that four soil-water properties i.e., sorptivity with positive head, sorptivity with negative head, soil hydraulic conductivity and the soil-water retention characteristic undergo significant temporal changes due to wetting and subsequent drying during tillage, with the first wetting and drying cycle being responsible for most of the temporal variability. The study by Diamond and Shanley (1998) with the aim of deriving soil properties from infiltration measurements in the summer and winter period in Ireland showed that infiltration tests are a poor discriminate of soil properties, particularly in the winter period. This is because infiltration rates are influenced more by the hydrologic regime than by soil properties. The method is however quite useful in classifying soil during the summer period and as such would perform well on tropical condition.

Soil surface characteristics (SSCs) have also been reported to influence the infiltration properties at the surface of the soil and could explain spatial variation in the infiltration properties observed under natural rainfall in uniform soil. In a study by Malet et al. (2003), the distribution of hydraulic conductivity curves near saturation for each SSCs type was developed and was helpful in distributing local hydraulic conductivity values on hillslopes. The study showed that it is possible to link SSCs in a catchment to hydrodynamic properties and will assist in identification and delineation of hydrological and geomorphological response units, based on the SSCs distribution of the catchment.

Both Hortonian and Dunne's runoff generation processes are strongly influenced and regulated by the infiltration property and saturated conductivity of the

soil layers. There is a consensus, though not unanimous on the spato - temporal changes in the magnitude of infiltration within a season and also in a during a rainfall event. This transient behavior of infiltration should be quantified and integrated in developed models, to represent field condition reasonably. This has led to the concept of interactive infiltration. Interactive infiltration assumes a small-scale dynamic interaction between the overland flow and infiltration process caused by spatially variable soil, ground surface characteristics, depth of overland flow and rainfall intensity (Fiedler and Ramirez, 2000). In this study, the concept was applied in the modeling technique by defining sorptivity value, which varies depending on the initial moisture conditions, and soil state before the runoff events.

2.6 Scale issues in runoff and infiltration processes

Modeling surface runoff and infiltration process over large area is always challenging particularly when such models are for predictive purposes. This is often the case because measurement of infiltration, hydraulic conductivity, rainfall, surface feature, etc., which serve as input for many rainfall - runoff models, are made at point or at the most on plot scale, whereas the developed models are required for application at basin or catchment scale. Consequently, great discrepancies exist in the results as most of the models do not explicitly account for spatial variability of soil hydraulic properties and the temporal dynamics associated with the processes. For example, the computational elements of kinematic wave overland models of large areas do not explicitly account for spatially variable infiltration characteristics or small-scale ground surface unevenness (microtopography). Effective or apparent parameters are assumed such that the model can fit observed data, but these parameters may not be valid at other input levels or application scales.

There have been several research efforts to understand these discrepancies, commonly referred to as scale dependency or scale effect. Early numerical investigations include the works of Julien and Moglen (1990), using kinematic wave approximation of the hydrodynamic equation. The study concludes that variability in runoff discharge depends primarily on the ratio of rainfall duration t_r to the time to equilibrium t_e defined as

$$t_e = \left(\frac{wL}{ai^{b-1}} \right)^{1/b} \qquad (2.1)$$

where w and L are width and the length of plot; b and a are the kinematic wave parameters; and i is the infiltration excess.

This study further defined a length scale factor that incorporates spatially averaged values of surface parameter, rainfall intensity and duration factors, to delineate similarity conditions for spatially varied runoff. In a follow-up study, Ogden and Julien (1993) partitioned the zone of effectiveness of both spatial and temporal variability factors in rainfall-runoff response systems as a function of the rainfall duration and the time to equilibrium. A similar study by Dunne et al. (1991) showed that apparent and effective infiltration rates depend on hillslope length, and consequently the steady state discharge will increase linearly with distance downslope thus initiating scale dependency. An analytical study on the effect of temporal variation of rainfall intensity on overland flow by Hjelmfelt (1981) showed that the peak discharge from an overland flow could be influenced by the rainfall intensity pattern. Recent contributions to the numerical investigation include those of Fiedler et al. (2002), who investigated the effect of grazing activities on scale response, concluding that grazing alters the microtopographic formation of the field. Fieldler and Ramirez (2000), Esteves et al. (2000), and van Loon and Keesman (2000) in their studies solved the full hydrodynamic equations using different methods, and showed that rainfall-runoff response depends on the combination of various factors, which include microtopography, spatial characteristic of hydraulic properties, etc. Wainright and Parson (2002), in their numerical investigation of scale dependency, showed that temporal characteristics of rainfall intensity might be an alternative explanation to the commonly assumed spatial variability of soil properties in explaining scale dependency. In a study focused on analysis of scale dependency of a lumped hydrological model, Koren et al. (1999) showed that the Hortonian overland flow process is more scale dependent than the Dunnes' flow and that all the models tested produced less surface and total runoff with increasing scale size.

In other studies, De Roo and Riezebos (1992) suggested the combination of stochastic methods with distributed hydrological models in evaluating the consequences of the large spatial variability of infiltration on scale dependency in rainfall-runoff

transformation. Jetten et al. (1999) concluded from their evaluation of runoff and erosion models that the spatial variability of infiltration-related variables is difficult to handle, due to differences in scale between observations (on small soil samples) and application (on entire watersheds). Scale dependency is also attributed to variability in soil conditions. Auzet et al. (1995) opined that the use of qualitative typologies of soil condition and rough empirical models of its evolution will constitute a considerable improvement over approaches ignoring the variability of soil surface state in space and time in scale dependency studies.

There have also been some efforts to investigate scale dependency in the rainfall-runoff process by field trials under natural rainfall or simulated rainfall. Esteves and Lapetite (2003) observed a decrease in the runoff coefficient with increasing plot area in their field experiment at four different scales under natural rainfall conditions in Niger. Joel et al. (2002) equally observed in their experiments under natural rainfall that large plots with an area of 50 m^2 only produced 40% of runoff quantities from 0.25 m^2 plots per unit area discharge, when compared even in periods of continuous rainfall. Van de Giesen et al. (2000) also observed a clear reduction in runoff coefficients with increasing slope length. Their result showed that between 30 to 50% of rainfall, is lost as runoff on a square meter plot as compared to 4% on a 130 Ha watershed. Lal (1997), Yair and Kossovsky (2002), and Wilcox et al. (1997) all concurred with the observation of a reduced runoff coefficient with increasing size of plots, at varying factors.

Summarily, scale dependency in the rainfall-runoff response system in all types of investigations has been attributed to several spatial and temporal factors. Spatial variability of several factors such as soil hydraulic conductivity, surface depression, initial soil water content, slope length, crack development, crust and seal formation, and rainfall has been given as source of scale dependency of rainfall-runoff response from catchments (Joel et al., 2003; Arnaud et al., 2002; Gomez et al., 2002; Julien and Moglen, 1990). Schmidt et al. (2000) showed that effective geomorphometric parameters such as landform structure, topology, local slope angle, convergence, and drain density influence scale dependency. They also noted that in small sub-region catchments, particularly those having low slope angles, the low flow lengths, concavities and spatial distribution of the soil types, are all important in scale dependency of the rainfall-runoff response system. Some authors, including de Lima

and Singh (2002), Wainright and Parson (2002), Ogden and Julien (1993), Dunne et al. (1991) and Julien and Moglen (1990), have cited temporal dynamics with special focus on rainfall dynamics. Lapatite and Esteves (2003) and van de Giesen et al. (2000) suppose that temporal dynamics in infiltration excess play a significant role in scale dependency.

Using a combination of field trial results and numerical simulation, this study will answer the following questions:

1. What are the principal factors that influence runoff formation in the Volta basin?
2. What is the relationship between runoff and catchment hydraulic properties at different scales?
3. Which are the effective parameters that influence scale response at each scale of simulation?
4. What role is played by the surface properties and the temporal dynamics of the rainfall in runoff response at the different scales?

3 MATERIALS AND METHODS

3.1 Study area description: location, geography and topography.

In investigating and understanding the hydrologic behavior of the Volta Basin, three pilot sites were selected for intensive observation of several hydro-ecological processes in the Ghana side of the catchment. The selected areas are Ejura in the middle belt, Tamale and Navorongo in the northern part. Among the three sites selected, Ejura has the highest annual rainfall average, and is characterized by undulating landforms that facilitate runoff process. Extensive flat terrains characterize Tamale and Navorongo sites. Plots and catchment investigation of the runoff process was consequently studied at a catchment in the Ejura study area. The research catchment is located about 14 Km north of Ejura and is locally named Kotokosu (latitude 07° 20' N and longitude 01° 16' W). The catchment is in the forest–savannah transition zone of Ghana and the study area has been christened the "food basket of Ghana". That implies very intense cultivation and other human activities that have significantly influenced changes in vegetation patterns and degradation of soil quality. Owing to centuries of human activities and high rural population density, virtually all natural vegetation in the study area has been destroyed and replaced by secondary re-growth vegetation, cashew and cocoa farms, and farms with field crops such as maize, cowpea, guinea corn, cassava and yams.

The climate is wet semi-equatorial with a long wet season lasting from April to mid-November. This alternates with a relatively short dry spell that lasts from mid-November to March. The major rainfall season begins in April and ends in July, and the minor season begins in September and ends mid-November, displaying large inter-and intra-season heterogeneity with regard to total rainfall as well as the occurrence of dry spells. Long-term mean annual rainfall is 1445 mm (Osei-Bonsu and Asibuo, 1998). The storms are mostly determined by the mesoscale convective system (MCS), which is a unique, well-organized convective cloud cluster that is well known for its production of extreme weather conditions and abundant rainfall. A MCS usually originates as a localized region of convection and subsequently spreads out like a ripple on a pond. However, unlike water waves, the convective wave rarely spreads in a symmetric fashion, and convection may be entirely absent from certain sectors. Therefore, an

expanding arc of convection is more often observed on satellite images than a full circle. This arc is usually referred to as a squall line (SL) (Raymond, 1976; Friesen, 2002; Abiodun, 2003). A front with high intensities and a tail of longer duration and lower intensities characterize the typical hyetograph generated by a squall line. Rainfall distribution in the study area is spatially variable with the intensity ranging between 2 $mmhr^{-1}$ to 240 $mmhr^{-1}$ and a median intensity of about 70 $mmhr^{-1}$. Rainfall duration is generally short with an average of about 30 to 50 minutes, but some events are longer especially the monsoonal rains also common in the study area. Average annual temperature in the study area is about 28°C with no marked seasonal or monthly departure from the annual average. The area lies in the Voltaian sandstone basin and is characterized by gently dipping or flat-bedded sandstones, shales, and mudstones, which are easily eroded. This has resulted in an almost flat and extensive plain, which is between 60 and 300 meters above sea level (Dickson and Benneh, 1995). The drainage network is composed of well-formed channels that developed from rills and concentrate the runoff water away from the shallow soil profile. Schist and granite are the major rock materials found in the catchment. The nature of soils in this landscape is largely associated with the parent material. The dominant soil types in the area are Luvisol, Phinthosols, Acrisol and Leptosols. The catchment consists of a large area of rock outcrops and soil depth is shallow. There are about four shallow ponds formed in the valley area that trap runoff water, and 3 other seasonal streams, which discharge into the one main stream used to monitor catchment discharge. Detail soil characterization for the study site is presented by Agyare (2004).

During the dry season preceding the 2002 rainfall season, a detailed topographical survey was conducted. Elevations data at several points were kinematically collected using ASHTEC Differential Global Positioning System (DGPS). The obtained data was used to generate a digital elevation model (DEM) of the study site. The study site can be classified as a medium to low land with elevation varying between 165 meter and 260 meter above the sea level (figure 3.1).

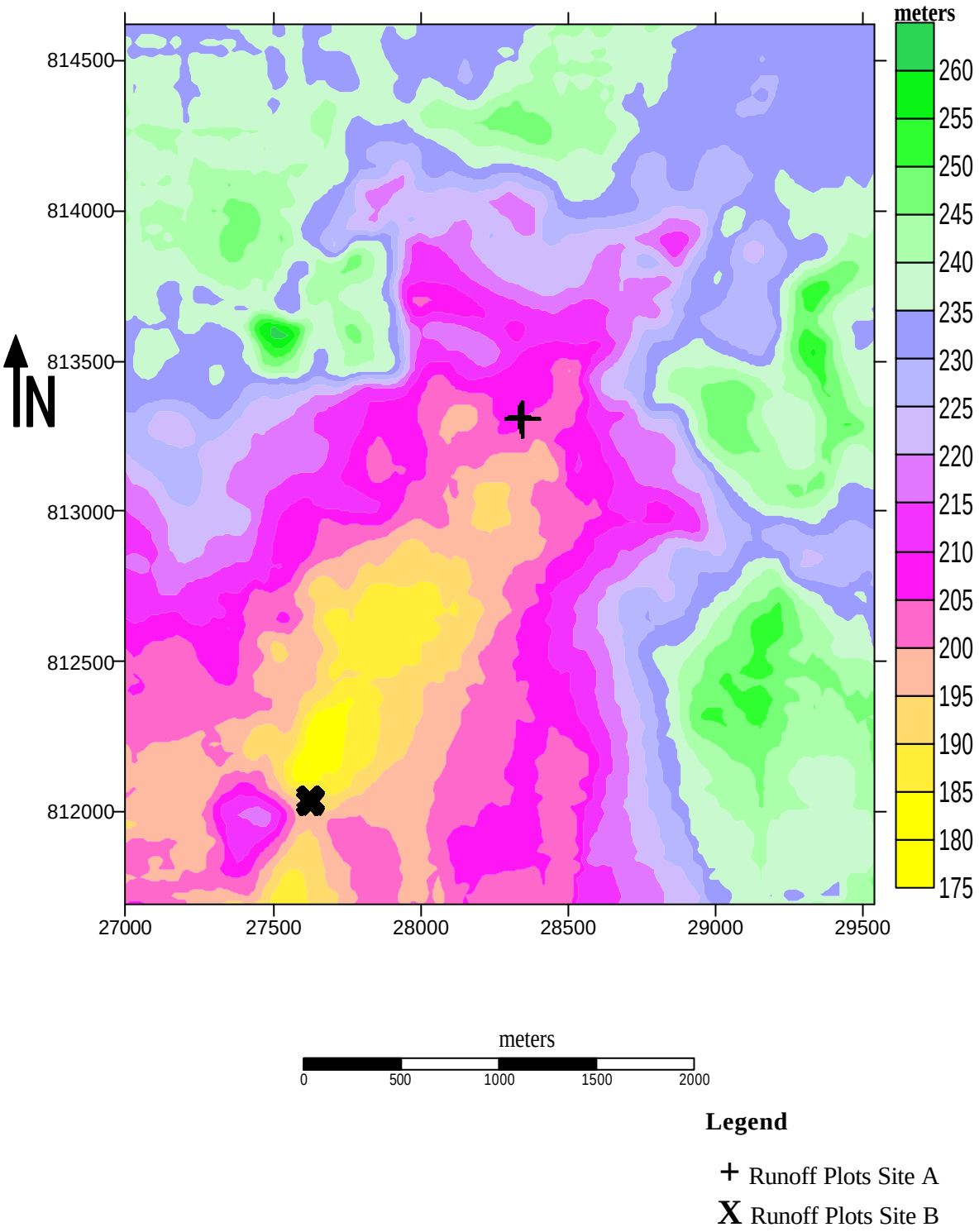

Figure 3. 1 Digital elevation map of the study site indicating the location of runoff plots.

The area of the study site as estimated from the survey data is about 8.75 Km^2. The digital elevation model was constructed from about 5000 GPS measurements over

the entire catchments, which was interpolated by Kriging. The first step involved modeling the spatial structure of the elevation data using the semi-variogram. The semi-variogram is a function of distance (lag) separating data points. With a set on n observation, there are $\frac{(n-1)n}{2}$ unique data pairs. The empirical variogram is computed as half the average of the squared difference of all data pairs (Chilés et al., 1999). The experimentally derived variogram was used to fit a linear model of the form:

$$j(h) = 45 + 0.32h \quad (3.1)$$

where j is the semi variogram and h is the distance in meters.

Kringing was used for interpolation, because it has been shown to be the best linear unbiased estimator (BLUE).

3.2 Site instrumentation

The study area as mentioned is one of the test sites selected for intensive observation and monitoring of agro-eco-hydrological variables within the scope of the overall project objectives. Instruments at the site include an automatic weather station, which records all weather variables (rainfall, minimum and maximum temperature, net radiation, relative air humidity, barometric pressure, wind speed and direction, and soil heat flux). These parameters are logged every 10minutes by a Campbell CR10 datalogger. The site is also equipped with a set scintilometer to capture the heat flux in the catchment transects. Networks of plastic access-tube were installed at strategically selected 16 locations to a depth of 100cm. Soil moisture at depths of 10cm, 20cm, 30cm, 40cm, 60cm, and 100cm were monitored with a Delta-T TDR profile moisture probe type PR1/6 during the study period. Profile soil moisture monitoring is also supplemented by another network of 15 aluminum tubes installed to a depth each of 120cm, which were monitored concurrently at depths 10cm, 20cm, 30cm, 40cm, 60cm, 100cm and 120cm with a neutron probe. Surface soil moisture in the first 10cm layer was monitored using the Delta-T TDR moisture probe regularly throughout the period of observation. At two locations, each close to one aluminum access tube, one plastic access tube and the runoff plots, soil moisture tension were monitored at the depths 30cm, 60cm, and 100cm from June to November of the 2002 rainfall season with 6 sets of tensiometers. Within the study period, vegetation development was monitored in a

series of biomass estimation experiments at various locations in the catchment and within the plots with Sunscan probe.

3.3 Design of runoff plots, construction materials and process

To capture the surface runoff process at a local scale, two sets of runoff plots were cited within the catchment to allow discharge measurement. They were composed of natural soil demarcated with aluminum sheets on three sides, which were driven 20cm into the soil and protruded 30cm. With this border, upstream flow from both surface and subsurface flowing into the runoff plots was effectively cut off. The downstream section of each plot was fitted with an aluminum gutter that discharged into a trough. Each trough housed a tipping bucket runoff meter designed basically for this field study. A mercury switch was attached to the base of each tipping bucket and connected to a HOBO state logger, which logged the date and time (to the nearest second) of each tip of the bucket as either open or closed state. The site selection for the plots was based on a reconnaissance survey of the catchment in the later part of the 2001 rainfall season. The two sets of plots were located close to the valley bottom on transects of discharge into the main stream which flows through the catchment, and oriented along the slope direction. Plate 3.1 shows the runoff plots layout.

Each set of plots consisted of a twin plot measuring 2 m x 18 m (long plot, LP), one 2m x 6 m plot (medium plot, MP) and one 2°m x 2°m square plot (short plot, SP). The plots were placed close enough to each other to avoid the influence of soil spatial variability on rainfall-runoff response monitoring. This implies that the soil in all the plots at each site was uniform and the soil physical characteristics of all the plots on both sites were similar. Table 3.1 shows the summary of the physical characteristics of the soil at each site. The sites were named A and B. The location of the plots within the catchment is shown in figure 3.1. All the plots were constructed at the end of the rainy season in 2001, so that all the plots would have sufficient time to stabilize, and return to natural conditions before the onset of the rainfall season in 2002, used for observation.

A: Long and Short runoff plot at site when freshly constructed

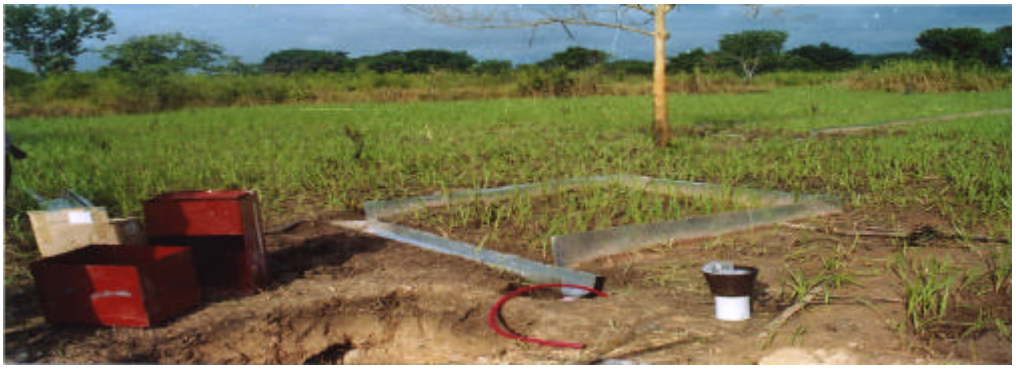

B: Short runoff plot at site A when freshly constructed

C: The twin runoff plots at site B

Plate 1: Runoff plots in picture

Table 3.1: Physical properties of soil in site A and B

Plots	Bulk Density	CEC	% Sand	%Silt	% Clay	Soil Class*
Site A	1.475	4.21	56.76	40.52	3.28	Silt loam
Site B	1.366	2.17	67.96	25.52	6.52	Sandy clay loam

*Based on van Genuchten parameter classification

The records of total discharge from each runoff plot during runoff events were manually measured at the end of each event with calibrated buckets combined with measuring cylinders. The HOBO event loggers ensured the automated measurement of total number of tips and frequency (time of tip to nearest seconds) during the runoff events. From the record of the cumulative tips, the total volumes were also obtained, and compare very well with the manually measured runoff volume. Between the plots on each site, a tipping bucket-rain gauge was placed to monitor the rainfall intensity at the plot level. Each gauge was connected to a HOBO event logger that registered date, cumulative tip number, and time of tip to the nearest second. The standard amount of rainfall per tip was between 0.1 and 0.2 mm, but the buckets were calibrated for the actual amount of discharge per tip that was estimated to be 0.17ml. Three other tipping - bucket rain gauges also fitted with HOBO event loggers were also distributed along defined transect within the catchment. This facilitated the comparison of rainfall intensity distribution on the catchment. The HOBO event and state loggers are normally read out with the Boxcar software provided with the loggers.

3.4 Hydraulic conductivity and infiltration measurement

In characterizing the hydraulic properties within each runoff plot, cumulative infiltration curves were obtained from the several-scaled points within the plots. The Decagon's 0.5cm suction minidisk infiltrometers were used for the infiltration experiment. The 0.5cm suction represents the suction at which raindrop infiltrate into the soil under natural field conditions. For each measurement, the initial and final moisture content at the point and its immediate environs were taken with the handheld TDR. These values were later related to the initial moisture content value.

This study also aim to examine the spatial variability of infiltration and hydraulic conductivity over the catchment in relation to the spatial distribution of the soil type and landscape position; consequently infiltration curves were obtained at selected grid points used to characterize the soil physio-chemical properties, using the

mini-disc infiltrometers. Measurements were taken at about 200 points within the catchment and the Philip two-term equation was used to obtain the cumulative infiltration curve. Using the polynomial fitting techniques of the cumulative infiltration curve, the van Genuchten parameters were obtained, which were then substituted in appropriate equations to compute the hydraulic conductivity values at all the measured points. These values were then analyzed for trend and distribution using statistical and geo-statistical methods. A summary of routine measurements of the parameters monitored during the field experiment, their frequency, spatial and temporal resolutions are given in Table 3.2

Table 3.2: Outline of measured parameters and equipment used during the field experiment.

Parameter	**No of points**	**Instrument used**	**Temporal resolution**
Rainfall total	3	Totaling rain gauge	Each rainfall event
Rainfall intensity	6	Rainfall tipping buckets	Intensity to the nearest seconds
Runoff intensity	8	Runoff tipping buckets	Each event
Plot discharge	8	Measuring cylinder	Each event
Catchment discharge	1	Barrow Divers	2002 rainfall season
Infiltration & hydraulic conductivity	Several within Runoff plots and catchment Area	Mini disk infiltrometers	2002 rainfall season
Surface soil moisture	Several point	ML2	Dec. 2001 to Dec. 2002
Profile soil moisture	16	PR1 profile probe	Dec. 2001 to Dec. 2002
Soil tension	2	TL2 Tensiometer	June 2002 to Nov. 2002
Leaf area index	Within Plot and 8 other experimental location.	Sunscan probe	2002 rainfall season

4 MODEL DEVELOPMENT

4.1 Background

The various mechanisms involved in most hydrological processes could be investigated and clearly understood, if adequate relationships that characterize the physics of the process is derived and applied. Consequently, most studies often rely on such numerical or statistical model(s) to elucidate on field trial results. In the study of surface runoff or overland flow processes and in many other environmental problems involving unsteady flow in waterways, mathematical models based on the shallow water wave equation have become and an accepted efficient tool for representation (Chow and Ben - Zvi, 1973; Zhang and Cundy, 1989; Fiedler, 1997; Singh and Bhallamudi, 1998; Zoppou and Roberts, 2003). This equation is either used in its complete form as the full hydrodynamic equation or in its approximate form as a kinematic or diffusion wave model as earlier discussed (section 2.2). Since this study aimed at improving the understanding of surface runoff processes at varying scale (spatial and temporal) of observations, the full hydrodynamic model was selected for application after a review of the different model. A detailed description of the development of the model and the solution for this study is given in the following sections.

4.2 Model outline

The two-dimensional unsteady flow equations commonly referred to as the Saint Venant equation is widely used to describe overland flow and surface runoff process. In deriving the Saint Venant equation, the four original Navier - Stokes hydrodynamic equations are vertically averaged over the flow depth using the following kinematic boundary conditions:

At the free surface $h = h_{sur}(x, y, t)$

$$\frac{dh}{dt} = \frac{\partial h_{sur}}{\partial t} + u_{sur}\frac{\partial h_{sur}}{\partial x} + v_{sur}\frac{\partial h_{sur}}{\partial y} = w_{sur} - R(x, y, t) \tag{4.1}$$

At the bed surface $h = h_{bed}(x, y, t)$

$$\frac{dh}{dt} = \frac{\partial h_{bed}}{\partial t} + u_{bed}\frac{\partial h_{bed}}{\partial x} + v_{bed}\frac{\partial h_{bed}}{\partial y} = w_{bed} + I(x, y, t) \tag{4.2}$$

where h_{sur} and h_{bed} are the free surface and bed surface elevations above the datum respectively; u_{sur}, v_{sur} and w_{sur} are the velocity components in the x, y, and z directions respectively at the free surface; u_{bed}, v_{bed} and w_{bed} are the velocity components in the x, y, and z direction at the bed surface; $R(x, y, t)$ is the spatially and temporally variable rainfall rate; and $I(x, y, t)$ is the spatially and temporally variable infiltration rate. The following assumptions are also used (1) velocity is constant across the various depths; (2) for a shallow water flow of long waves, the vertical velocity and acceleration of the fluid particles are small compared to the acceleration due to gravity; (3) pressure distribution is hydrostatic, and, (4) horizontal shear stresses components are small compared to the vertical shear stress components (Zhang and Cundy, 1989; Fiedler and Ramirez, 2000). The derived equations (by neglecting all small terms) comprise of the equation of continuity and two equations of motion, one for each of the planar coordinate directions x and y. These equations in Cartesian coordinates may be stated as (Zhang and Cundy, 1989; Esteves et al., 2000).

$$\frac{\partial h}{\partial t} + u\frac{\partial h}{\partial x} + v\frac{\partial h}{\partial y} = R(t) - I(x, y, t) \tag{4.3}$$

$$\frac{\partial u}{\partial t} + u\frac{\partial u}{\partial x} + v\frac{\partial u}{\partial y} + g\left[\frac{\partial h}{\partial x} + S_{fx} - S_{ox}\right] = 0 \tag{4.4}$$

$$\frac{\partial v}{\partial t} + u\frac{\partial v}{\partial x} + v\frac{\partial v}{\partial y} + g\left[\frac{\partial h}{\partial y} + S_{fy} - S_{oy}\right] = 0 \tag{4.5}$$

where

h= depth; u= local depth-averaged velocity in the x - direction; v = local depth - averaged velocity in the y - direction; g = gravitational acceleration; S_{ox} = bed slope in the x - direction; S_{oy} = bed slope in the y-direction; S_{fx} = friction slope in the x - direction; S_{fy} = friction slope in the y-direction; $R(t)$ = rainfall intensity assumed to be uniform in space but varied in time; and $I(x,y,t)$ = rate of infiltration which could be spatially varied and time dependent.

The equation could be re - written in terms of the dependent variables, depth, h and unit discharges $(q_x=u\,h)$, $(q_x=v\,h)$ in the x and y planar directions, by multiplying the two equations of motion (4.4, and 4.5) by the depth of flow (h) for surface runoff problems resulting in:

$$\frac{\partial h}{\partial t}+\frac{\partial q_x}{\partial x}+\frac{\partial q_y}{\partial y}-q_l(x,y,t)=0, \tag{4.6}$$

$$\frac{\partial q_x}{\partial t}+\frac{\partial}{\partial x}\left(\frac{q_x^2}{h}+\frac{gh^2}{2}\right)+\frac{\partial}{\partial y}\left(\frac{q_x q_y}{h}\right)+gh(S_{fx}-S_{ox})=0 \tag{4.7}$$

$$\frac{\partial q_y}{\partial t}+\frac{\partial}{\partial y}\left(\frac{q_y^2}{h}+\frac{gh^2}{2}\right)+\frac{\partial}{\partial x}\left(\frac{q_x q_y}{h}\right)+gh(S_{fy}-S_{oy})=0 \tag{4.8}$$

$q_l(x, y, t)$ represents the net lateral inflow i.e., the rate at which water is vertically added to or removed from the control volume $[R(t)-I(x,y,t)]$, and it could be spatially and temporally varied. Equation (4.6) results from conservation of mass over a control volume, and its first term connote the variation of depth over time in an unsteady flow condition. The various differential terms in the momentum equations represent different quantities related to conservation of momentum. Comparing the equation in this form to the classical St. Venant equation, the local acceleration, convective acceleration and pressure force terms in both x and y directions could be extracted as follows:

$\frac{\partial q_x}{\partial t}, \frac{\partial q_y}{\partial t}$ — Local acceleration in x- and y - directions

$\frac{\partial}{\partial x}\left(\frac{q_x^2}{h}\right), \frac{\partial}{\partial y}\left(\frac{q_x q_y}{h}\right), \frac{\partial}{\partial y}\left(\frac{q_y^2}{h}\right), \frac{\partial}{\partial x}\left(\frac{q_x q_y}{h}\right)$ — Convective acceleration in x - y directions,

$\frac{\partial}{\partial x}\left(\frac{gh^2}{2}\right); \frac{\partial}{\partial y}\left(\frac{gh^2}{2}\right)$ — Pressure force in x - y directions

Some of the terms of the surface runoff equations must be derived or approximated from other equations and relationships. These relationships are based either on field measurements, empirical models or published data. The following sections describe in detail, the method of estimation or derivation of the parameters used for the surface runoff equation in the study.

4.3 Bed and friction slopes

The bed slope, which connotes the ground surface topography and variation of local slope gradient in the x - y planar directions, S_{0x} and S_{0y}, were estimated from the relative

ground surface elevation in the z-plane. Data for the computation can were obtained from the digital elevation model (DEM) data. Mathematically, the bed slope is computed from the expressions:

$$S_{0x} = -\frac{\partial h_{mt}}{\partial x} \tag{4.9}$$

$$S_{0y} = -\frac{\partial h_{mt}}{\partial y} \tag{4.10}$$

where h_{mt} is the bed elevation from an arbitrary datum (m). In the numerical code developed for the solution, point elevations at regular grids were defined, which enable the computation of local bed slope at each grid cell.

The friction slopes depict the slope of the energy grade line and can be calculated from a number of equations. It constitutes the resistance to overland flow by soil and vegetation and is an important factor included in the model. The friction factor varies depending on the type of flow under consideration as it is related to the shear stress at the bed. It is moderated by several factors including soil texture, soil surface roughness (microtopography), vegetation type, distribution and density among other factors. For any prevailing flow condition, there is interplay of significance between the viscous stress and the Reynolds' stress. For example, in laminar flow condition, viscous stress dominates, and consequently, the Reynolds' stress effect can be ignored and vice-versa.

The simplest form of the Darcy – Weisbach equation is the one derived for a steady and uniform flow and is given as:

$$S_{fx} = f\frac{u^2}{8gh} \tag{4.11}$$

$$S_{fy} = f\frac{v^2}{8gh} \tag{4.12}$$

where f is the Darcy – Weisbach factor and u and v are the velocity in the two direction. This is a very simple form of representation, which however rarely occurs in field observation, since surface runoff can hardly be uniform because of the various disturbances in the process. This approach was used by Esteves et al. (2000) to represent the friction slope factor in their solution developed for the surface runoff equation.

Another form of the Darcy–Weisbach equation for two-dimensional laminar flow (i.e., viscous stress dominates and Reynold stress can be ignored) situation is given as:

$$S_{fx} = \frac{f}{8g}\frac{q_x(q_x^2 + q_y^2)^{1/2}}{h^3} \tag{4.13}$$

$$S_{fy} = \frac{f}{8g}\frac{q_y(q_x^2 + q_y^2)^{1/2}}{h^3} \tag{4.14}$$

where q_x and q_y are the fluxes of the velocities in both x and y directions; h is the flow depth; g is gravitational acceleration and f is the flow resistance factor. In the laminar flow regime, in which viscous stresses are much larger than Reynolds stresses, f is computed as a function of the Reynolds-number, R_e, captured in the relationship

$$f = \frac{K_o}{R_e} \tag{4.15}$$

The parameter K_o is a resistance parameter, which relates to the ground surface characteristics. It has been estimated for some surface characteristics and other biotic factors including vegetation type and density, root volume. Table 4.1 shows the estimated range of K_o for different surfaces from the study by Woolhiser, (1975).

Table: 4.1 Estimated values of K_o for different surfaces

Surface type	***K*$_o$ (range)**
Bare sand	30-120
Sparse vegetation	1000-4000
Short grass	3000-10000

The Reynolds number for two-dimensional flow is computed from the equation:

$$R_e = \frac{\sqrt{(q_x^2 + q_y^2)}}{n} \tag{4.16}$$

where $\nu = 10^{-6}$ m/s is the kinematic viscosity of water. When the expression for K_o and R_e are substituted in equations 4.13 and 4.14, the relationship for the friction slope factor in laminar flow conditions takes the form:

$$S_{fx} = \frac{K_0 n q_x}{8gh^3} \tag{4.17}$$

$$S_{fy} = \frac{K_0 n q_y}{8gh^3} \tag{4.18}$$

Fiedler and Ramirez (2000) applied equations 4.17 and 4.18 in their study, by assuming laminar flow dominate surface runoff processes.

The friction slope factor for turbulent flow (i.e. where Reynolds' stress dominate and viscous stress can be ignored) is mainly calculated from the Manning equation using the relationship:

$$S_{fx} = \frac{n^2 \left(q_x^2 + q_y^2\right)^{1/2}}{h^{4/3}} \tag{4.19}$$

$$S_{fy} = \frac{n^2 \left(q_x^2 + q_y^2\right)^{1/2}}{h^{4/3}} \tag{4.20}$$

where n is the Manning's roughness coefficient. This form was applied in surface irrigation modeling by Playan et al. (1994).

Another form of the Darcy – Weisbach equation, which accounts for the effect of rainfall resistance on the frictional resistance, is given by the relationship (Singh and Bhallamudi, 1998):

$$S_{fx} = f_d \frac{q_x^2}{8gh^3} \tag{4.21}$$

$$S_{fy} = f_d \frac{q_y^2}{8gh^3} \tag{4.22}$$

where f_d is the frictional resistance, whose evaluation depends on the instantaneous state of flow. It is calculated for laminar flow from the relationship:

$$f_d = \frac{C_l}{R_e} \tag{4.23}$$

where C_l factor is proportional to rainfall intensity.

In this study, all the above-described methods of computing the friction slope were evaluated and the numerical code for the solution is developed in a way that any of the described methods can be activated. To account for the interaction of both temporal nature of rainfall (which was not considered by Fieldler and Ramirez (2000) since time constant rainfall was used) and soil surface feature (which was not considered by Singh and Bhallamudi (1998) since one dimensional form of the equation was solved and this neglect surface feature), the equation by Zhang and Cundy (1989) was revisited.

According to Zhang and Cundy (1989), the friction slope factor is the difference between the shear stresses at the free surface and at the bed i.e.

$$S_{fx} = (S_{fx_{sur}} - S_{fx_{bed}}) \quad \text{and} \quad S_{fy} = (S_{fy_{sur}} - S_{fy_{bed}}) \tag{4.24}$$

where $S_{fx_{bed}} = \frac{f}{8g}\frac{q_x(q_x^2+q_y^2)^{1/2}}{h^3}$; $S_{fy_{bed}} = \frac{f}{8g}\frac{q_y(q_x^2+q_y^2)^{1/2}}{h^3}$; accounts for the friction factor at the bed and is often used alone by ignoring the friction factor at the surface. The friction slope at the surface in the x and y directions, which takes into account, the effect of rainfall is stated given as:

$S_{fx_{sur}} = -R\frac{q_x}{h}$ and $S_{fy_{sur}} = -R\frac{q_y}{h}$. Combining the surface and bed shear stress, and substituting for *f*, the friction factor, the friction slope in both directions becomes:

$$S_{fx} = \frac{f}{8g}\frac{q_x(q_x^2+q_y^2)^{1/2}}{h^3} + R\frac{q_x}{gh^2} \tag{4.25}$$

$$S_{fx} = \frac{f}{8g}\frac{q_x(q_x^2+q_y^2)^{1/2}}{h^3} + R\frac{q_y}{gh^2} \tag{4.26}$$

The inclusion of rainfall effect is necessary in view of the shallow nature of overland flow and the peculiar high intensity associated with tropical rain. As raindrops fall into flowing water, they generate splashing craters on the water surface, and turbulence in the flow. These can cause energy loss and increase flow resistance (Zhang and Cundy, 1989). Laminar flow relationship was used for simplicity and any turbulence that might develop is accounted for in the instantaneous rainfall factor (*R*).

4.4 Net lateral inflow

Net lateral inflow is literarily the difference between rainfall and infiltration, thus the value of lateral inflow at any point in time and space varies depending on several factors, including the time since the beginning of the rainfall, the intensity of the rainfall event and its distribution, initial moisture condition and hydraulic characteristics of the soil. Soil hydraulic behavior depends on the type of soil and the landscape position. A negative net inflow will imply that the rainfall intensity is lower than the infiltration capacity of the soil; consequently, all the rainwater infiltrates into the soil. To compute

net lateral inflow, the effect of vegetation on rainfall and the interactive process of infiltration were considered as discussed below.

4.4.1 Rainfall and vegetation

Rainfall intensity values used as an input in this study are directly computed from records obtained from the tipping-bucket rainfall gauges installed at the experimental site. These data are prepared in the frequency format, i.e., cumulative number of tips and the corresponding time in seconds since the onset of the particular rainfall event.

Average Leaf Area index (LAI) defined as the cumulative one-sided area of (healthy) leaves per unit area (Watson, 1947) per plot was monitored during the experiment. The analysis of these record was used to account for rainfall interception by introducing a reduction factor on the volume of rainfall per tip of the tipping bucket rainfall gauge as a function of the canopy cover fraction *c*. Van Dijk and Bruijnzeel (2001a, b) gave a detailed review of the various analytical model of rainfall interception for use with vegetation of variable density. A modified equation relating canopy cover fraction and Leaf Area Index (*LAI*) was proposed in that study and is expressed as:

$$c = 1 - e^{-kL} \tag{4.27}$$

where k is a dimensionless extinction coefficient. The value of k depends on leaf distribution and inclination angle and usually ranges between 0.6 and 0.8 in forests (Ross, 1975). For a number of agricultural crops, van Heemst (1988) reported values between 0.2 and 0.8, with values of 0.5 to 0.7 being the most common. The canopy cover fraction was later used to estimate interception loses from a mixed cropping system, very similar to the cropping practice in the Volta Basin. This was achieved by relating the canopy cover fraction to the relative evaporation rate and a range of 5% to 14% of the gross rainfall was found to be lost to vegetation interception. However, the estimation does not include stemflow. Stemflow may however have no significant effect on the range, since stem losses are mostly estimated from through fall and not from gross rainfall.

Calculated rainfall intensity from the tipping bucket is therefore reduced by the canopy cover fraction to obtain the “effective” rainfall intensity. The characteristic graph of the average LAI representing the major vegetation covers in the catchment against the week(s) since the beginning of the rainfall season was used to select an

appropriate factor for use in the simulation. This enhance large scale application of the model over the basin, since vegetation development in the basin has a predictable trend moderated by the widely practiced bush burning during the dry season, which destroys most of the undergrowth that dominates the basin vegetal cover. The interception-reduced rainfall intensity $R(t)_{ri}$ could then be defined as:

$$R(t)_{ri} = R(t) \times c \tag{4.28}$$

4.4.2 Infiltration

The representations of temporal and spatial dynamics of the infiltration process during an event need to match observation in field studies. Infiltration components can be incorporated by the use of empirical model including the Green-Ampt equation, Philip two-term equations, Smith-Parlange, etc. Another approach is the Richards equation for unsaturated flow in the sub-surface, in one or two dimensions. Both methods have been applied in different studies (Wainright and Parson, 2002; Fiedler and Ramirez, 2000; Esteves et al., 2000; Singh and Bhallamudi, 1997).

The study by Fiedler and Ramirez (2000) and Esteves et al. (2000) outline the importance of incorporating an infiltration model, if the simulation results are to be used for explaining practical field observation. The use of a spatially and temporally dynamic infiltration model creates a scenario of interactive infiltration. Based on the outlined significance, the infiltration and movement of water through the soil as described by the Philip-Two-Term (PTT) infiltration equation (Philip, 1957) was adopted for the developed model. This is given as:

$$I(t) = St^{-1/2} + C \tag{4.29}$$

where $I(t)$ is the instantaneous infiltration rate [m/s] as a function of time, t [s]; S is sorptivity [m/s^{½}], and C is the effective hydraulic conductivity [m/s]. The physical properties of the soil influences the van Genuchten parameters used for the estimation of effective hydraulic conductivity from field data. The choice of the PTT is influenced by several factors including: adequate representation of the infiltration process in most tropical soils, the ease and simplicity of estimation of its model parameters from short-time field measurements. In this study, infiltration curves were obtained for most of the nodes within the plots and the catchment from field measurements with the Decagon

0.5cm mini-disc infiltrometers (Zhang, 1997). Spatial interpolation technique (Kringing) was used to estimate values at grid point that were not measured using the interpolation procedure in 'Surfer' software (Golden software, Inc. 2000). With the interpolation, the PTT hydraulic parameters at all the computational grid points were obtained.

Infiltration values according to the PTT are time dependent; its computation begins with the onset of rain and interactively changes with rainfall duration. This interactive behavior of the infiltration rate and rainfall intensity results in the three possible scenarios of rainfall-runoff response. In the first few seconds or minutes since the onset of a rainfall event, all the rain water tends to infiltrate depending on rainfall intensity and hydraulic conductivity of the soil. At this time, actual infiltration is equivalent to the amount of rainfall. When the infiltration capacity of the soil is attained or when the rainfall intensity becomes greater than the infiltration rate, point runoff begins to forms. In computing the time interval for this to occur, the Time Compression Approximation (TCA) approach is used (Revees and Miller 1975). The TCA method assumes that the infiltration capacity is a function of the cumulative infiltration, since the onset of a typical rainfall event. TCA eliminates variations in rainfall by theoretically condensing time. All other re-distributional processes of infiltrating water are ignored. This assumption has been shown to be properly suited for West African storm patterns (van de Giesen et al., 2000). The TCA has been shown to be very reliable in its estimations (Parlange et al., 2000; Gómez et al., 2001). From this phase and subsequently, most rainfall are converted to surface runoff. Infiltration values in a field can vary spatially depending on the value of the hydraulic conductivity defined at the grids. The lateral inflow equation for the developed solution can be given as:

$$q_l(x,y,t) = \left[R(t)_{ri}\right] - \left[St^{-\frac{1}{2}} + C(x,y)\right] \tag{4.30}$$

The developed flow equations for used in this study after all the substitution could be summarily given as:

$$\frac{\partial h}{\partial t} + \frac{\partial q_x}{\partial x} + \frac{\partial q_y}{\partial y} + St^{-\frac{1}{2}} + C(x,y) - R(t)_{ri} = 0, \tag{4.31}$$

$$\frac{\partial q_x}{\partial t}+\frac{\partial}{\partial x}\left(\frac{q_x^2}{h}+\frac{gh^2}{2}\right)+\frac{\partial}{\partial y}\left(\frac{q_x q_y}{h}\right)+\frac{K_0 u q_x}{8h^2}+R\frac{q_x}{h}-gh\frac{\partial h_{mt}}{\partial x}=0 \quad (4.32)$$

$$\frac{\partial q_y}{\partial t}+\frac{\partial}{\partial y}\left(\frac{q_y^2}{h}+\frac{gh^2}{2}\right)+\frac{\partial}{\partial x}\left(\frac{q_x q_y}{h}\right)+\frac{K_0 u q_y}{8h^2}+R\frac{q_y}{h}-gh\frac{\partial h_{mt}}{\partial y}=0 \quad (4.33)$$

4.5 Numerical methods for solution of surface runoff equation

Numerical schemes are still the most valid method of solving the surface runoff equation, since no analytical solution exists for this system of partial differential equations (Dibike, 2002). The schemes are, however, much easier to apply in deep-water flows such as occur in lakes and estuaries, where the shock and discontinuities often encountered in shallow water equations are not present. The observed shock and discontinuities are difficult to accommodate in numerical schemes. Shocks capable of truncating the numerical process can result from any of the following processes and they represent a major challenge in the process:

(1) At the onset of rainfall, i.e., before ponding occurs in the runoff process, the depth of overland flow is zero, since all raindrops infiltrate into the soil. This implies that the flow depth (h) will be equal to zero (dry bed). This condition cannot be accommodated by any known numerical scheme, for solving the hydrodynamic equation, because depth is a denominator in several terms.

(2) In field condition, surfaces are ponded differentially and ponding is not instantaneous and often not uniform. It varies spatially depending on the spatially varied initial moisture condition, hydraulic properties and rainfall properties. These conditions lead to discontinuity in the flow regime and consequently introduce large gradients in the dependent variables, and thus, affecting the stability of the numerical solution.

(3) At the onset of ponding, and even for several flow situations observed in the surface runoff process, the depth of overland flow is very shallow (sometimes in the millimeter and at the most in the centimeters range). This is because overland flows develop and move towards the discharge outlet, thus the build-up is gradual, except during very intense storms, which often result in flood problems. This shallow depth demands a small magnitude of computational oscillation, which will lead to truncation of the solution as negatives depth is computed (negative depth is impossible in field conditions). The computational instability and collapse is due to the oscillatory nature of

the hydrodynamic equation (Zoppou and Roberts, 2003). Even in flood situations, depth change is unstable and such sudden changes will lead to instability of the solution.

(4) The effect of ground surface roughness and microtopographical forms that characterize most runoff plots, cultivated fields, tilled surfaces, rill channel and other overland flow surfaces. This surface roughness and the corresponding local slope gradients significantly regulate overland flow depth and vertical amplitude, particularly in regions of rapidly varying surfaces. This triggers oscillation in the numerical solution; consequently the solution becomes unstable.

In view of the above problems associated with the solution of the hydrodynamic equation, most numerical schemes commonly used in the solution of the shallow water equation or its overland flow form (surface runoff equation) may not adequately handle the problem at hand. It was then expedient to critically assess most of these schemes and modify the selected scheme to achieve the goal of this study.

4.6 Selection of method

The first step in obtaining the solution of the hydrodynamic equation is the re-presentation of the partial differential equation in a Cartesian matrix form as:

$$\frac{\partial H}{\partial t}+\frac{\partial U}{\partial x}+\frac{\partial V}{\partial y}+E=0 \tag{4.34}$$

where *H*, *U*, *V* and *E* are the cartesian components of the flux vectors. The vectors *H*, *U*, *V* and *E* are then presented in the matrix formulation of the unit discharge q_x, q_y and flow depth *h* as

$$H=\begin{bmatrix} h \\ q_x \\ q_y \end{bmatrix},\ U=\begin{bmatrix} q_x \\ \frac{q_x^2}{h}+\frac{gh^2}{2} \\ \frac{q_x q_y}{h} \end{bmatrix},\ V=\begin{bmatrix} q_y \\ \frac{q_y^2}{h}+\frac{gh^2}{2} \\ \frac{q_x q_y}{h} \end{bmatrix},\ E=\begin{bmatrix} R(t)_{ri}-I(t) \\ \left(\frac{K_0 u q_x}{8h^2}+R\frac{q_x}{h}\right)-gh\frac{\partial h_{mt}}{\partial x} \\ \left(\frac{K_0 u q_y}{8h^2}+R\frac{q_y}{h}\right)-gh\frac{\partial h_{mt}}{\partial y} \end{bmatrix} \tag{4.35}$$

Four major methods are applied to obtain the solution to the matrices that result from this transformation. These are (1) method of characteristics; (2) finite element method (FEM); (3) finite difference method (FDM); and (4) finite volume method (FVM).

The method of characteristics (MOC) is an analysis-based method, which involves the transformation of the partial differential equations (PDE) to ordinary differential equations (ODE) along the characteristics. These transformed ODE are then solved numerically using explicit or implicit schemes. The application of this method is limited to general overland flow cases, since spatial variability, slope, surface roughness, and infiltration pattern cannot be adequately characterized. MOC can be used to define the appropriate boundary conditions for use in numerical methods and to account for the stability conditions. Katapode and Strelkoff (1979) used the method of characteristics to solve the two-dimensional flow resulting from a dam break.

Most practical applications of the hydrodynamic equation especially (from the two-dimension) do not have analytical solutions, therefore, analysis-based methods, like the MOCs, cannot be applied. Consequently, the governing equations, which are in continuous forms, are transformed into discrete forms, which then result in series of algebraic equations that can be solved with the computer. The solution of these discrete algebraic equations represents an approximation of the continuous problem, and several methods have been developed to find the most appropriate discrete representation of the actual continuous equation. Such numerical techniques are the basis of other methods described in the following paragraphs.

The Finite Element Method (FEM) involves the discretization of the system into a series of sub-domains (triangular or quadrilaterals), called finite elements, connected at a discrete number of nodal points. Thereafter, each of the dependent variables (e.g., h, v and u) is approximated in terms of the unknown values and the known shape function at the nodal points. Subsequently, an appropriate measure of error from the set of simultaneous equations at each nodal point is minimized and the resulting set of equations is solved for the unknowns at the nodal points. The Galerkin form of the FEM has been used in some studies on the runoff process. Taylor et al. (1974) used this form to solve the two-dimensional shallow water equations for modeling watershed runoff. He reported the occurrence of shocks at points where there are sudden changes in the bed slope. This could be attributed to the method of solution

in which the entire flow domain was represented and solved as a set of matrix equations. Al-Mashidani and Taylor (1974) also used this form of FEM to solve the one-dimensional form of the shallow water wave equation for surface runoff. Kawahara and Yokoyama (1980) used a regular triangular grid discretization of the FEM method to solve the two-dimensional model of overland flow. Akanbi and Katapodes (1988) used a Petro-Galerkin form of FEM to model two-dimensional overland flow on a deforming moving-grid system. The coordinates of these moving grids were transformed in simulating the flooding of an impervious square plain from one of its corners. This method produced a very good output when compared to the field data from the border irrigation system used for the validation. Improvements were made on the FEM method to accommodate sudden changes in bed slope resulting from changes in surface slope and soil surface roughness, so that the problem of shock in the solution is removed (Vieux et al., 1990).

Julien and Moglen (1990) used the FEM method to solve a one-dimensional hydrodynamic equation for investigating overland flow generated under spatially varied surface slope, width roughness, and excess rainfall intensity. Ogden and Julien (1993) also applied the method to study surface runoff sensitivity to spatial and temporal variability of rainfall. Both studies attest to the usefulness of the method in numerical investigations. Other possibilities with the FEM methods include the integration with digital elevation models of catchments to delineate watersheds and consequently route the surface runoff paths (Goodrich et al., 1991). The FEM method is often credited with flexibility and a wide range application, and its consistency in the numeric solutions. A common limitation of the method is that every improvement in the predictive ability implies a corresponding increase in number of nodal points to be handled, which consequently increases number of points for solution. This always results in increased time for efficient computations, particularly when the variable surface properties and time-varying rainfall intended in this study are used.

The most frequently used method of solution of the hydrodynamic equation is the finite difference method (FDM). There are three basic steps in the application of this method to differential equations (Singh, 1996). In the first step, the continuous solution domain is discretized and replaced by a grid point called the finite-difference mesh. Secondly, the continuous derivatives of the differential equation are replaced by finite

differences on the grid points, thus the solution equations, their variables and coefficients are established at all grid points (nodes). In the final step, for each node, all the equations are solved using the values of the dependent variable given by the initial and boundary conditions. This set of solutions is used as initial and boundary conditions when the solution at the next time step is desired.

Finite difference methods can be solved implicitly or explicitly, depending on the number of points at which the solutions are obtained in a time step. In implicit schemes, the sets of difference equations for a complete row of points are solved simultaneously in a time step, while in the explicit scheme, the difference equations are solved point by point from one time level to the next. Both schemes have been applied in numerical solutions of the hydrodynamic equations and have been shown to have comparative advantages and limitations. Implicit schemes are best applied when the computer resource is large and a time accurate solution is not so important in the process under study. The number of points for iterations in each time step necessitates an increase in time step (lag), for stability purposes. Such increase in time step could cloud some important processes, particularly in problems that require high time resolution to appreciate like the one under study in which high-resolution rainfall intensity data is used. Implicit schemes are unconditionally stable and the accuracy depends on the grid ratio of distance (Δx) to time lag (Δt). On the other hand, explicit schemes could accommodate smaller time step, such that the processes could be understood at very fine time resolutions. These schemes are always preferred when time accuracy is desired. Explicit schemes (particularly from the second-order schemes) are generally noted for efficiency in handling shocks and discontinuity. Such discontinuities originate from sudden changes in depth of flow, which characterize most tropical runoff processes especially where spatial variability of soil physical and hydrological properties can be observed even in centimeter ranges, and high rainfall intensity leads to a abrupt increase in the depth of overland flow.

The finite volume method (FVM) involves the discretization of the continuous equation into number of finite volumes. In each of these finite volumes, the integral equations are applied to obtain the exact conservation within each cell. It is particularly useful in hydrodynamic models, since most of the equation is solved based on the principle of conservation of momentum. By the discretization of the integral form of the

conservation equation, the mass and momentum remain conserved. The resulting expression in the FVM solution appears similar to finite difference approximation depending on the techniques applied. As such, it is often considered as a finite difference method applied to the differential conservative form of the conservation law in arbitrary coordinates. The method can be applied also using an unstructured grid system as FEM, but will generally require less computational effort than FEM. The key problem in FVM is the estimation of the normal flux through each cell interface. Valiani et al. (2002) developed a FVM that was tested in predicting dam break problems in the Malpasset dam in Italy. The FVM was also used by Bellos et al. (1991) in computation of two-dimensional dam break induced flow and was found to perform very well with respect to prediction. The FVM was also applied to capture hydraulic shock commonly encountered in river modeling; the developed scheme worked well in its ability to represent shock without a collapse of the solution (Zhao et al., 1996). A major limitation of the FVM is the inability to handle flow over rough surfaces (Valiani et al. 2002), thus limiting its application in this study.

In selecting a numerical scheme that could handle the overland flow under varying surface and hydraulic conditions similar to the one under consideration in this study, Fiedler (1997) extensively reviewed and in some cases tested the performance of several higher order schemes i.e., third- and fourth-order schemes. He concluded that most of the higher order schemes could not correct the dispersive errors and numerical oscillations observed in lower-order schemes. There was, therefore, no incentive to select them for solution. He also examined a new generation of high-resolution FDM, but noted that the scope of development of the model could still not match the requirement in overland flow situations. A form of the high-resolution scheme, the total variation diminishing (TVD), was used by Valiani et al. (2003) in predicting flood events in the Toce river in Italy; and their findings confirm the conclusion of Fiedler (1997) concerning the scope of application and the suitability of the scheme for overland flow situations. Consequently, the search for the solution in this study was limited to the second-order finite difference scheme.

Recent studies on the solution of the full hydrodynamic equation in surface runoff and overland flow processes with the second-order finite difference scheme have basically used the MacCormack scheme (Zhang and Cundy, 1989; Esteves et al, 2000;

Fiedler and Ramirez, 2000), because of its simplicity and robustness. It is also second-order accurate in space and time. It was observed during the review of the various studies that the original form of the MacCormack scheme could not handle flow on rough terrain. It requires some modification to accommodate this physical reality. A variant is the application of the Leapfrog scheme by Playan et al. (1994, 1999). They applied the Leapfrog scheme to the simulation of overland flow in basin irrigation schemes on both simple and complex terrains. This scheme was shown to be numerically stable in solution, but was criticized for being inflexible with respect to stability at odd grid points and the requirements of artificial viscosity terms due limited dissipative properties. To correct the problem of stability at odd grid points, a Leapfrog scheme with centered time and space derivatives was used for this study; the scheme is described below. A major incentive for the use of the scheme is its ability to accurately handle very complex terrain and the ease of extension of the simulation area under study without loss of prediction accuracy. The computational process ensures the efficiency of computer resources, since the solutions are in staggered form.

4.7 Leapfrog scheme

The Leapfrog scheme is a second-order method for solving differential equations. It is a three-time-level scheme that is second-order accurate in both space and time as depicted graphically in Figure 4.1b. It present an attractive alternative for solution of numerical problem in several fields of study, including meteorology, engineering physics, astronautics, environment and economics etc, where systematic observations are normally made.

The Leapfrog scheme has been successfully applied for computational purposes in hydrology and its efficiency has been evaluated in comparison with other schemes (Foreman, 1984; Akanbi, 1986; Playan, 1994). A major advantage of the scheme is the staggered approach to the solution of equations (figure 4.2). Staggering of the numerical solution, ensures that the numerical fluxes are not calculated the grid cell interfaces, where jump and discontinuities occur, but rather at the gridcell centers (figure 4.1a), where the variable varies smoothly (Erbes, 1994). When applied to the surface runoff equation, the estimation of flow depth and discharges are staggered in time by a half-time step, enhancing the stability of the scheme. A detailed description of

the Leapfrog scheme as applied to shallow water equations in a basin irrigation scheme is found in Playan (1992). However, there is no documented record of the application of the scheme to surface runoff or overland flow modeling despite the itemized advantages.

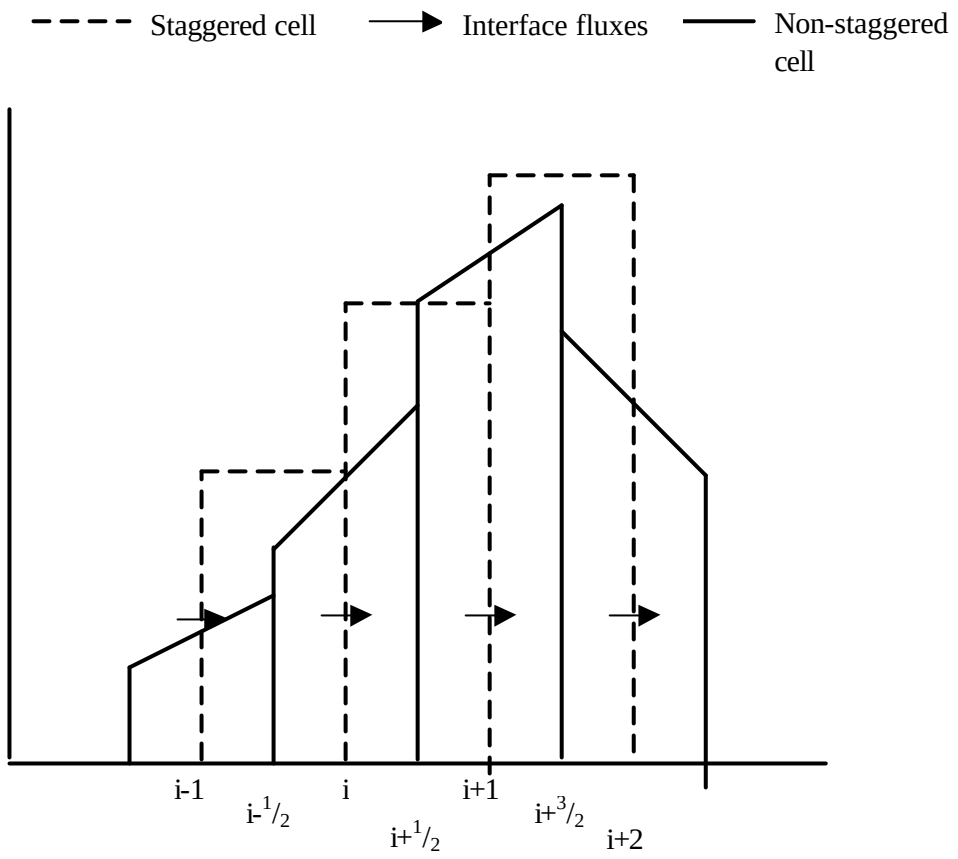

Figure 4.1a: Gridcell structure for staggered and non-staggered method using piecewise linear reconstructions.

Adapted from Erbes, 1994

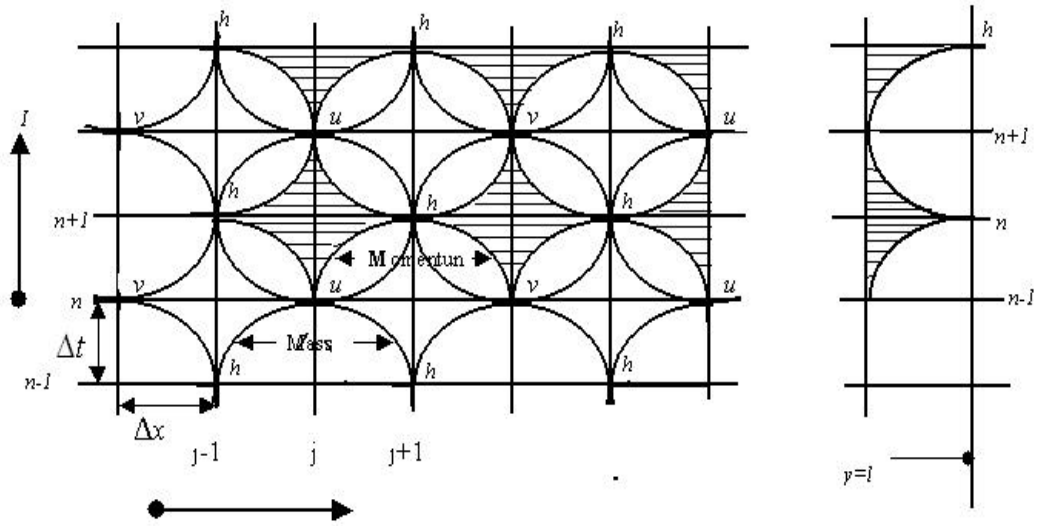

Figure 4.1b: Schematization of a staggered grid (leapfrog method).

4.8 Adaptation of Leapfrog scheme

The general form of solution in the Leapfrog scheme is centered in time, but not in space. Haltiner and William (1980) have, however, shown that centered differencing in space is more accurate than forward or backward differencing, and it is used for the derivative in equations 4.28 – 4.30. Using the leapfrog centered time and space-differencing scheme; the derived surface runoff equation in finite form could be stated as:

$$\frac{h_{i,j}^{n+1} - h_{i,j}^{n-1}}{2\Delta t} + \frac{q_{x_{i+1,j}}^{n} - q_{x_{i-1,j}}^{n}}{2\Delta x} + \frac{q_{y_{i,j+1}}^{n} - q_{y_{i,j-1}}^{n}}{2\Delta y} - q_{l_{i,j}}^{n} = 0 \tag{4.36}$$

$$\frac{q_{x_{i,j}}^{n+1} - q_{x_{i,j}}^{n-1}}{2\Delta t} + \frac{1}{h_0}\frac{q_{x_{i+1,j}}^{n} - q_{x_{i-1,j}}^{n}}{2\Delta x} + g\frac{h_{i+1,j}^{n} - h_{i-1,j}^{n}}{4\Delta x} + \frac{1}{h_{0_{i,j}}}\frac{q_{x_{i+1,j}}^{n} - q_{x_{i-1,j}}^{n}}{2\Delta x}\frac{q_{y_{i,j+1}}^{n} - q_{y_{i,j-1}}^{n}}{2\Delta y} = gh_{0_{i,j}}(S_{0_{i,j}}^{n} - S_{f_{i,j}}^{n}) \tag{4.37}$$

$$\frac{q_{y_{i,j}}^{n+1} - q_{y_{i,j}}^{n-1}}{2\Delta t} + \frac{1}{h_0}\frac{q_{y_{i,j+1}}^{n} - q_{y_{i,j-1}}^{n}}{2\Delta y}$$
$$+ g\frac{h_{i,j+1}^{n} - h_{i,j-1}^{n}}{4\Delta y} + \frac{1}{h_{0_{i,j}}}\frac{q_{x_{i+1,j}}^{n} - q_{x_{i-1,j}}^{n}}{2\Delta x}\frac{q_{y_{i,j+1}}^{n} - q_{y_{i,j-1}}^{n}}{2\Delta y} = gh_{0_{i,j}}(S_{0_{i,j}}^{n} - S_{f_{i,j}}^{n}) \quad (4.38)$$

where i and j are the spatial indices and n is the time indices. The scheme is neutral and is conditionally stable for problems involving non-linear advection terms, but may be unstable for dissipative terms, because a short wave component of the solution emerges. In this case, the profiles of the solution become uncontrollable (Cunge et al., 1980), implying that two solutions will exist for the problem, whereas the differential equation that is supposed to be approximated has one solution only. The false solution is simply an artifact of the numerical scheme and has no bearing with reality.

Various methods have been proposed to handle this undesired condition. An artificial viscous dissipation term may be introduced in the relationships. This damped the numerical noise by ensuring smooth results in **space** (i.e. consecutive grid point), while still maintaining the stability of the scheme. Another way of solving this problem is to carry out grid refinement, in which the grid spacing and combination are carefully selected. This often leads to increase in computational effort.

In this study, the second order turbulent viscosity used to account for turbulent momentum transfer (Reynolds Stresses) in shallow water equation was applied (Erbes, 1994; Fieldler and Ramirez, 2000). This method involves the introduction of two terms in second partial derivatives, which are added to the three equations developed for surface runoff (4.31 – 4.33), thus we have:

$$k_{diff}\left(\frac{\partial^2 h_x}{\partial x^2} + \frac{\partial^2 h_y}{\partial y^2}\right) = \frac{\partial}{\partial x^2}k_{diff}\left[h_{i+1,j} - 2h_{ij} + h_{i-1,j}\right]$$
$$+ \frac{\partial}{\partial y^2}k_{diff}\left[h_{i,j+1} - 2h_{i,j} + h_{i,j-1}\right] \quad (4.39)$$

$$k_{diff}\left(\frac{\partial^2 q_x}{\partial x^2} + \frac{\partial^2 q_y}{\partial y^2}\right) = \frac{\partial}{\partial x^2}k_{diff}\left[q_{x_{i+1,j}} - 2q_{x_{i,j}} + q_{x_{i-1,j}}\right]$$
$$+ \frac{\partial}{\partial y^2}k_{diff}\left[q_{x_{i,j+1}} - 2q_{x_{i,j}} + q_{x_{i,j-1}}\right] \quad (4.40)$$

and

$$k_{diff}\left(\frac{\partial^2 q_x}{\partial x^2}+\frac{\partial^2 q_y}{\partial y^2}\right)=\frac{\partial}{\partial x^2}k_{diff}\left[q_{y_{i+1,j}}-2q_{y_{i,j}}+q_{y_{i-1,j}}\right]$$
$$+\frac{\partial}{\partial y^2}k_{diff}\left[q_{y_{i,j+1}}-2q_{y_{i,j}}+q_{y_{i,j-1}}\right] \quad (4.41)$$

for the three equations respectively. h = height difference along x-axis over a staggered grid; $h_{i,j+1}-h_{i,j-1}$ = height difference along y-axis over a staggered grid; $q_{x_{i+1,j}}-q_{x_{i-1,j}}$ = difference in q_x along x-axis over a staggered grid; $q_{x_{i,j+1}}-q_{x_{i,j-1}}$ = difference in q_x along y-axis in a single staggered grid; $q_{y_{i+1,j}}-q_{y_{i-1,j}}$ = difference in q_y along x - axis over a staggered grid; $q_{y_{i,j+1}}-q_{y_{i,j-1}}$ = difference in q_y along y-axis over a staggered grid; $q_{x_{i,j}}$; $q_{y_{i,j}}$; and $h_{i,j}$ are the middle grids values of q_x, q_y, and h, while k_{diff} is the coefficient of diffusion. The value of this coefficient depends on the type of problem being handled and must be adjusted until the stability of the solution is achieved. Values of the diffusion factor tried with this model range between 0.5 and 5, but the $k_{diff\,c} = 1$ is used in all computation processes in the numerical tests reported in this thesis, since it effectively smears these discontinuities. The introduction of this coefficient did not in any way affect the accuracy of the scheme.

4.9 Computational process

Numerical computational process in the Leapfrog scheme follows a staggered implementation process, in which computation proceeds in half-time intervals (Figure 4.3). At the start of the computation process, the fluxes of the discharge momentum, and that of the height at the nodes *(i.e. i = 1, npx and j = 1,npy)* in the x and y direction are estimated from the equations (4.31 - 4.33). The fluxes for the friction slope in the two directions are also calculated from equation (4.25 - 4.27).

At the whole-time steps, the continuity equation is solved to evaluate flow depth at necessary nodes. The equation is discretized as:

$$\frac{h^{t+\Delta t}-h^t}{2\Delta t}+\frac{\partial q_x}{2\Delta x}+\frac{\partial q_y}{2\Delta y}+q_l=0 \quad (4.42)$$

where the spatial partial derivatives of the fluxes and the net lateral inflow are evaluated at the time $t+Dt/2$ and the discretized equation allows for the solution of h^{t+Dt} explicitly as:

$$h^{t+\Delta t} = h^t - \left(\frac{\partial q_x}{2\Delta x} + \frac{\partial q_y}{2\Delta y} + q_l \right) \Delta t \tag{4.43}$$

The centered-in-time formulation is implemented in the numerical scheme as:

$$\begin{aligned} h_{i,j}^{n+1} = h_{i,j}^{n-1} &- \frac{\Delta t}{\Delta x}\left[Qx_{i+1,j}^{n} - Qx_{i-1,j}^{n} \right] - \frac{\Delta t}{\Delta y}\left[Qy_{i,j+1}^{n} - Qy_{i,j-1}^{n} \right] \\ &+ \frac{2\Delta t}{\Delta x^2} k_{diff} \left[h_{i+1,j}^{n-1} - 2h_{i,j}^{n-1} + h_{i-1,j}^{n-1} \right] \\ &+ \frac{2\Delta t}{\Delta y^2} k_{diff} \left[h_{i,j+1}^{n-1} - 2h_{i,j}^{n-1} + h_{i,j-1}^{n-1} \right] + (h_{rate})_{i,j}^{n-1} \end{aligned} \tag{4.44}$$

where h_{rate} is:

$$h_{rate_{i,j}} = R(t)_{ri} - I(t)_{i,j} \tag{4.45}$$

Infiltration rate is averaged over the discretized time, and the maximum h_{rate} is used.

To obtain the transient value for the flux q_x and q_y in both x - and y - directions at the nodal points i = *2* to *npx-1*, on the x - axis, and *j = 2, to npy - 1* on the y - axis. The finite differencing process, i.e., centered – in - time step, is discretized in the scheme as:

$$\begin{aligned} q_{x_{i,j}}^{n+1} = q_{x_{i,j}}^{n-1} &- \frac{\Delta t}{\Delta x}\left[F_{xx_{i+1,j}}^{n} - F_{xx_{i-1,j}}^{n} \right] - \frac{\Delta t}{\Delta y}\left[F_{xy_{i,j+1}}^{n} - F_{xy_{i,j-1}}^{n} \right] \\ &- \frac{\Delta t}{\Delta x} g h_{i,j}^{n} \left[(h_{mt})_{i+1,j}^{n} - (h_{mt})_{i-1,j}^{n} \right] - 2\Delta t (F_{rsu})_{i,j}^{n} \\ &+ \frac{2\Delta t}{\Delta x^2} k_{diff} \left[q_{x_{i+1,j}}^{n-1} - 2q_{x_{i,j}}^{n-1} + q_{x_{i-1,j}}^{n-1} \right] \\ &+ \frac{2\Delta t}{\Delta y^2} k_{diff} \left[q_{x_{i,j+1}}^{n-1} - 2q_{x_{i,j}}^{n-1} + q_{x_{i,j-1}}^{n-1} \right] \end{aligned} \tag{4.46}$$

$$q_{y_{i,j}}^{n+1} = q_{y_{i,j}}^{n-1} - \frac{\Delta t}{\Delta x}\left[G_{xy_{i+1,j}}^{n} - G_{xy_{i-1,j}}^{n}\right] - \frac{\Delta t}{\Delta y}\left[G_{yy_{i,j+1}}^{n} - G_{yy_{i,j-1}}^{n}\right]$$
$$- \frac{\Delta t}{\Delta y} g h_{i,j}^{n}\left[(h_{mt})_{i,j+1}^{n} - (h_{mt})_{i,j-1}^{n}\right] - 2\Delta t (F_{rsv})_{i,j}^{n}$$
$$+ \frac{2\Delta t}{\Delta x^2} k_{diff}\left[q_{y_{i+1,j}}^{n-1} - 2q_{y_{i,j}}^{n-1} + q_{x_{i-1,j}}^{n-1}\right]$$
$$+ \frac{2\Delta t}{\Delta y^2} k_{diff}\left[q_{y_{i,j+1}}^{n-1} - 2q_{y_{i,j}}^{n-1} + q_{y_{i,j-1}}^{n-1}\right] \qquad (4.47)$$

where

$\Delta x = x_{i+1} - x_i$; $\Delta y = y_{j+1} - y_j$

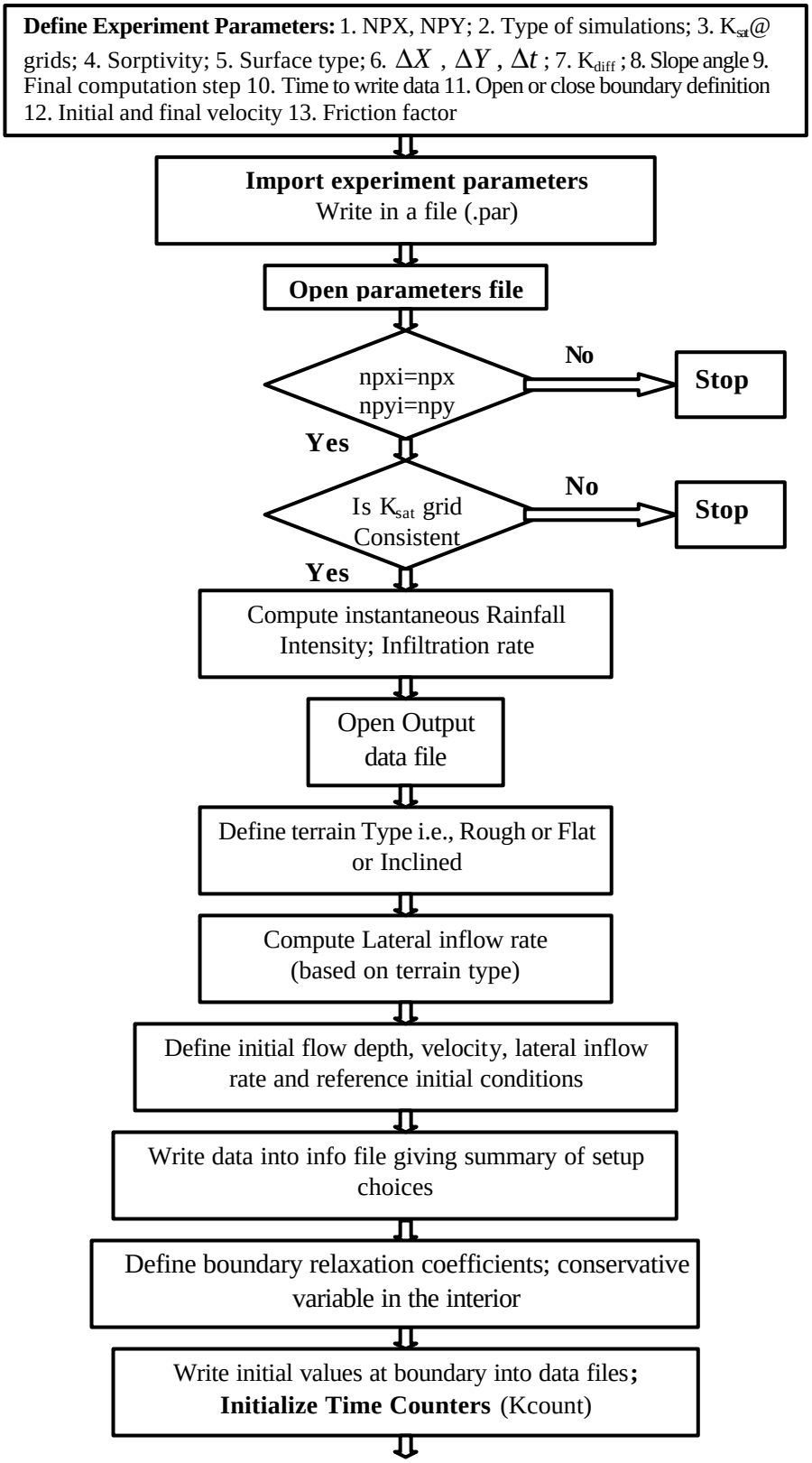
Define Experiment Parameters: 1. NPX, NPY; 2. Type of simulations; 3. K_{sat}@ grids; 4. Sorptivity; 5. Surface type; 6. ΔX , ΔY , Δt ; 7. K_{diff} ; 8. Slope angle 9. Final computation step 10. Time to write data 11. Open or close boundary definition 12. Initial and final velocity 13. Friction factor
Import experiment parameters
Write in a file (.par)
Open parameters file
npxi=npx
npyi=npy
No
Stop
Yes
Is K_{sat} grid Consistent
No
Stop
Yes
Compute instantaneous Rainfall Intensity; Infiltration rate
Open Output data file
Define terrain Type i.e., Rough or Flat or Inclined
Compute Lateral inflow rate (based on terrain type)
Define initial flow depth, velocity, lateral inflow rate and reference initial conditions
Write data into info file giving summary of setup choices
Define boundary relaxation coefficients; conservative variable in the interior
Write initial values at boundary into data files;
Initialize Time Counters (Kcount)

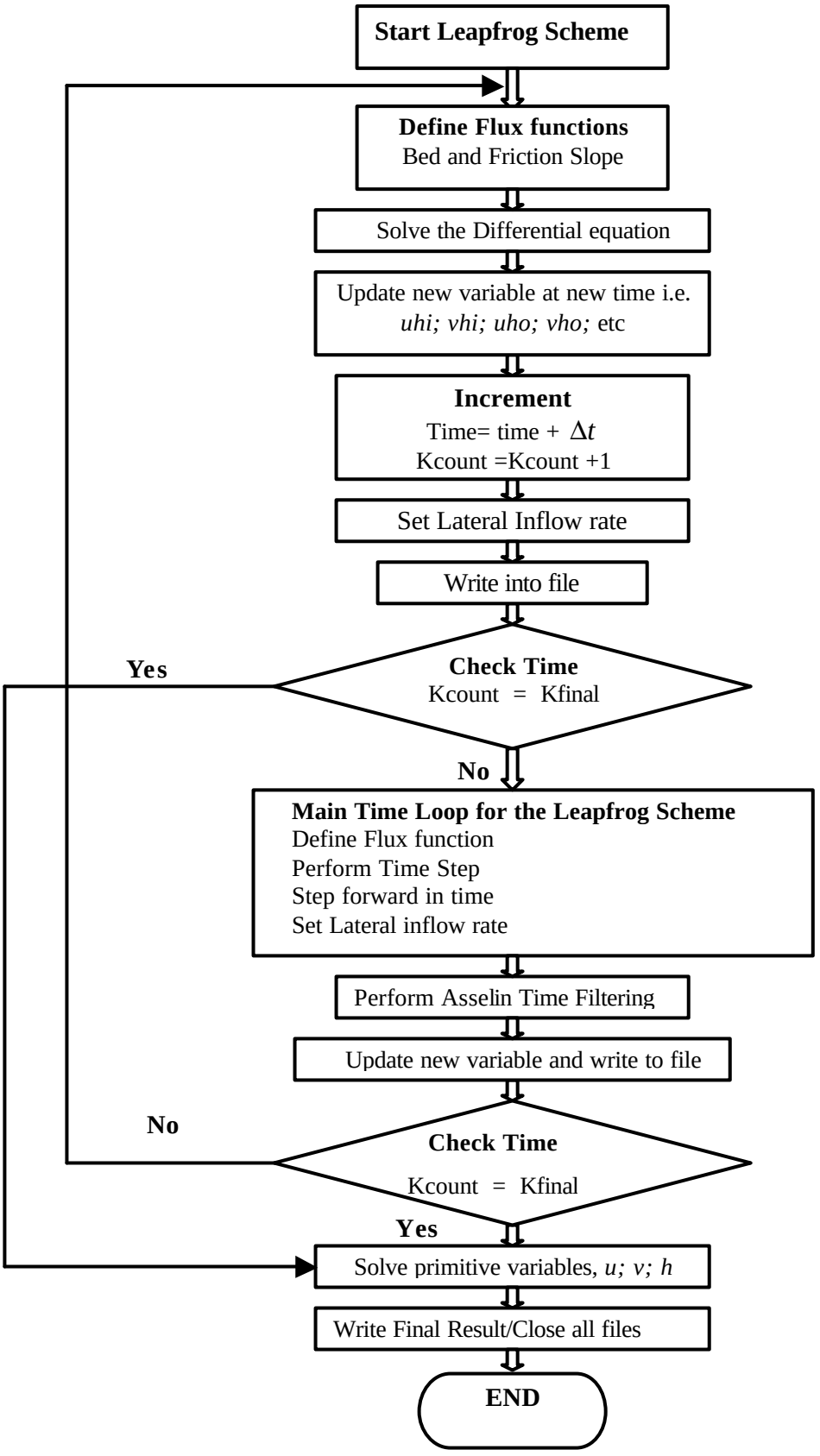

Figure 4.2 Flow chart of the sequence of computations in the developed model

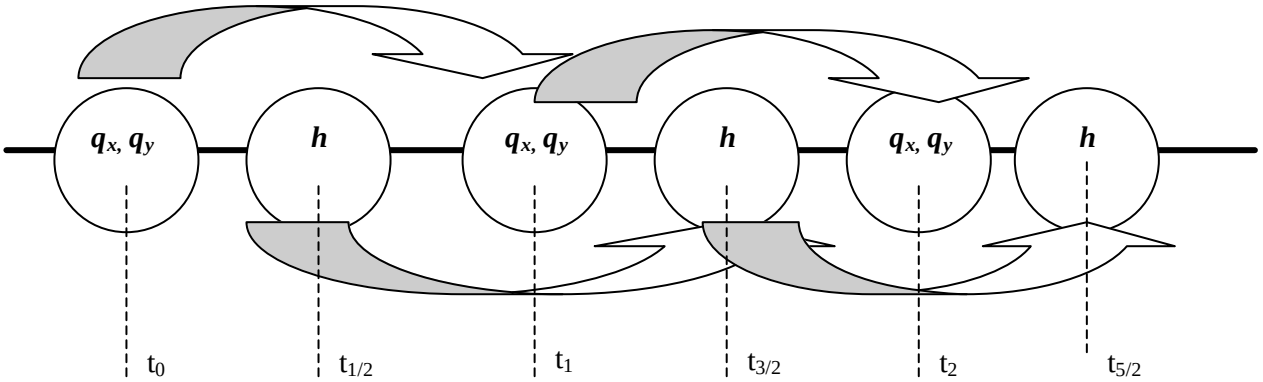

Figure 4.3 A grid with three dependent variables that are computed at alternate grid points.

It should be noted in each stage of the leapfrog scheme, both space and time differencing are implemented. The computation of the same variables at each node is separated by an entire time step.

4.10 Initial and boundary conditions

The numerical computational procedure in the developed model required the specification of appropriate initial and boundary conditions. For the purpose of stability in the solution, a practical situation of zero initial flow depth, which holds before the onset of a rainfall event till ponding, could not be applied. This necessitates the definition of an initial overland flow depth, which should be small and insignificant in the computational procedure. This technique has been applied in several numerical studies on the overland flow process (Chow and Ben-Zvi, 1967; Zhang and Cundy, 1989; Tayfur et al., 1993; Esteves et al., 2000 and Fiedler and Ramirez, 2000). In this study, a consistent value of initial depths was used so that the effect on the output will be uniform and could be corrected.

The model is a limited area model (LAM), implying that it can only describe or predict variables over the applied domain, not outside the domain. However, it also requires the variables from this outside domain (i.e., boundaries) to predict those in the

applied domain. A boundary relaxation coefficient and a boundary relaxation zone is defined appropriately. The boundary relaxation zone provide space to handle efficiently, the error that might have occurred due to reconstruction of the oscillatory behavior by the finite process. Consequently, in the experimental plot simulations, the closed boundaries on the three sides of the plots are set such that there is no flow through them. The fluxes of q_x and q_y perpendicular to these boundaries ($q_{xb}\ q_{yb}$) are set to zero. Depths at close boundaries (h_b) are defined using inward differences in both the continuity and momentum equations. For example, when the south boundary is opened, the following condition is applied from *i*=1, to *i*=*npx*

$$\begin{aligned} q_{xb} &= q_{x_{i,1}} = q_{x_{i,2}} \\ q_{yb} &= q_{y_{i,1}} = q_{y_{i,2}} \\ h_b &= h_{i,1} = h_{i,2} \end{aligned} \tag{4.47}$$

and when it is fixed or closed:

$$\begin{aligned} q_{xb} &= q_{x_{i,1}} = 0 \\ q_{yb} &= q_{y_{i,1}} = 0 \\ h_b &= h_{i,1} = h_{init_{i,1}} \end{aligned} \tag{4.48}$$

The values of all the fluxes at the boundary relaxation zones, in each time step is corrected with the boundary relaxation coefficient from the expression:

$$\left(q_x\right)_{i,j}^{n+1} = (1-g_{i,j})\left(q_x\right)_{i,j}^{n+1} + g_{i,j}\left(q_{xb}\right)_{i,j}^{n} \tag{4.49}$$

$$\left(q_y\right)_{i,j}^{n+1} = (1-g_{i,j})\left(q_y\right)_{i,j}^{n+1} + g_{i,j}\left(q_{yb}\right)_{i,j}^{n} \tag{4.50}$$

$$h_{i,j}^{n+1} = (1-g_{i,j})h_{i,j}^{n+1} + g_{i,j}(h_b)_{i,j}^{n+1} \tag{4.51}$$

where $g_{i,j}$ is the boundary relaxation coefficient. $0 \le g_{i,j} \le 1$, and it is given by

$$g_k \equiv 1 - \tanh\left\{\frac{2}{ndamp-4}(k-1)\right\}; \quad k \ge 1 \tag{4.52}$$

where *ndamp* is the width of the relaxation zone, k is the current gridpoint, and k-1 is the number of grid points to the nearest boundary from the current grid point.

4.11 Computational time optimization

The maximum allowable time step and horizontal resolution of the Leapfrog scheme as in all other finite difference schemes are constrained by the Courant-Friedrichs-Lewy (CFL) condition. The CFL condition provides a framework for the stability of the numerical scheme, and basically implies that the flow must not progress farther than the grid size during a time step. The CFL condition used for one-dimension flow is generally expressed as:

$$CN = \frac{c\Delta t}{\Delta x} \tag{4.53}$$

where c is the celerity (the phase speed) or an advection velocity of a small flow disturbance (cm/s), Δt is the time increment (s), and Δx is the grid spacing in the x-direction and $0 \le CN \le 1$.

For the two-dimension solution applied in this study, the maximum admissible time step is defined according to Bellos et al. (1988) as:

$$\Delta t = CN_{\min}\left(\frac{\Delta x}{u+c}, \frac{\Delta y}{v+c}\right) \tag{4.54}$$

where Dx and Dy are the grid spacing in both directions, u and v are the initial velocity at a point in time, in both directions, and CN_{min} indicates the minimum of the two possible values the CN number. However, the source terms introduces further restrictions on the admissible time step for simulation. This extent of restriction is dependent on the rainfall intensity, inclination angle, microtopography, and the defined artificial diffusion coefficient. Consequently rigorous stability analysis for the developed equation is difficult. Fiedler, (1997) also reports the same limitation in the application of MacCormack scheme, implying that the difficulty is not peculiar to the Leapfrog scheme.

4.12 Time filtering

To reduce the amplitude of the computational mode, ensure smooth results in time (i.e., consecutive time steps) and avoid a decoupling of the solutions at odd and even time steps (time splitting of the solution), an Asselin time-filter is applied at each time step (Asselin 1972) to the computed values. The variables (q_x, q_y,) being time stepped is operated on as follows

$$\left(\overline{q_x}\right)_{i,j}^{n} = \left(q_x\right)_{i,j}^{n} + a\left[\left(\overline{q_x}\right)_{i,j}^{n-1} - 2\left(q_x\right)_{i,j}^{n} + \left(q_x\right)_{i,j}^{n+1}\right] \tag{4.54}$$

$$\left(\overline{q_y}\right)_{i,j}^{n} = \left(q_y\right)_{i,j}^{n} + a\left[\left(\overline{q_y}\right)_{i,j}^{n-1} - 2\left(q_y\right)_{i,j}^{n} + \left(q_y\right)_{i,j}^{n+1}\right] \tag{4.55}$$

and

$$\left(\overline{h}\right)_{i,j}^{n} = \left(h\right)_{i,j}^{n} + a\left[\left(\overline{h}\right)_{i,j}^{n-1} - 2\left(h\right)_{i,j}^{n} + \left(h\right)_{i,j}^{n+1}\right] \tag{4.56}$$

where a is the time filtering coefficient. $\overline{q_x}$, $\overline{q_y}$ and $\overline{h}$ are the filtered variables, which is the model output.

At the first time step and after each time that an Asselin time filter has been applied, a forward in time step is performed as:

$$\begin{aligned} q_{x_{i,j}}^{n+1} = {} & q_{x_{i,j}}^{n} - \frac{\Delta t}{2\Delta x}\left[F_{xx_{i+1,j}}^{n} - F_{xx_{i-1,j}}^{n}\right] - \frac{\Delta t}{2\Delta y}\left[F_{xy_{i,j+1}}^{n} - F_{xy_{i,j-1}}^{n}\right] \\ & - \frac{\Delta t}{2\Delta x} g h_{i,j}^{n}\left[h_{mt_{i+1,j}}^{n} - h_{mt_{i-1,j}}^{n}\right] - \Delta t F_{rsu_{i,j}}^{n} \\ & + \frac{\Delta t}{\Delta x^2} k_{diff}\left[q_{x_{i+1,j}}^{n} - 2q_{x_{i,j}}^{n} + q_{x_{i-1,j}}^{n}\right] \\ & + \frac{\Delta t}{\Delta y^2} k_{diff}\left[q_{x_{i,j+1}}^{n} - 2q_{x_{i\,j}}^{n} + q_{x_{i,j-1}}^{n}\right] \end{aligned} \tag{4.57}$$

$$\begin{aligned} q_{y_{i,j}}^{n+1} = {} & q_{y_{i,j}}^{n} - \frac{\Delta t}{2\Delta x}\left[G_{xy_{i+1,j}}^{n} - G_{xy_{i-1,j}}^{n}\right] - \frac{\Delta t}{2\Delta y}\left[G_{yy_{i,j+1}}^{n} - G_{yy_{i,j-1}}^{n}\right] \\ & - \frac{\Delta t}{2\Delta y} g h_{i,j}^{n}\left[h_{mt_{i,j+1}}^{n} - h_{mt_{i,j-1}}^{n}\right] - \Delta t F_{rsv_{i,j}}^{n} \\ & + \frac{\Delta t}{\Delta x^2} k_{diff}\left[q_{y_{i+1,j}}^{n} - 2q_{y_{i,j}}^{n} + q_{x_{i-1,j}}^{n}\right] \\ & + \frac{\Delta t}{\Delta y^2} k_{diff}\left[q_{y_{i,j+1}}^{n} - 2q_{y_{i,j}}^{n} + q_{y_{i,j-1}}^{n}\right] \end{aligned} \tag{4.58}$$

$$h_{i,j}^{n+1} = h_{i,j}^{n} - \frac{\Delta t}{2\Delta x}\left[Qx_{i+1,j}^{n} - Qx_{i-1,j}^{n}\right] - \frac{\Delta t}{2\Delta y}\left[Qy_{i,j+1}^{n} - Qy_{i,j-1}^{n}\right]$$

$$+ \frac{\Delta t}{\Delta x^{2}} k_{diff}\left[h_{i+1,j}^{n} - 2h_{i,j}^{n} + h_{i-1,j}^{n}\right]$$

$$+ \frac{2\Delta t}{\Delta y^{2}} k_{diff}\left[h_{i,j+1}^{n} - 2h_{i,j}^{n} + h_{i,j-1}^{n}\right] + (h_{rate})_{i,j}^{n} \qquad (4.59)$$

The second-order finite-difference approximation for the numerical process for space and time derivatives is represented as in the following the expressions:

$$\frac{\partial^2 g^{n-1}}{\partial x^2} \approx \frac{q_{x_{i+1}}^{n-1} + q_{x_{i-1}}^{n-1} + 2q_{x_i}^{n-1}}{\Delta x \Delta x} \qquad (4.60)$$

$$\frac{\partial^2 g^{n-1}}{\partial y^2} \approx \frac{q_{y_{j+1}}^{n-1} + q_{y_{j-1}}^{n-1} + 2q_{y_j}^{n-1}}{\Delta y \Delta y} \qquad (4.61)$$

$$\frac{\partial^2 g^{n-1}}{\partial y^2} \approx \frac{h_{j+1}^{n-1} + h_{j-1}^{n-1} + h_j^{n-1}}{\Delta x \Delta y} \qquad (4.62)$$

where g^{n-1} is a generic variable describing the flow at each and every point in the domain of the solution at all times. Figure 4.2 shows the flow chart of the computational process in the developed solution applied in this study. Detailed descriptions of other differentiation processes are provided in the numerical code. The solution of the differential equations at the various boundaries is discussed in the section on boundary and initial condition.

4.13 End of simulation

The end of the simulation processes in this model is determined by the defined maximum time steps allowed and the computational time interval Δt. During simulation run with actual rainfall data, the maximum time step is determined by dividing the duration in seconds of the rainfall event by the time interval. During simulation with constant rainfall intensity, the end of the simulation is determined by the time defined in the initializing file.

4.14 Numerical test for the developed solution

No analytical solution exists for the full hydrodynamic equation. However, there are some analytical solutions for the approximate form of the equation, which could be used to verify the validity of the developed model. In testing the possibility of a mass balance problem in the solution, the model output was compared with analytical solution of the steady state kinematic wave solution for a plane of length 30.48m, with constant lateral inflow rate of 25.4 mm h^{-1} developed by Woolhiser et al, 1996, which was also applied by Fieldler et al. (2000) in validating the developed MacCormack scheme. The bed slope for the test was 0.05 and the Darcy-Weisbach friction factor is 0.265. Table 4.2 present the result and a mass balance problem would have resulted in marked discrepancies in computed discharge and flow depth.

Table 4.2 Comparison of output with the steady state kinematic wave test

	Analytical solution (Woolhiser et al., 1976)	**MacCormack Solution (Fieldler and Ramirez, 2000)**	**Leapfrog Solution (Ajayi 2004)**
Depth (cm)	0.1462	0.1471	0.1470
Discharge (cm^2s^{-1})	2.1505	2.1418	2.1420

Another example, which is generally accepted as a benchmark test problem for the hydrodynamic equation, is the dam-break problem (Fennema and Chaudhry, 1990; Jha et al, 1995; Fiedler and Ramirez, 2000; Zoppou and Roberts, 2003). The problem is based on a scenario in which a shock wave develops at the moment of failure of a dam wall measuring 1000 m with upstream water depth of the dam remaining constant at 10 m. The downstream water depth is 5m. This problem has a known analytical solution given by Stoker (1957) and Wu et al. (1999). In simulating the dam break problem in this model, the channel bed is assumed to be horizontal and frictionless. The time interval for computation Δt is =0.2s and the horizontal and vertical distance, Δx and Δy were kept at 25cm. The result compared very well with both the analytical solution and the solution of Fiedler and Ramirez (2000) produced with the MacCormack scheme (Figure 4.4). The dam break problem is a measure of the ability of any developed solution to adequately simulate the surface water component of the hydrodynamic

model and capture non-physical rarefaction or and expansion shock. The performance of the developed solution is quite interesting and shows the ability to handle such shock.

The study by Alcurdo and Garcia-Navarro (1994), which was also confirmed by study by Zoppou and Roberts (2003), noted that at a downstream water depth of 5 m, sub-critical flow still exists, which could easily cloud the problems in numerical schemes, by providing a buffer for shocks. They therefore suggested the use of a downstream water depth of 0.1 m, which they argue is a severe test case (transition between subcritical and supercritical flows). This has been successfully used to highlight problems with a number of numerical schemes that passed the first test. Zoppou and Robert (2003) applied this version of the dam break test in analyzing the performance of twenty explicit numerical schemes that solve the shallow water equation. In trying out the second test, the parameters used for the first test were adopted, but the downstream water depth level was reduced to 0.1 m. The developed solution successfully captured even the shock initiated by such level of supercritical flow, a condition in which a number of second-and higher-order schemes including MacCormack failed to handle. This clearly shows that the developed solution is a good shock-fitting numerical scheme, which is efficient, accurate and robust and would be suitable for solving the full hydrodynamic equations when discontinuities are encountered in the problem.

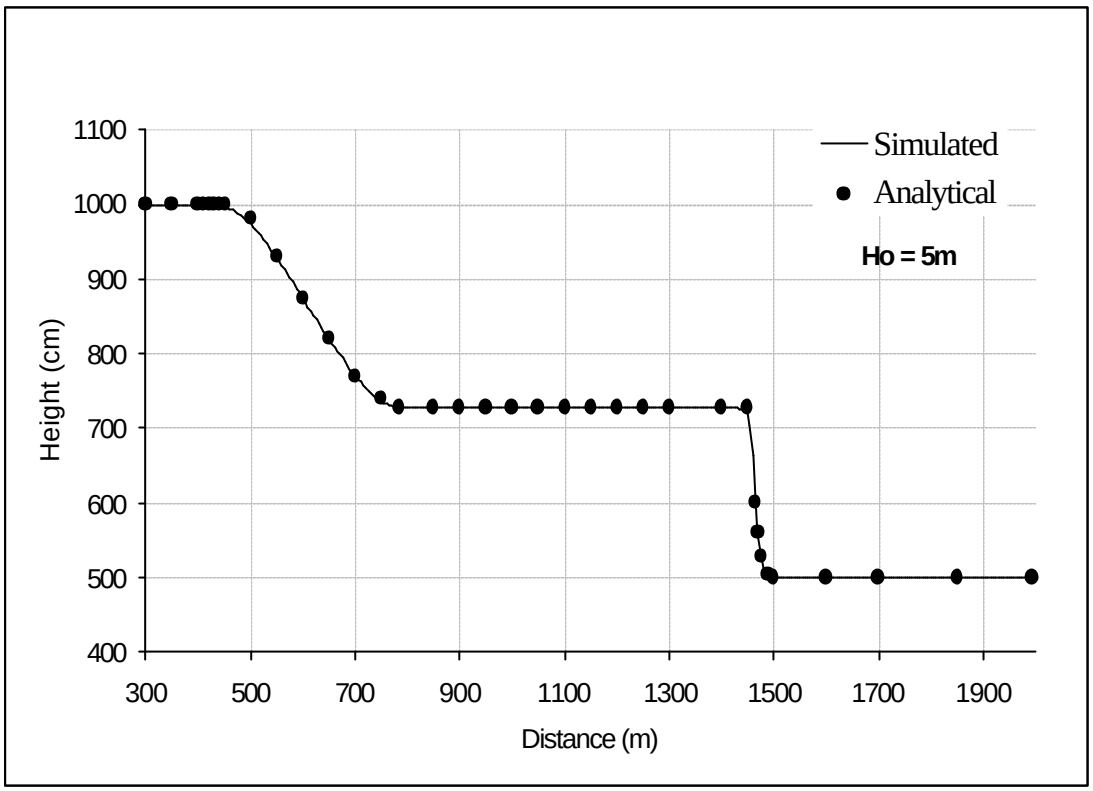

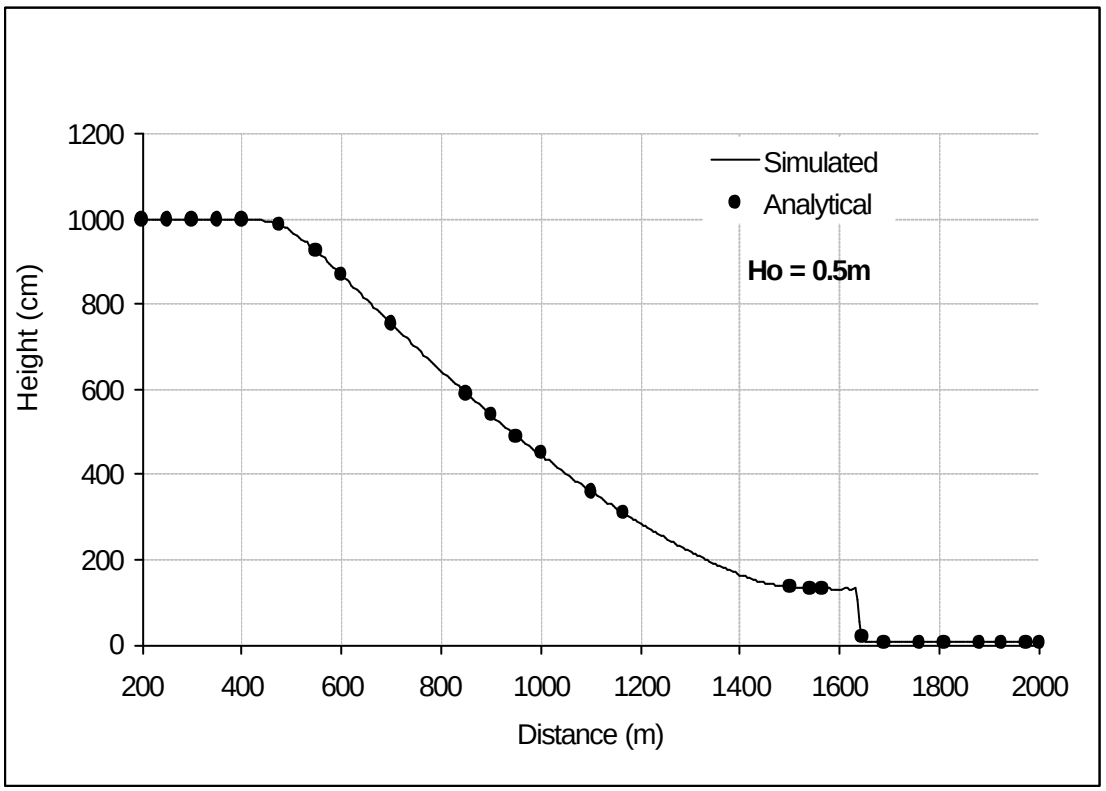

Figure 4.4 Model solution for dam break problem where ho=5m and ho=0.1m compared with analytical solutions.

5 FIELD RESULTS AND DISCUSSION

5.1 Rainfall and runoff distribution

Figure 5.1 presents the distribution of rainfall within the catchment in the 2002 season. A total of 96 rainstorm events were observed, out of which 17 were trace events, therefore, the total number of effective events were 79. The average rainfall depth for the season was 17.5mm, and the total rainfall for the season was 1684mm. Mean rainfall intensity for the season ranged between 49.2mmh^{-1} – 90mmh^{-1} and the maximum intensity range between 115 mmh^{-1} and 180 mmh^{-1}. Higher intensity (up to 240 mmh^{-1}) was observed in some events. There were no significant differences in the total seasonal rainfall recorded with the different rain gauges, but a measure of spatial variation in rainfall depth were observed in most high intensity storms.

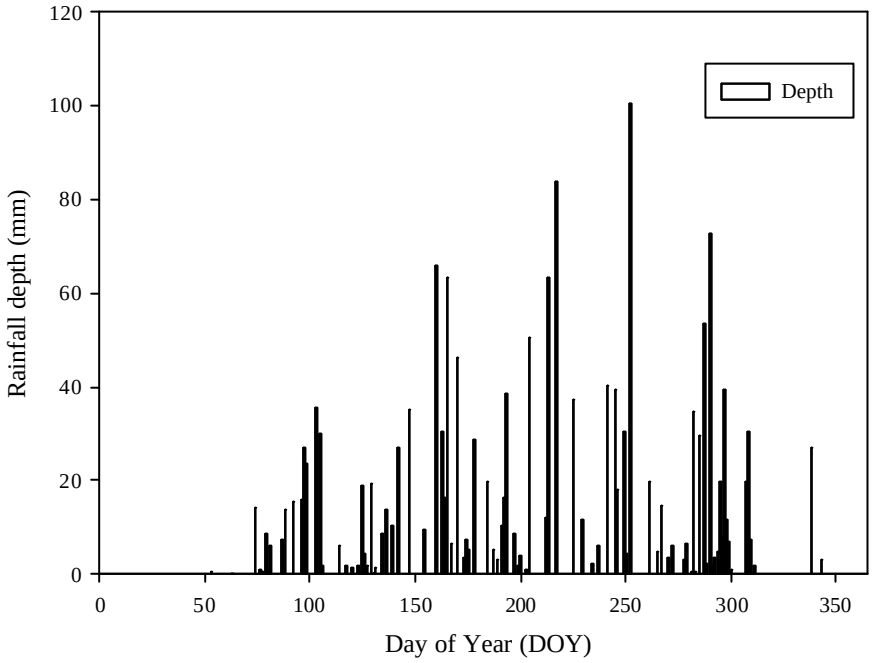

Figure 5.1 Rainfall distributions in Kotokosu catchment in 2002 season

A linear relationship, with a coefficient of determination of 0.60, (r^2 = 0.60) defines the relationship between the number of rainfall events per month and the monthly rainfall total (Figure 5.2a,b). The period is characterized by high inter-seasonal rainfall variability (c.v. = 0.87), synonymous with most tropical areas. Figure 5.2b compares the cumulated monthly rainfall and number of events per month. With fewer

numbers of events, in comparison to October, the cumulative depth of rainfall in August was higher, indicating that the rainfall in the month of August has longer duration.

The runoff producing events for the season were selected for further analysis. The maximum and mean rainfall intensities of the separate events were related to the rainfall depth, to appraise any possible effect of intensity on rainfall depth. Exponential equations produce the best fit for the variables (figure 5.3). Both curves have low coefficient of determination, but the maximum rainfall intensity is better correlated to rainfall depth (r^2=0.43), compared to the mean rainfall intensity (r^2=0.18) for the season. This suggests that, the maximum rainfall intensity will be expected to play a more significant role in the hydrological processes over the catchment. Van Dijk (2002) obtained a similar result (r^2=0.30) while determining the relationships between depth-averaged rainfall intensity (*R*) values derived from both original (*R* -orig.) and resampled (*R*-resampl.*)* tipping bucket data and the respective storm rainfall depth (*P*) values in West Java, Indonesia. The simple exponential relationship formed the basis for an analytical expression used to derive the model parameters, for characterizing the (R)USLE and GUEST models used in his study.

During the study period, there were in all about 40 runoff events at both sites. Thirty-three events were selected, based on the criteria that, at least two plots per sites (A & B) generate measurable runoff volume. Twenty-three joint events were further selected in which all the eight runoff plots, simultaneously produced measurable runoff. Some events could not be monitored at site A due to flash flooding, which submerged the plots and the measuring equipment in June. Also, substantial contributions from subsurface flow were noted in some events in the season, i.e., mostly prolonged events with low intensity.

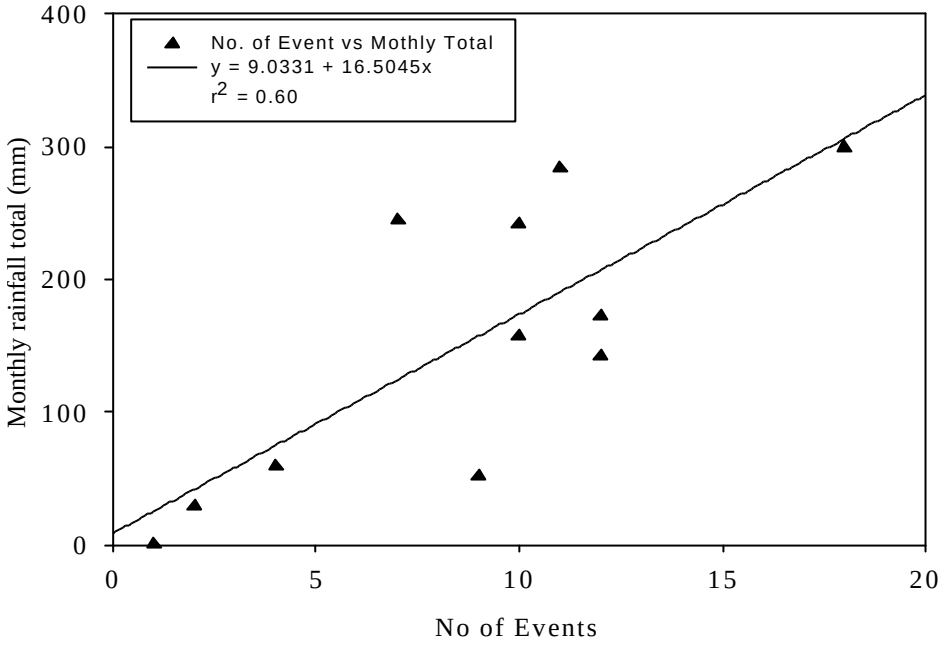

Figure 5.2a: Frequency of rainfall event against total depth on a monthly basis

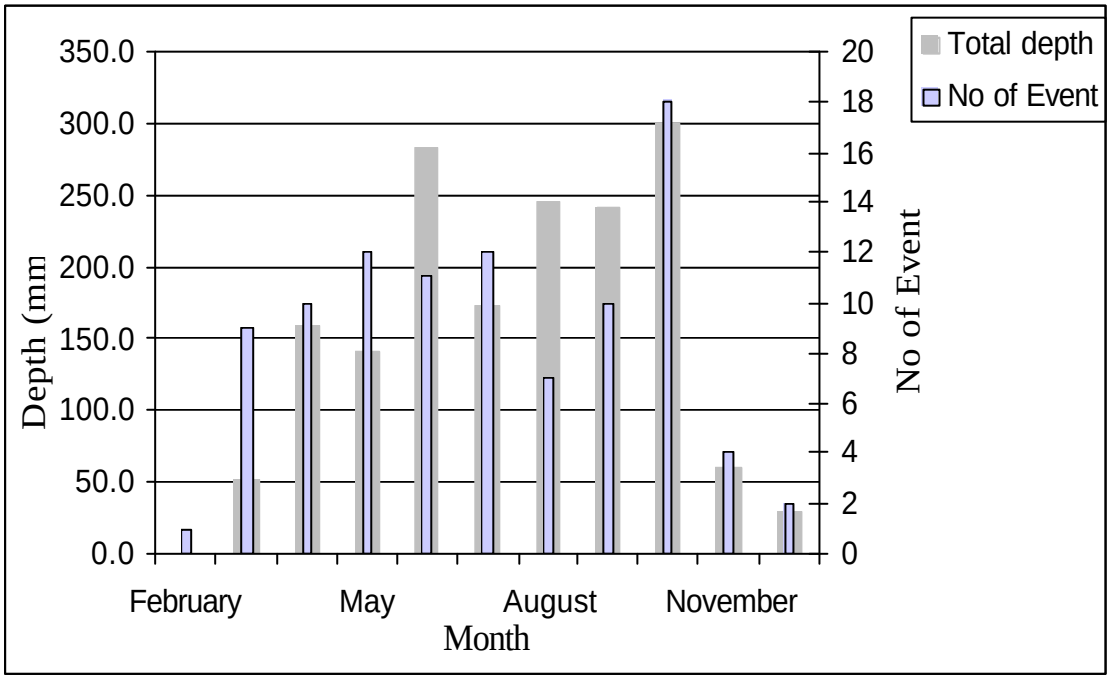

Figure 5.2b Monthly total rainfall depth and number of events

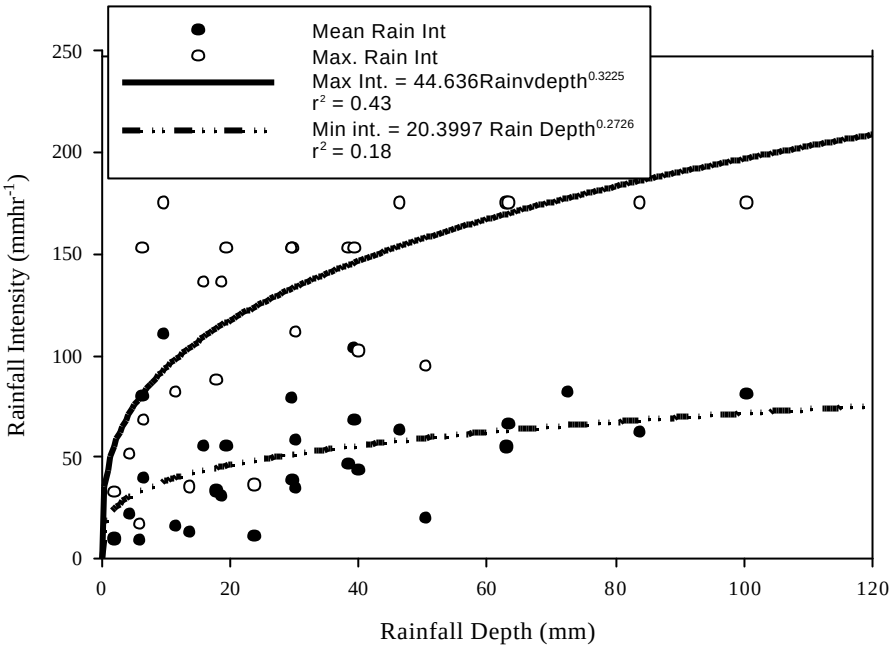

Figure 5.3 The relationship between mean and maximum rainfall intensity and rainfall depth

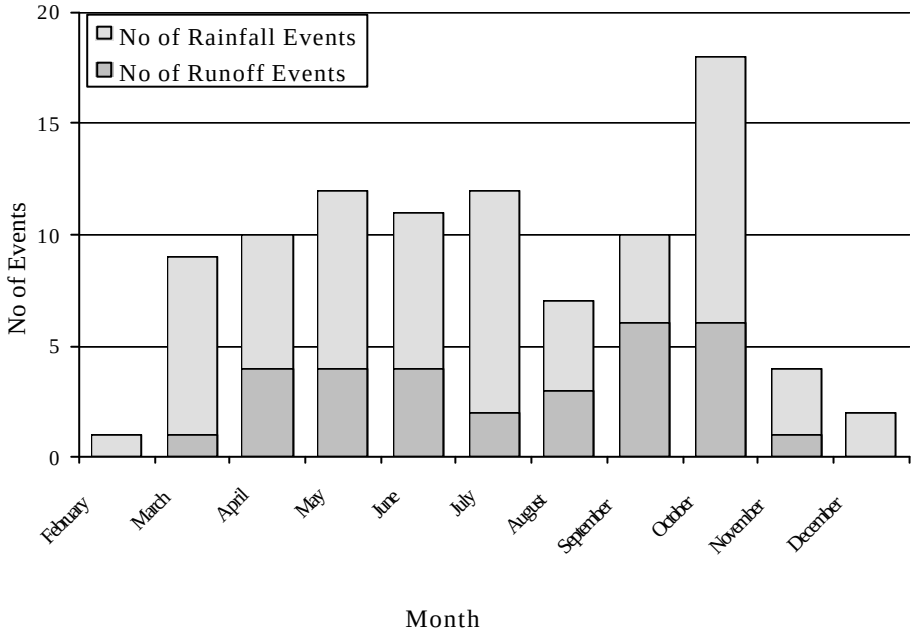

Fig 5.4 Comparison of number of rainfall and runoff events per month for the season

A breakdown of total number of runoff events compared with the number of rainfall events on a monthly basis is shown in Figure 5.4. The graph shows that there

isn't a strict linear relationship between the frequency of rainfall and runoff events. In spite of recoding the highest number of rainfall events, there is no difference in the number of runoff events in September and October. This indicates that the observation of a rainstorm event, do not linearly translate to the occurrence of runoff in the months compared.

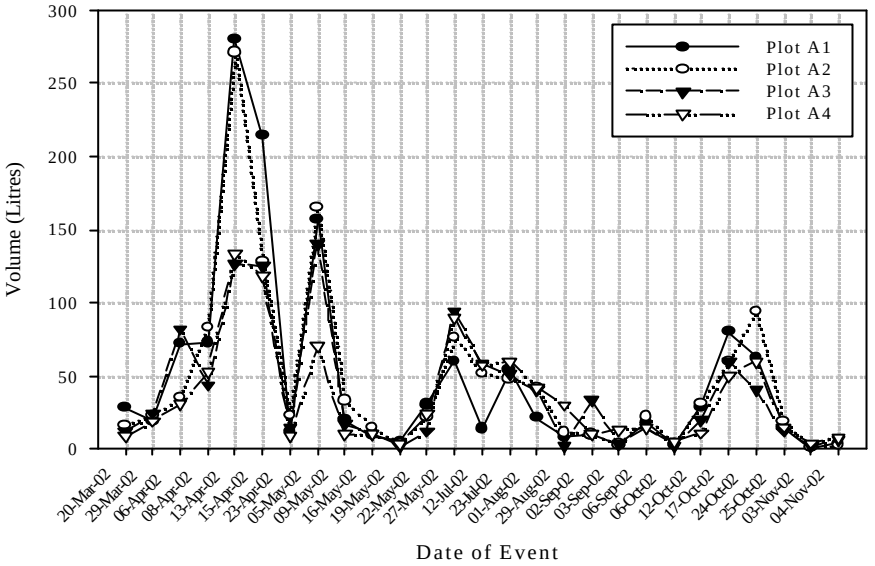

Figure 5.5a Runoff volume per event at site A in 2002 rainfall season

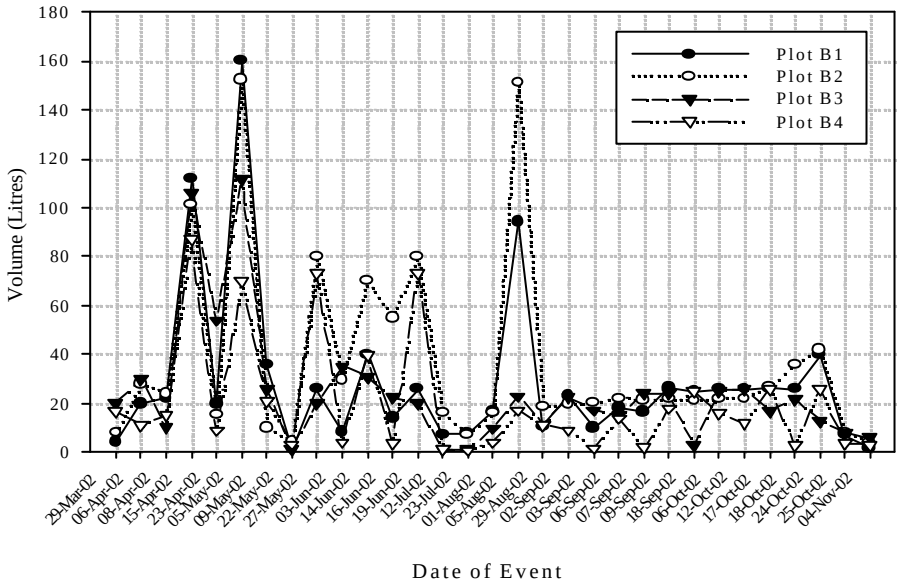

Figure 5.5b Runoff volume per event at site B in 2002 rainfall season

Figures 5.5a and 5.5b present the volume of runoff per event in each of the four plots, in the two sites (site A and site B) used for observation. The total depth of rainfall during the period of occurrence of the runoff events amounted to 747.6 mm in site A and 995.6 in site B. These figures reveal some differences in the hydrological behavior of the two sites used for investigation. The following salient points, which can be interpreted form the graphs deserves mention.

Consistently, the runoff volumes recorded in most events from site (A) are higher than those from site (B). The causative factor(s) of this observation will be discussed at a later section in this thesis.

Except on one occasion in site B, the runoff volume generally decreased as the season progresses, and only picked up towards the end of the season. The declining trend of runoff volume could among other factors be associated with the change in the vegetation canopy on all the plots, which apparently reduce the impact of rainfall. The difference in the type of vegetation that developed from the two sites is also reflected in the amount of runoff observed. Whereas narrow leave grasses developed at site (A), wide leaf shrubs developed on the plots at site B.

Vegetation development reduces substantially the flow velocity of surface runoff and simultaneously increases the friction resistance to the overland flow, and the time required for initiation of a runoff process. With increasing period since the beginning of the season, the canopy covers fraction and the vegetation density on all the plots increases, thereby increasing the effect of vegetative microtopography (mostly for low intensity events), and frictional resistance to overland flow. The combination of these processes significantly reduces the discharge volume.

The period during which, the decreasing trend of runoff volume changed, coincided with the period the whole vegetation on all the plots were carefully removed to plant maize. The observation show that vegetation cover significantly impact surface runoff and infiltration process in the catchment.

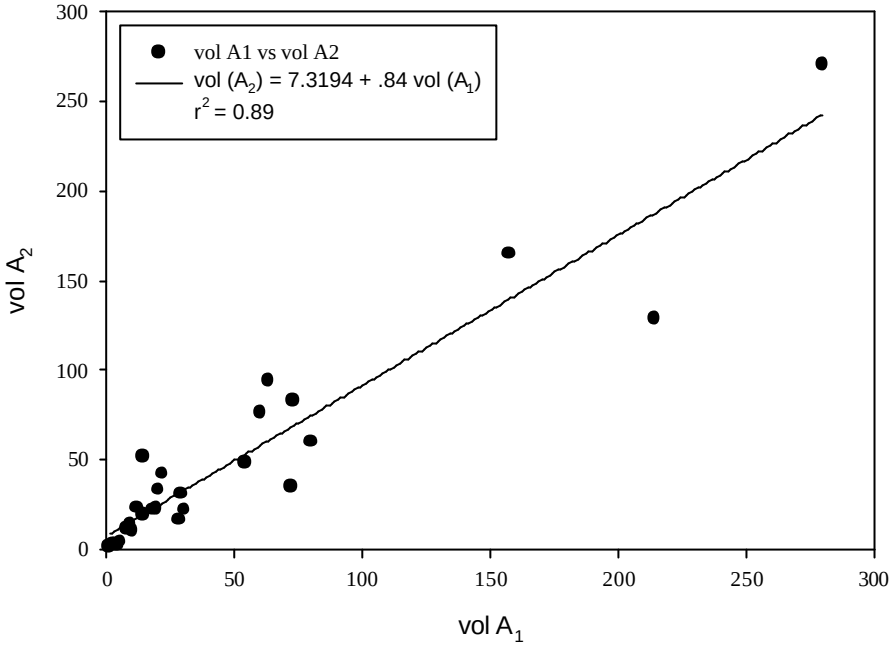

Figure 5.6a Comparison of runoff volume from the twin long plots at site A

In both sites, the highest runoff volumes were recorded early in the season i.e. April and May. These could be explained by the impact of vegetal cover already described above. In evaluating the possible effect of random noise in the runoff responses, the volumes of runoff from the twin long plots A_1 vs. A_2, and B_1 vs. B_2 at each sites were compared. To appreciate inter-site variability in response and random noise from the two sites, the runoff volume from one selected long plots from each site i.e. A_1 vs. B_2 and the short plots i.e. A_4 and B_4 were compared.

The high coefficient of determination of the linear equations between the runoff volume, and the narrow dispersion of the data from the twin-runoff plots at site A (r^2 = 0.89) and site B (r^2 = 0.75) indicate reasonable similarity in the response from the runoff plots at each site and that the measurement did not present large random noise. The small difference in the response, not captured by the linear equations could result from the natural differences in plot characteristics and the characteristic non-linearity in Hortonian runoff process.

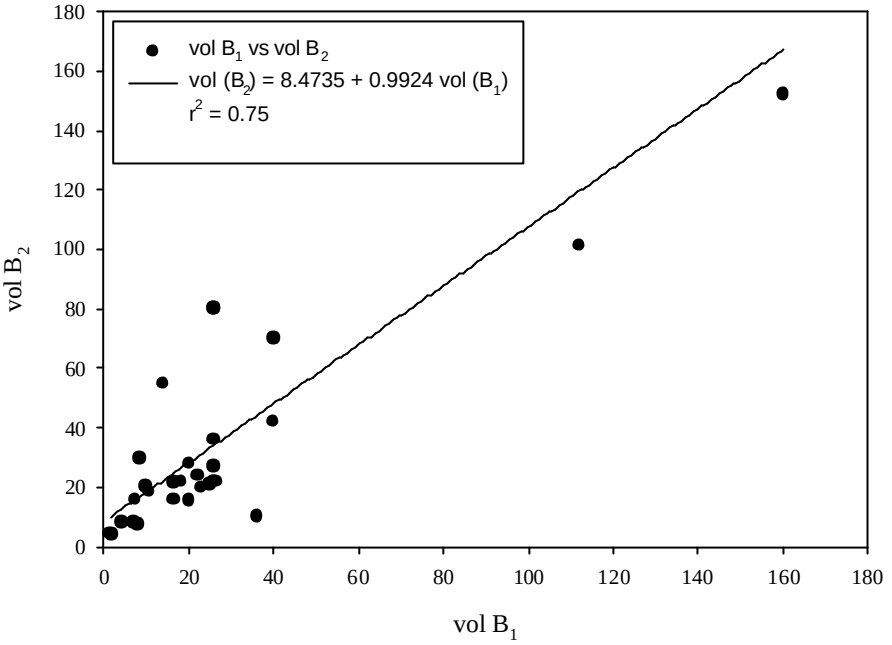

Figure 5.6b Comparison of runoff volume from the twin long plots at site B

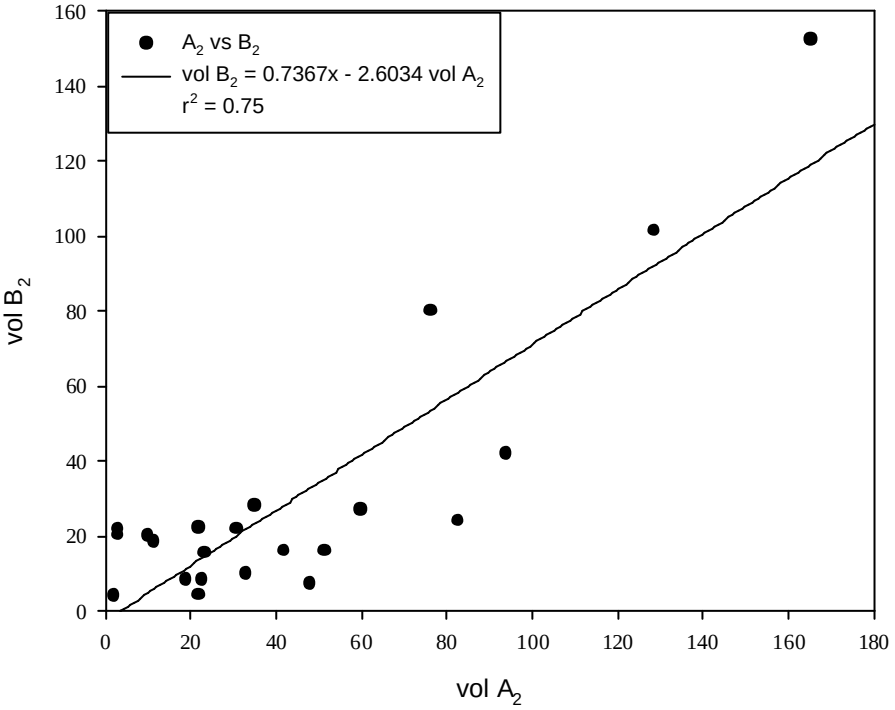

Figure 5.6c Comparison of runoff volume from selected long plot (LP) at site A and B

For the runoff volume for the long plots and short plots from the two different sites (i.e. A_1 vs. B_2 and A_4 and B_4), the coefficients of determination were 0.75 and 0.58 respectively. These figure show that there is a reasonable similarity in the response from the two sites particularly from the response from the long plots. As will be seen later, the variation in response of the two-site revolved around the difference in the in-situ hydraulic characteristics of the soil and other soil feature at the sites.

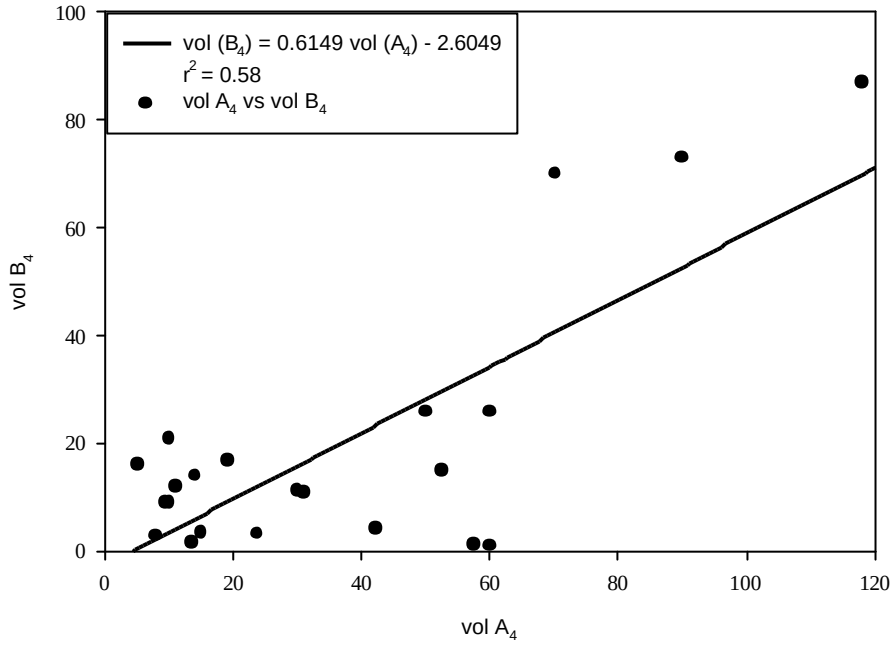

Figure 5.6d Comparison of runoff volume from the short plots (SP) at site A and B

5.2 Unit runoff discharge

To enhance a clearer understanding of the response of the different runoff plots vis-a-vis the plot size, the unit runoff discharge (runoff volume per unit area of plot) for each plot was calculated for all the runoff events. The unit runoff discharge is calculated by dividing the volume in Liters of recorded runoff per event by the area bordered by the respective plot (figures 5.7a, b).

The figures clearly show that unit runoff discharge reduces with increasing plot size in both sites. There is a consistent trend of higher runoff per unit area fom the small plots (SP) relative to the medium (MP) and long plots (LP). This underscores the effect of the scale of observation on results from runoff experiment and will be further explained under the section on scale effect and scale dependency. It is noteworthy that

the twin runoff plots in both sites, records comparable unit runoff for most of the events. This observation shows the consistency in the effect of runoff plot size in rainfall-runoff response and confirm that the observation is not accidental, but rather, a reflection of the effect of slope length.

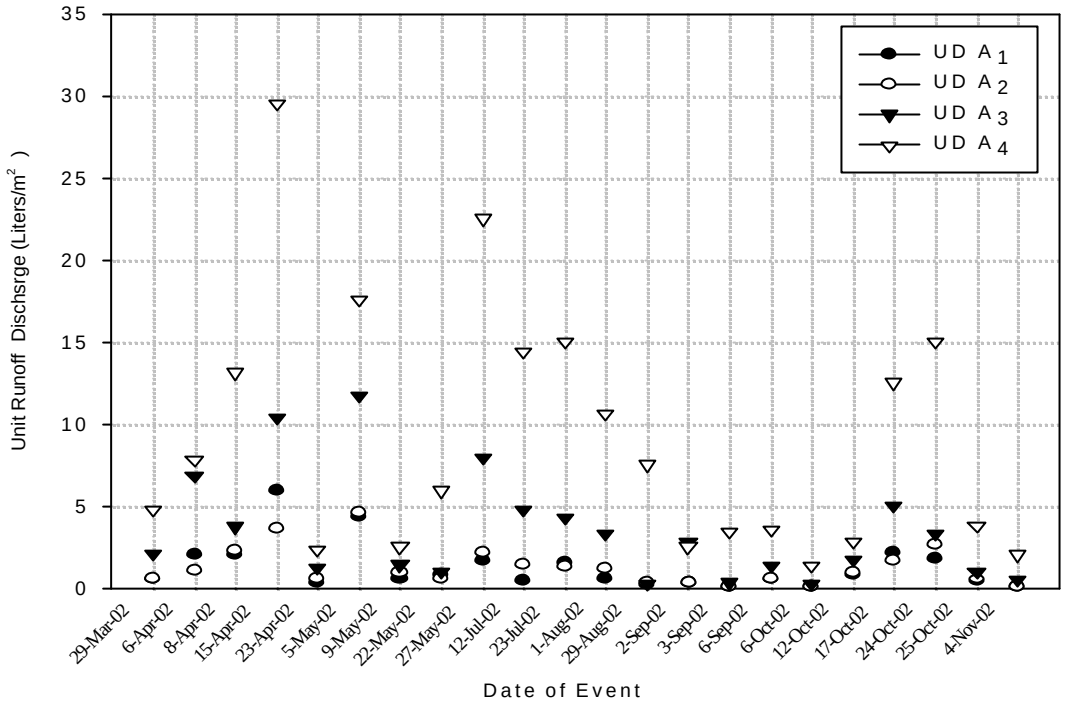

Figure 5.7a Unit runoff discharge (UD) per event for the different plot sizes at site A

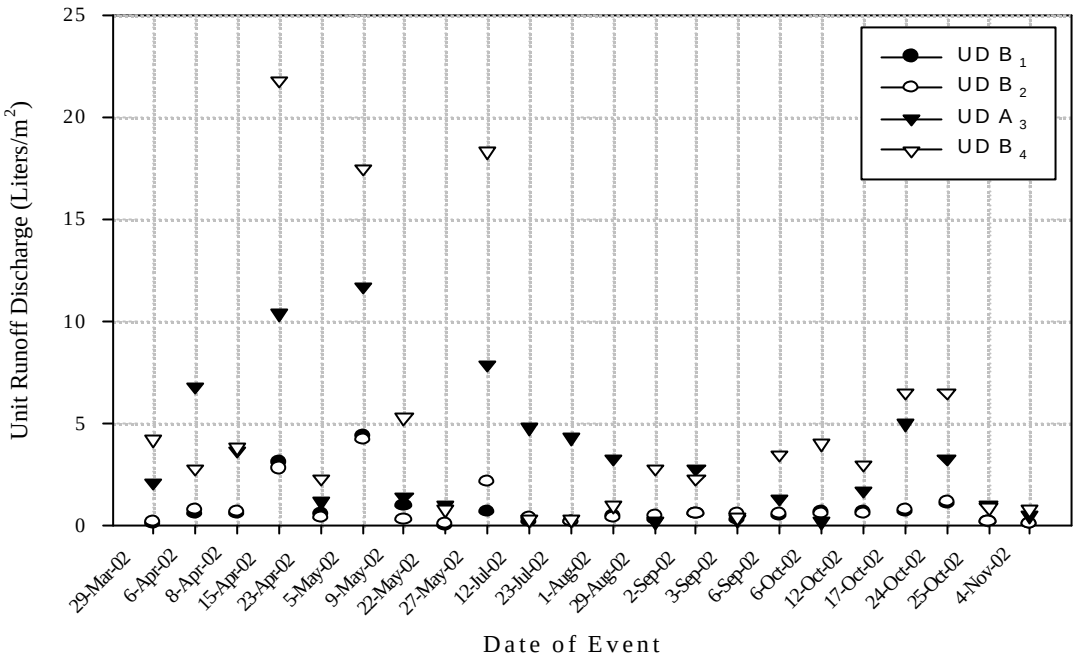

Figure 5.7b Unit runoff discharge (UD) per event for the different plot sizes at site B

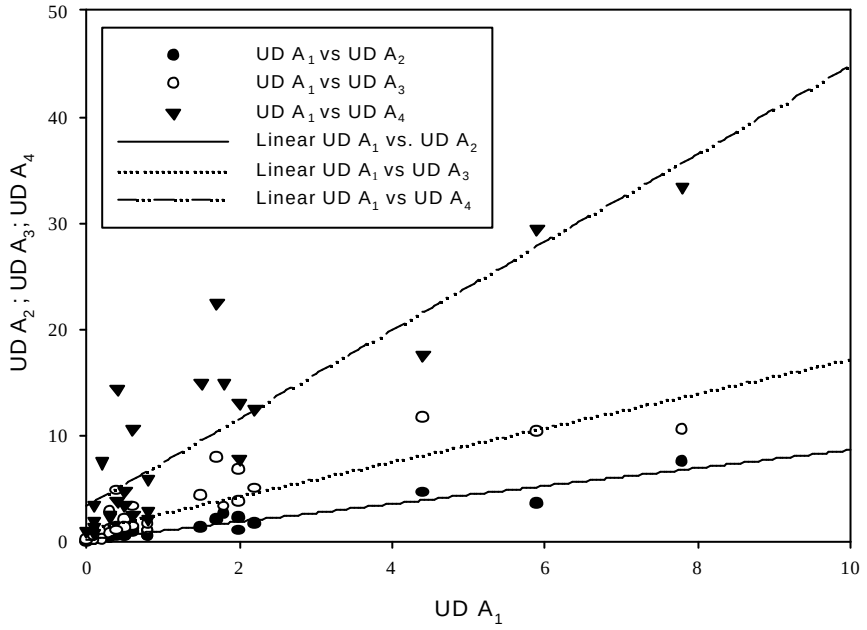

Figure 5.8a Relationship between the unit runoff discharge amongst plots in site A

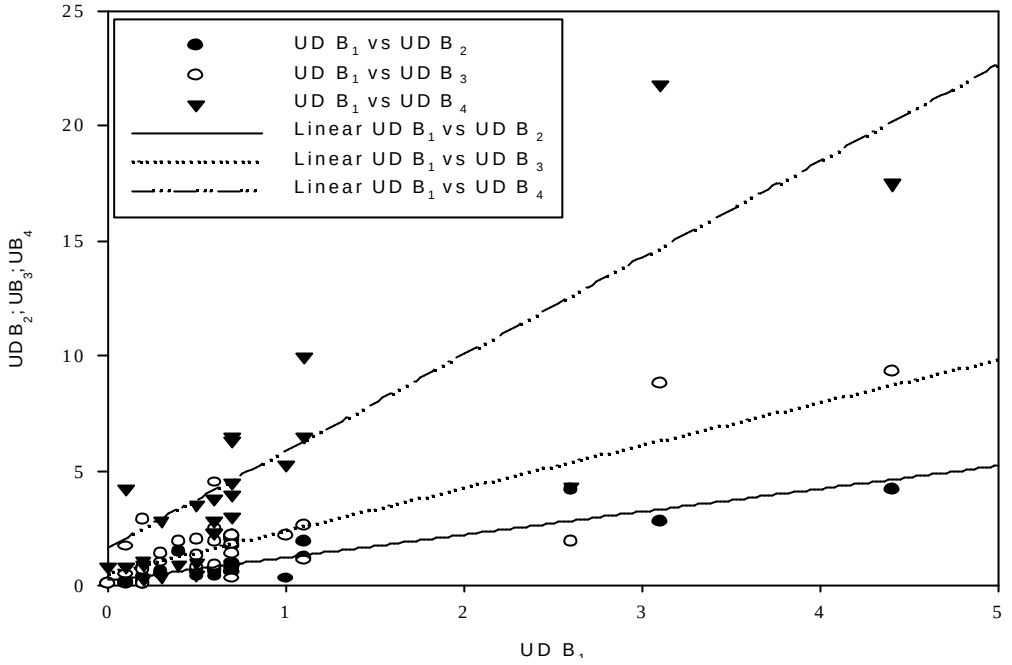

Figure 5.8b Relationship between the unit runoff discharge amongst plots in site B

Other plots (i.e. MP and SP), with identical dimension at both sites, also respond similarly in most the runoff events. To further explain this observation, the relationship between unit runoff in the runoff plots on each side was investigated in a regression model. Table 5.1 gives a summary of linear models relating the runoff discharges to one long plot (LP) in site A and B. The high coefficient of determination (r^2) between the twin long plots on sites A_1 and A_2 attest to the uniformity of hydraulic conditions between the pair of plots. Even in comparison with the medium and long plot, the r^2 values are still commensurate. Since slope, vegetation density, soil hydro-physio-chemical properties and rainfall distribution amongst the plots are uniform, it is imperative that the observed differences in response by the plots; particularly those located in the same site, is influenced by the heterogeneous factor of slope length (plot size). This conclusion becomes more clears, considering the fact that the soils in the plots are comparably similar in hydraulic properties. The low value of the coefficient of determination of the linear relationship between the twin-plot B_1 and B_2 results from the varied effect of macro-pores caused by the activities of earthworms, which are common on the site. These observations concur with the results from several studies including Esteves and Lapetite (2003), Joel et al. (2002) Gómez et al. (2001) and van de Giesen et al. (2000). A wide of intra-event variability was observed in the value of unit runoff

discharge in the season. Differences are more pronounced for short duration high intensity events and low intensity events. For rainstorm with long duration, and high depth, the unit runoff discharge differs only slightly.

Higher unit runoff discharge in small plots is more often associated with the spatial variability of the hydrological properties. This is equally observed in this study, but as will be better discussed in the section on scale effect, spatial variability of soil properties could not wholly explain the observation. Rainfall duration and directions are equally uniform; consequently, the temporal dynamics associated with different opportunities for overland flow reduction or increse in transit, which vary depending on slope lengths, would be necessary to make the explicit, the difference in unit discharge. In the analysis of time before onset of runoff and duration of runoff, the time lag between the onset and cessation of runoff event in different plot size are very close.

Table 5.1 Relationship between unit runoff on all plots at site A and B

Variables	**Equations**	**r^2**
UDA_1 vs. UDA_2	y = 0.2000 + 0.8425 x	0.90
UDA_1 vs. UDA_3	y = 1.0920 + 1.6082 x	0.77
UDA_1 vs. UDA_4	y = 3.3419 + 4.1456 x	0.78
UDB_1 vs. UDB_2	y = 0.2312 + 0.9973 x	0.75
UDB_1 vs. UDB_3	y = 0.5550 + 1.8628 x	0.69
UDB_1 vs. UDB_4	y = 4.2143 + 4.7704 x	0.43

5.3 Runoff coefficient

Runoff coefficient in percentages or as ratios is a widely accepted statistic in explaining rainfall-runoff response (van de Giesen et al., 2000; Esteves and Lapetite, 2003; Wainwright and Parsons, 2003). In this study, the runoff coefficient for all the runoff events were computed to further elucidate on the response of each of the scaled-plot to the rainfall events. Rainfall depth for the individual events was converted to volume of rainfall (per event) over the area enclosed by each runoff plot. The obtained rainfall volume per plot is then divided by the volume of runoff collected from the corresponding plots for the event. This value gives an idea of the proportion of rainfall that is converted to runoff during an event for each runoff plot. Figures 5.9 a and b show the temporal pattern of the runoff coefficient in the rainfall season under study. It is very clear from the figures that the runoff coefficient is strongly influenced by the scale of

observation and the rainfall depth (amount). The small runoff plots A_4 and B_4 has higher coefficient for all the events, in comparison to the long and medium runoff plots.

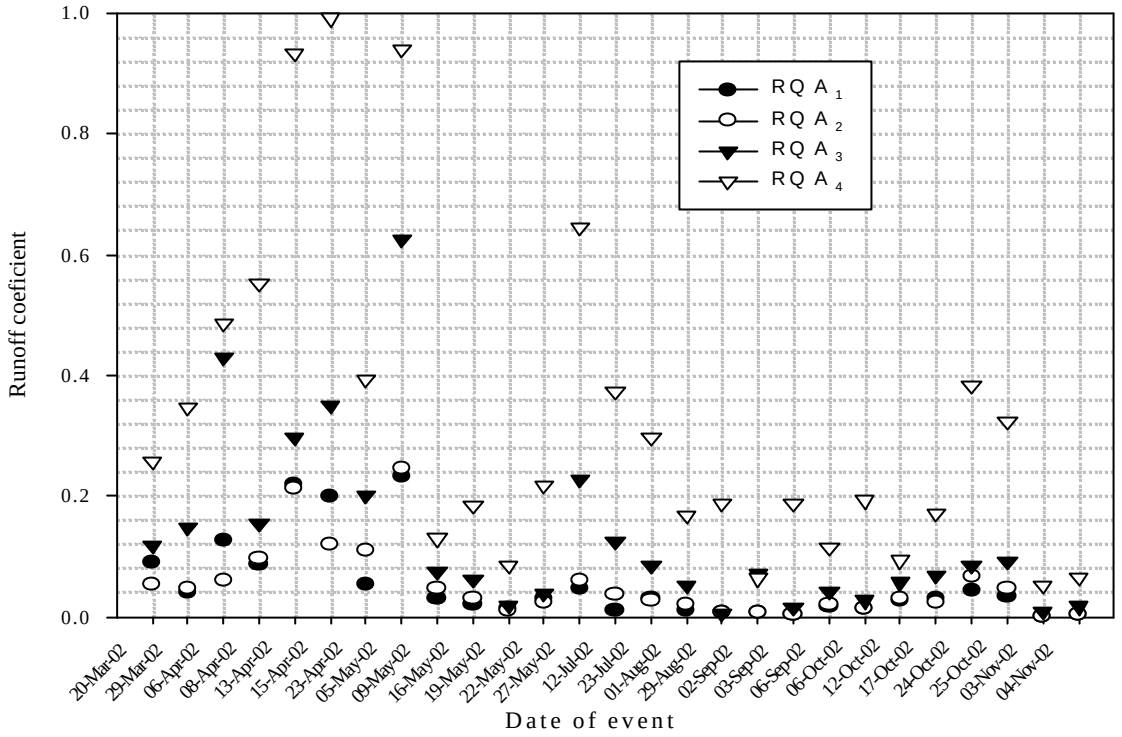

Figure 5.9a Runoff coefficient per event in site A

During rainfall events with high rainfall depth, the small plots records close to unity in runoff coefficient (Figures 5.10a and b). This implies a large proportion of the rainfall is converted to runoff. This can be simply explained by two possible developments during such events. In the first instance, high rainfall depth may result from very high intensity event that last a short time. Such events often lead to clogging and surface sealing, which reduces infiltration significantly and increase runoff. In a short plot, the effect of surface sealing is more pronounced due to a short slope length. Short slope lengths translate to reduced time for infiltration downslope and faster opportunity to reach the gutter. This results in the very high runoff volume for the short plot and consequently, a high runoff coefficient. Secondly, high rainfall intensity and the associated surface sealing in a short plot stimulate ponding of the plot in a short time. Subsequent raindrop after ponding directly contributes to runoff. The volume of runoff discharged at moments after rain had stopped also enhances the high value of runoff coefficient.

High depth rainfall events could also arise from low intensity events with prolonged duration. Low intensity prevents surface sealing and will therefore increase infiltration rate, and may allow pseudo-saturation in short time interval. Such soil saturation state is very easily attained in a short plot in comparison to a long plot, due to the differences in area be covered. From the moment of saturation, any additional rainfall directly contributes to runoff and such scenarios result in a condition in which the proportion of runoff volume may be increased in the short plot.

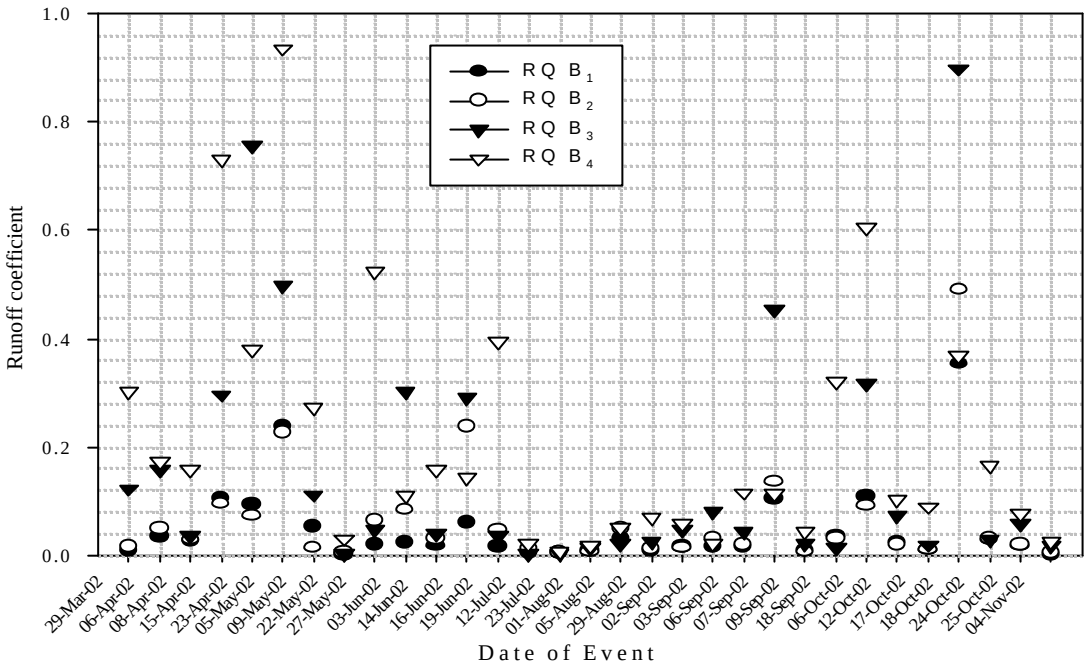

Figure 5.9b Runoff coefficient per event in site B

For some low depth rainfall event, the difference in runoff coefficient between the long and short is minimal. Such observation probably occurs with events coming after a period of dry spell, which would have increase, the infiltration potential of the soil. In such events, the soil is not saturated, and the low intensity nature of the rain prevents surface sealing of the soil. Surface sealing would have increased the runoff volume differentially. It is also evident that the set of twin plots (A_1-A_2, B_1-B_2) exhibits marked similarity in response to the rainfall event.

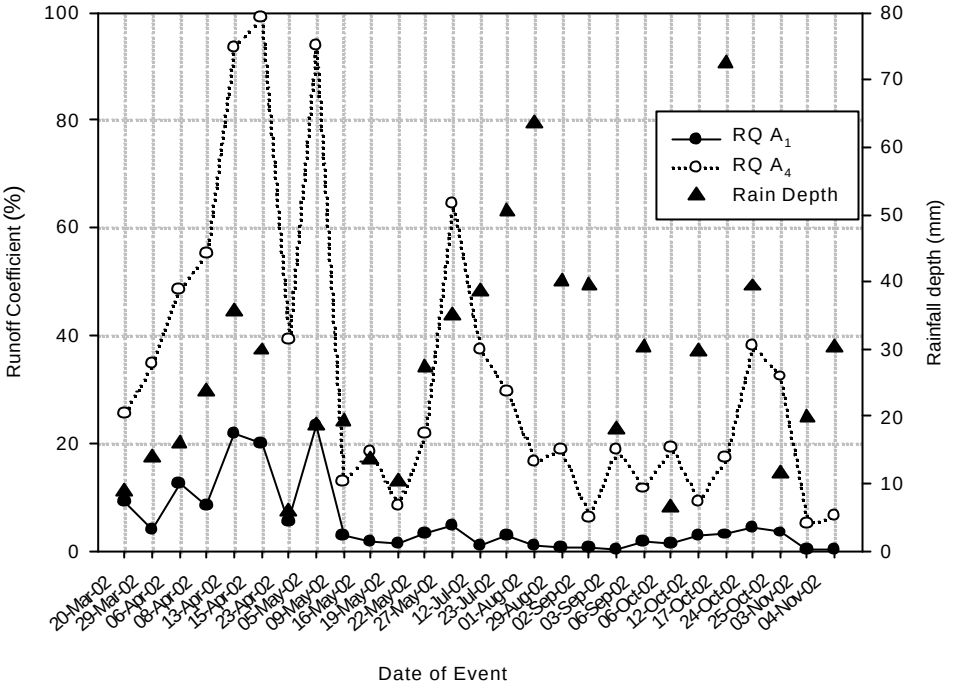

Figure 5.10a: Trend of runoff coefficient and rainfall depth from LP and SP plots at site A

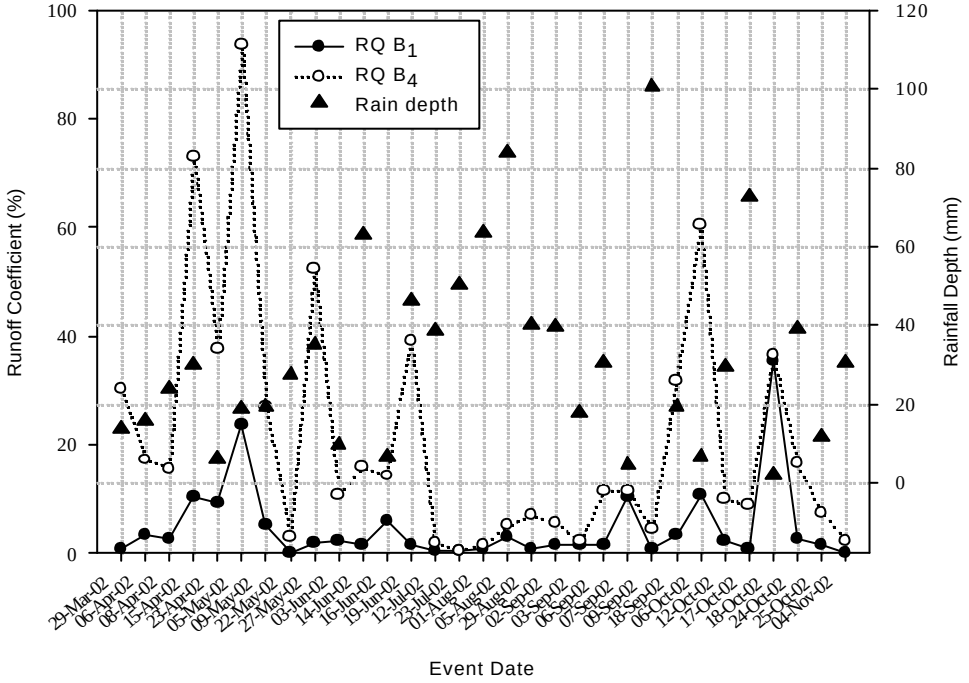

Figure 5.10b: Trend of runoff coefficient and rainfall depth from LP and SP plots at site B

Some studies have reported a strong relationship between runoff coefficient and rainfall intensity (Kang et al., 2001; Chaplot and Le Bissonnais, 2003). In this study, the possibility of such relationship between the runoff coefficients from the different plot sizes and maximum rainfall intensity for the event was explored. However, there was no significant relationship between the maximum rainfall intensity and rainfall coefficient values from the different plot size at both sites (figure 5.11a and b). The apparent lack of correlation has also be similarly reported by Kirdon and Yair (1997) in a field study conducted in Western Negev, Israel and Joel et al. (2002) from the field work in central region of Chile.

Table 5.2: Average value of runoff coefficient from the different plot.

Plot	**Plot dimension**	**Runoff coefficient**	**Runoff coefficient (%)**
A_1	18 m x 2 m	0.053	5.3
A_2	18 m x 2 m	0.052	5.2
A_3	6 m x 2m	0.129	12.9
A_4	2 m x 2 m	0.327	32.7
B_1	18 m x 2 m	0.048	4.8
B_2	18 m x 2 m	0.063	6.3
B_3	6 m x 2 m	0.156	15.6
B_4	2 m x 2 m	0.212	21.2

The average value of the runoff coefficient for the different plots sizes for the joint rainfall-runoff events for the 2002 rainfall season is presented in Table 5.2. Similar to the findings in a number of previous studies, the average runoff coefficient of reduces with increasing slope length. Slope length (area of runoff plot) was observed to be important in determining the proportion of rainfall in an event that is converted to runoff. For the long runoff plot at site A, about 5% of the rainfall is converted into runoff, whereas in site B, the proportion varied between 5% and 6%. On the short runoff plot at site A, 33% of the rainfall is converted to runoff, while at site B, only 21.2% is converted to runoff. The differences in this response as earlier mentioned showed that, apart from the slope length, difference in the in the value of saturated hydraulic conductivity may influence flow paths and in general affect the rainfall-runoff response.

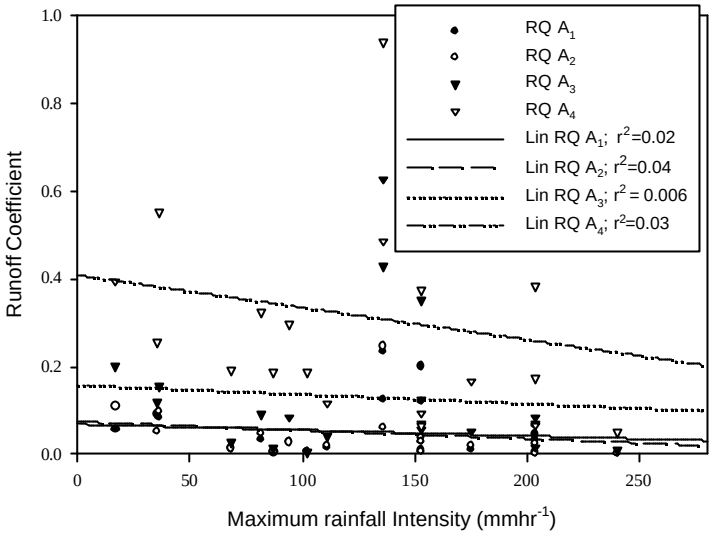

Figure 5.11a Relationship between maximum rainfall intensity and runoff coefficient in site A

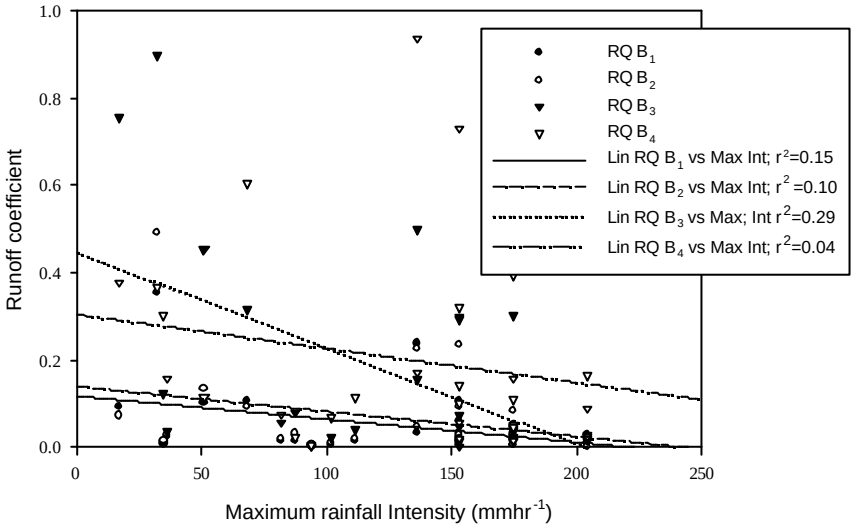

Figure 5.11b Relationship between maximum rainfall intensity and runoff coefficient in site B

Consequent upon the dependence of both the unit runoff discharge and runoff coefficient on slope length, an empirical power equation between plot (hillslope) length and runoff coefficient was derived based on the averages of the measured value during the field trial was derived for application in the catchment. With an r^2 value of 0.89, the

model explains the strong relationship existing between quantity of runoff discharge in response to rainfall event and the length of travel of the overland flow. Wainwright and Parsons (2003) in a model study of surface runoff processes similarly obtained power equations, relating runoff coefficient and slope length, although the effect of slope length will change with the slope angle and the microtopographic form. The digital elevation model of the study site show that the average slope angle in all part of the catchment ranges between 4° and 7°, thus the derived equation could be which was based on 5° slope could be applied in most part of the catchment.

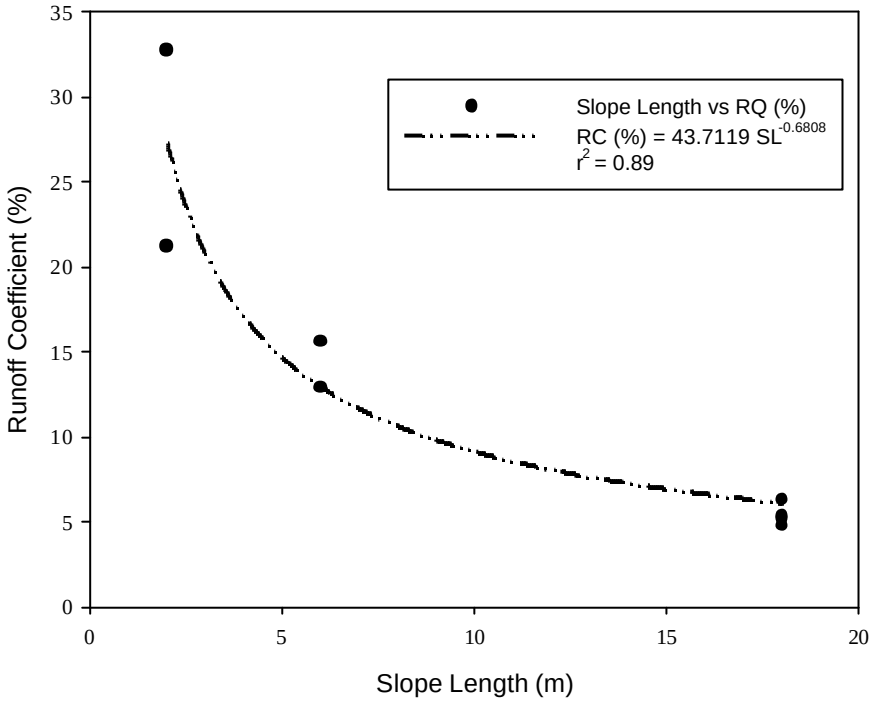

Figure 5.12 Relationship between runoff coefficient and plot length

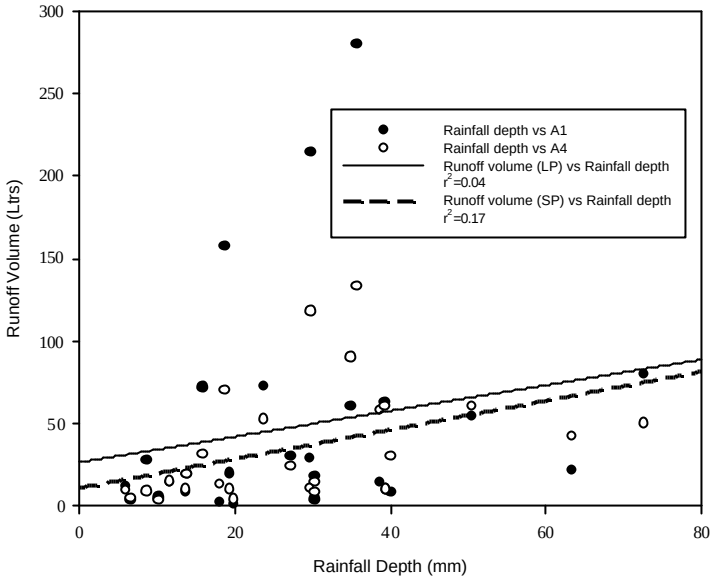

Figure 5.13a Relationships between rainfall depth and runoff volume in site A

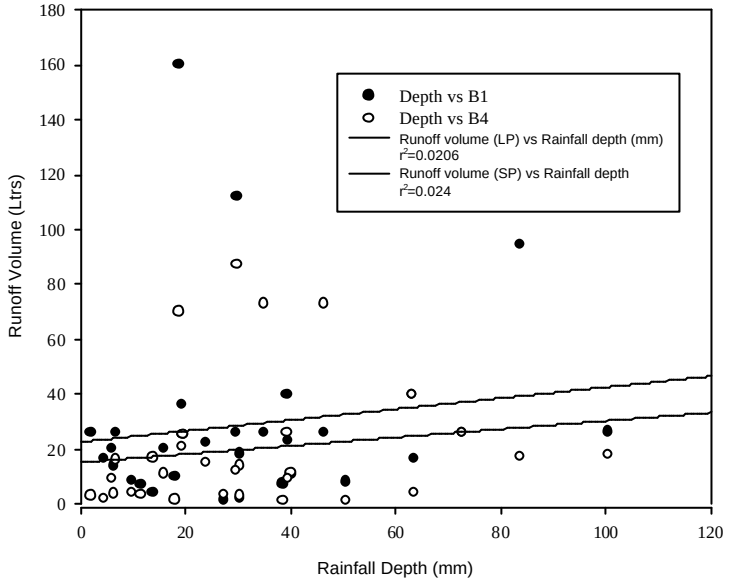

Figure 5.13b Relationships between rainfall depth and runoff volume in site B

To further test the possibility of predicting runoff volume from easily measured parameters like rainfall depth per event, the relationship between rainfall depth and runoff volume was investigated in both linear and non-linear analysis, for a selected long plot and a short plot at each site. The result (figure 5.13a and b) shows a very low r^2 value in all the cases. This further outlines the difficulty of predicting runoff volume without an appropriate processed based model. The difference in the value of

the r^2 from one plot size to the other further confirms the significant influence of the scale of observation on the rainfall - runoff response system.

5.4 Hydraulic characteristics of runoff plots

A number of analyses from the previous sections showed the influence of infiltration properties and hydraulic conductivity in rainfall-runoff response. Therefore, an adequate characterization of the hydrodynamic properties of soil is very important for understanding rainfall-runoff systems, and in general catchment hydrology. Among various hydrodynamic variables, the saturated hydraulic conductivity play significant role. It determines the maximum capacity of soil to transmit water, thus determining infiltration potential. The effect is important in this study, considering the previous conclusion that, the timing and magnitude of flow from smaller catchments depends on the processes in the landscape, more than processes in the stream channels (Schmidt et al., 2000). These processes are controlled by soil hydraulic properties and topography; thus, the decision was taken in this study to determine by field measurement, the hydraulic conductivity and microtopography of all study plots.

It is apparent that the value of hydraulic conductivity cannot be determined at every point in the plots or catchment; therefore, representative points were selected within each plot. The measured saturated hydraulic conductivity were geostatistically interpolated. The use of geostatistical techniques (measuring the correlation between neighboring points) has been shown to be very efficient for hydrological purposes (Mallant et. al, 1997).

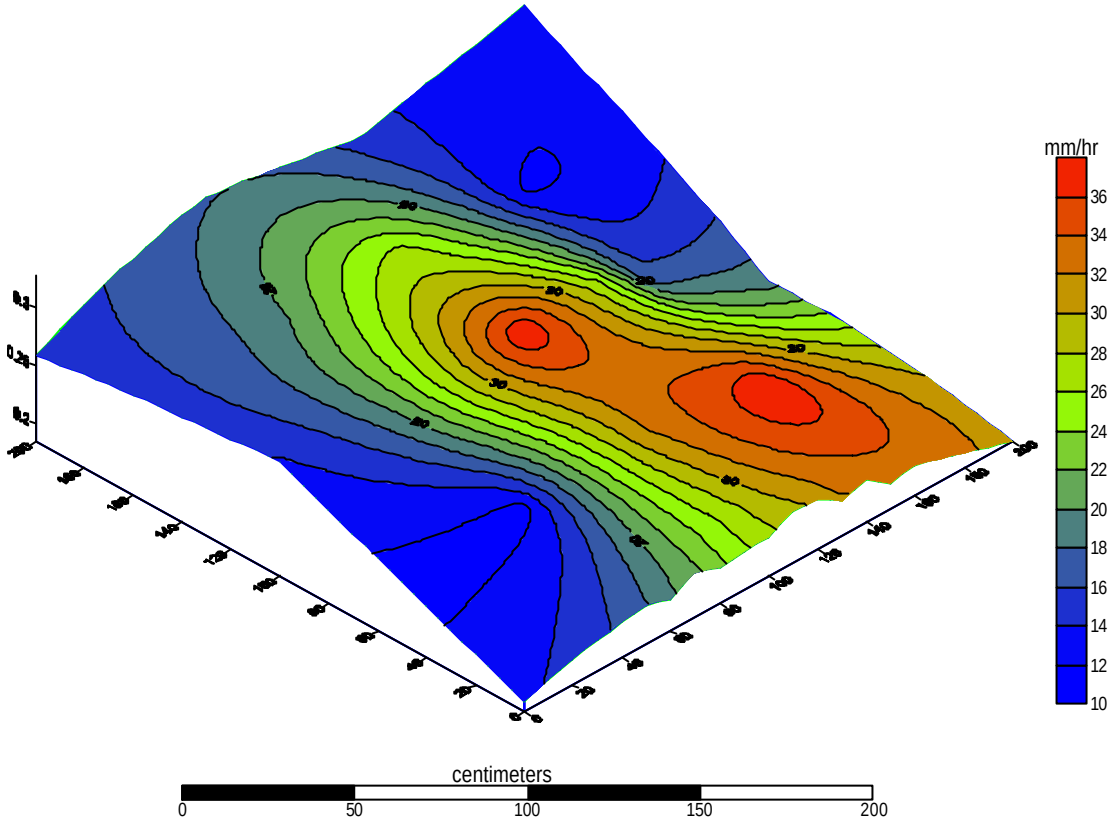

Figure 5.14a Spatial distribution of saturated hydraulic conductivity (K_{sat}) in plot A_4

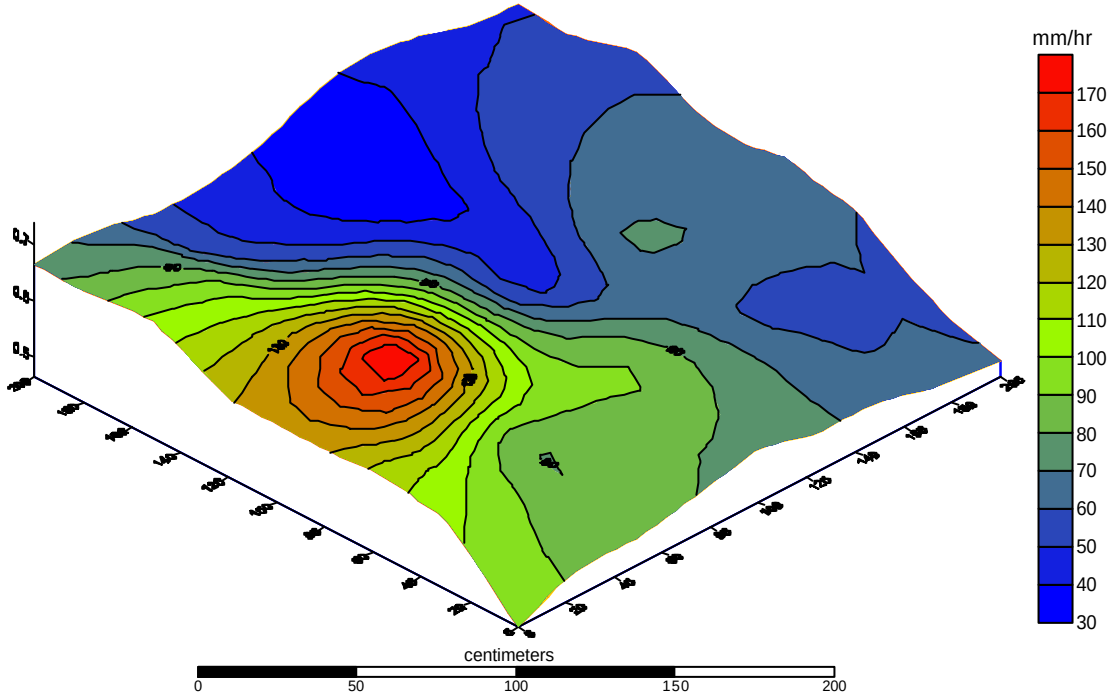

Figure 5.15b Spatial distribution of saturated hydraulic conductivity (K_{sat}) in plot B_4

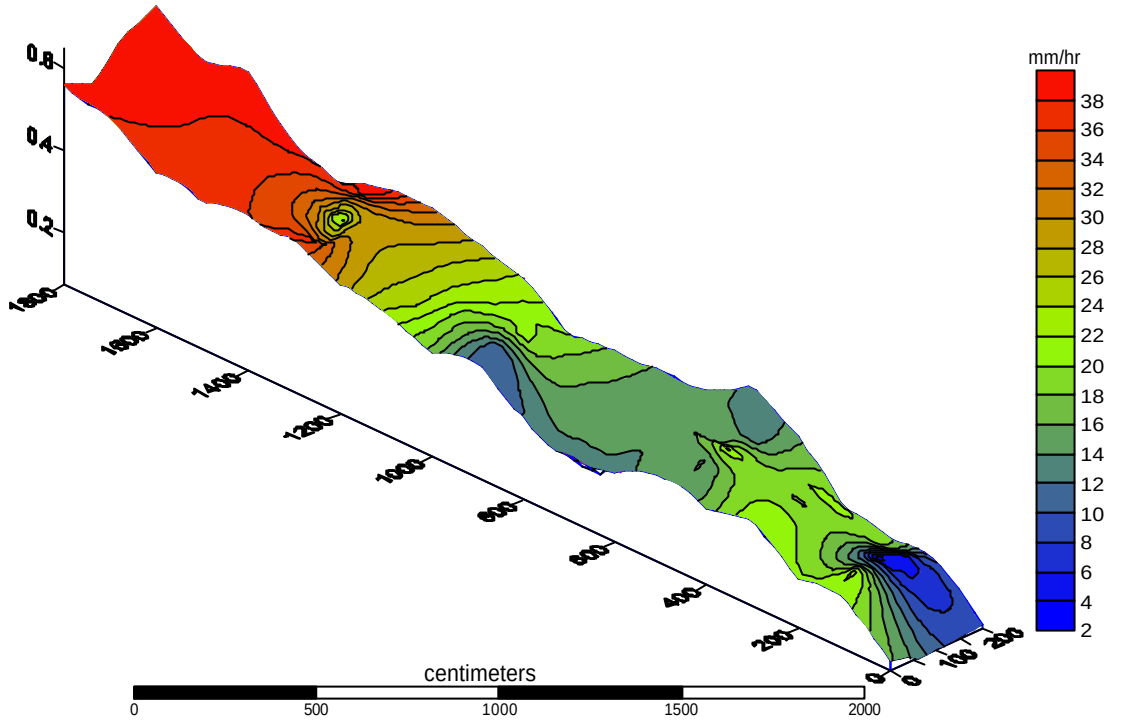

Figure 5.15c Spatial distribution of saturated hydraulic conductivity (K_{sat}) in LPA

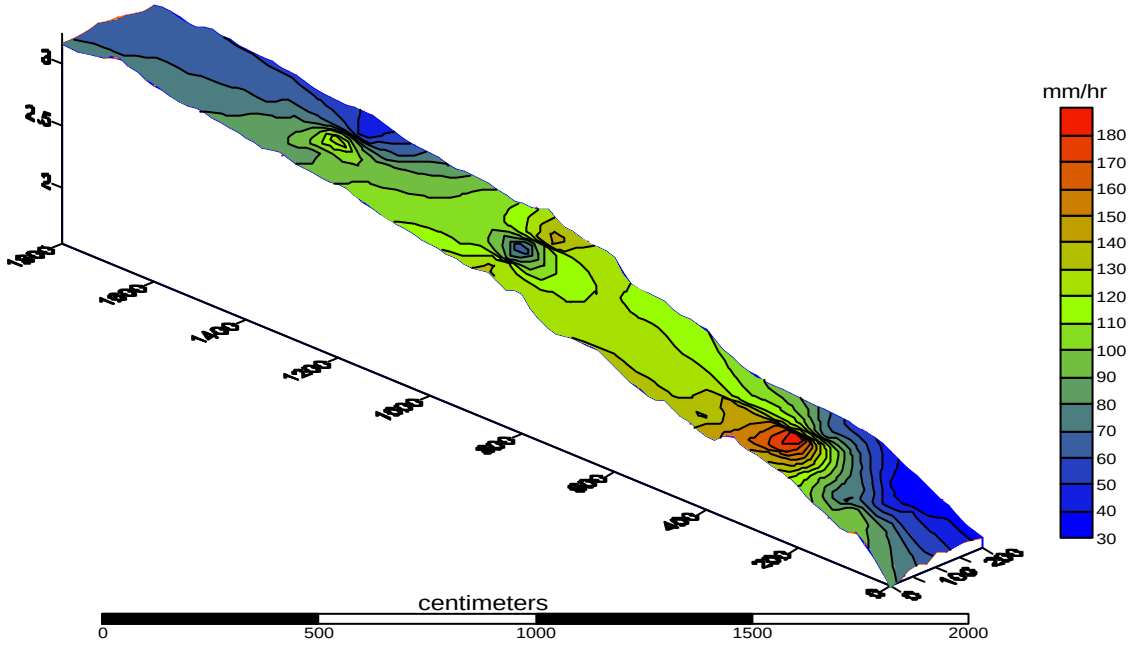

Figure 5.15d Spatial distributions of saturated hydraulic conductivity (K_{sat}) in Plot B_1

Figures 5.14a-d present the saturated hydraulic conductivity maps for one long plot each, and for the short plots, at both sites. The hydraulic conductivity values are overlaid on the plot's DEM. These figures show the uniformity and consistency in the ranges of value of saturated hydraulic conductivity in plots at the same site, while

revealing the wide variation in the values between the two sites. The intra-site variations is most likely influenced by the difference in the class of soil at the two sites, and the effect of macropores prevalent in site B. Site A is made up of silt loam while site B is a sandy clay loam. The difference in the proportions of sand and clay in the two soil types influence the movement of water. Site A consists of lower proportion of both sand and clay compared to site B.

Examination of the four figures shows the extent of spatial variability over very short distance in the distribution of hydraulic conductivity. This is consistent with the description of the hydrologic behavior of tropical soil, thus placing an extra demand in the selection of a representative model, when there is a need to characterize infiltration behavior. There is also a pattern of the prevalence of lower saturated conductivity values at the slope bottom close to the gutter. Upon the examination of the distribution of saturated hydraulic conductivity over the whole catchment, it was observed that hydraulic properties vary largely with the landscape position. An understanding of this interrelationship between soil hydraulic conductivity and landscape features is a key to understanding soil hydrologic environment (Mohanty and Mousli, 2000; Sobieraj at al., 2004). The high values of hydraulic conductivity at site B attest to the significant influence of macropores resulting from the activities of earthworms in the site. Earthworms create macropores in form of permanent burrows deep into the soil, which constitute a major conduit for drainage, particularly under low intensity rainfall. The increased infiltration capability due to the macropores reduces the magnitude of overland flow. Moreover, earthworms fragment the organic matter, thereby increasing soil porosity and aggregation. This significantly increases the water-holding capacity of soils, thereby reducing runoff volume. Therefore, it can be inferred that the discrepancies in hydraulic conductivity values to a large extent account for the consistent difference in runoff volume from the two sites despite substantial spatial uniformity in the rainfall distribution within the catchment.

Table 5.3 presents the statistical properties of the saturated hydraulic conductivity within the plots used in the field study. The values also outline the consistency of K_{sat} at the two selected sites and the clear difference between one site and the other.

Table 5.3: Summary statistics of measured and interpolated unsaturated hydraulic conductivity per runoff plot

Plot Name	Maximum ($mmhr^{-1}$)	Minimum ($mmhr^{-1}$)	Average ($mmhr^{-1}$)	Standard deviation	Coefficient of variation
A_1	39.1	2.7	23.7	10.1	0.42
A_2	33.7	2.6	17.7	6.6	0.37
A_3	49.5	5.8	23.8	8.4	0.35
A_4	37.8	11.5	21.7	7.5	0.35
B_1	188.4	30.0	95.8	30.1	0.31
B_2	204.9	25.9	68.4	31.5	0.46
B_3	160.9	42.8	87.3	20.2	0.23
B_4	187.2	29.6	75.2	29.3	0.39

In spite of the obvious spatial variation in the saturated hydraulic conductivity within the catchment, there is a need to derive effective (pseudo average) hydraulic properties for the varied (vertical and horizontal) soil hydraulic parameters. The effective parameters will be used in the developed numeric model for simulating the hydrologic response of the catchment. This is necessary because the simulated response is quite sensitive to soil hydraulic parameters (Jhorar et al. 2004), and hydraulic parameters are site specific.

In translating the measured saturated hydraulic conductivity from the different sites into effective hydraulic conductivity (K_{eff}); representative of all the plots at a particular site, the van Genuchten (1980) model was used to parameterize the soil-water and tension characteristics data obtained from the field measurement. Soil moisture and tension properties in the 1000mm profile were monitored at locations cited within the set of runoff plots at each site used for the field campaign. Soil tension was monitored with sets of tensiometers installed at three depths, while a TDR profile probe measure the corresponding soil water at those depth (detailed description already given in Chapter three). The van Genuchten model is presented as:

$$S_e(y) = \frac{q(y) - q(r)}{q_s - q_r} = \frac{1}{\left[1 + (-a\,y)^n\right]^{1-1/n}} \tag{5.1}$$

where S_e is the effective water saturation, also called the reduced water content ($0 = S_e = 1$), and q_r and q_s are the residual and saturated volumetric water contents respectively. The effective saturation describes the rate of flow of water through a

porous medium that contains more than one fluid, such as water and air in the unsaturated zone, and which should be specified in terms of both the fluid type and content and the existing pressure. The representative soil water parameters were obtained by iteration of the field data with RETC optimization software (van Genuchten et al., 1991) for the two sites are presented in Table 5.4. In applying the van Genuchten model in this study, the residual and saturated water content selected by examination of the 1 - year data, of soil moisture (0-1000mm) collected as part of the study, and the ***'n'*** parameter were obtained from the neural network fitting of soil physical properties at both sites using DISC (USDA) software.

Table 5.4 Summary data of soil water characteristics and hydraulic function for site A & B.

Site	**Soil type**	q_s **m^3 m$^-$**	q_r **m^3 m^{-3}**	a **/mm^{-1}**	n	S_e	$K_{s\ eff}$ **mmh^{-1}**
A	Silt loam	0.51	0.10	0.0633	1.8322	0.53	15.8
B	Sandy clay loam	0.57	0.07	0.0610	1.5716	0.68	53.6

Figure 5.16 and Figure 5.17 present the fitted hydraulic characteristics curves for sites A and B. The coefficient of determination (r^2) for the regression of observed against fitted values for site A is 0 .71, while for site B it is 0.43.

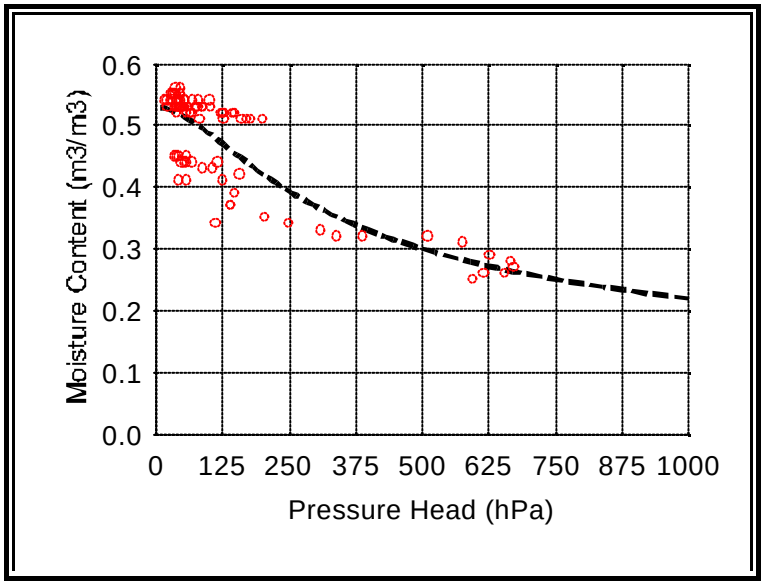

A: Moisture Content vs. Pressure Head

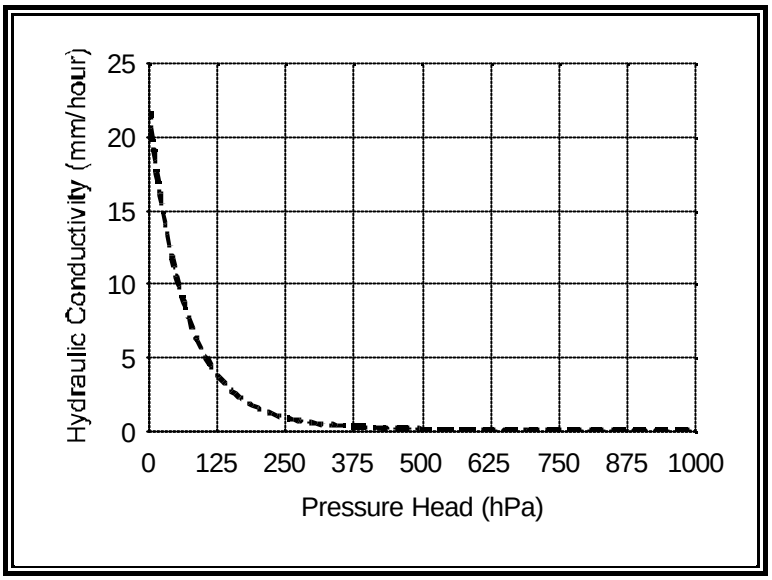

B: Pressure Head vs. Hydraulic Conductivity

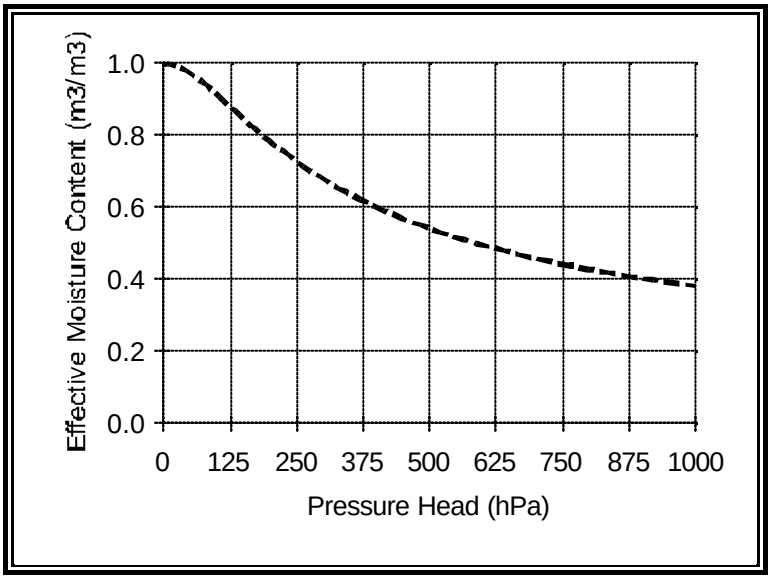

C: Pressure Head vs. Effective Moisture Content

Figure 5.16: Fitted hydraulic characteristics curves for site A based on simultaneously measured soil moisture and tension at 3 depths (30cm, 60cm and 100cm) during the study period.

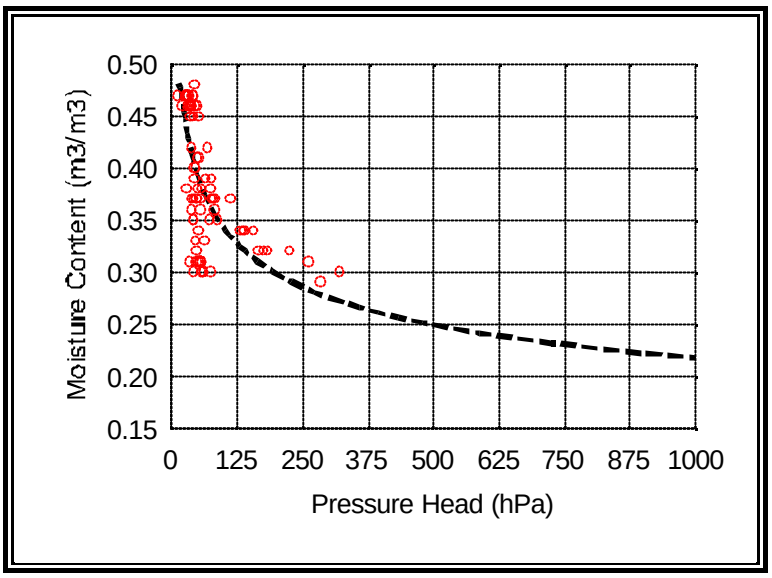

A: Moisture Content vs. Pressure Head

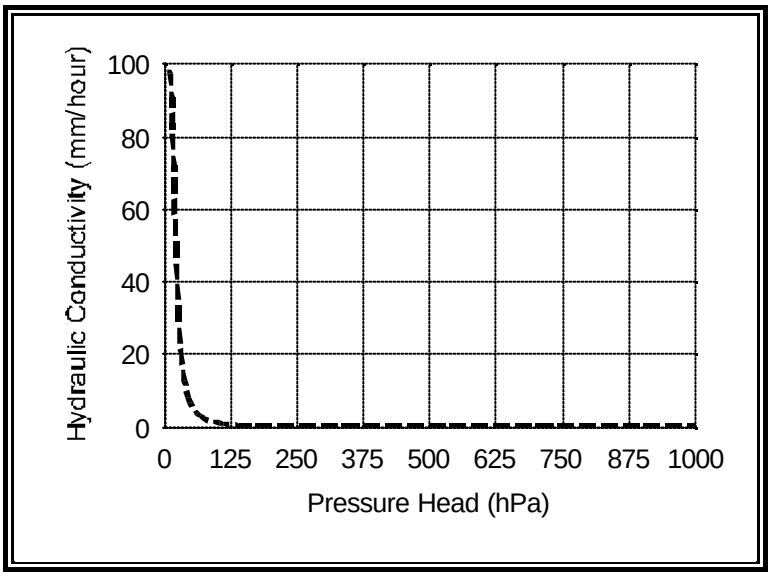

B: Pressure Head vs. Hydraulic Conductivity

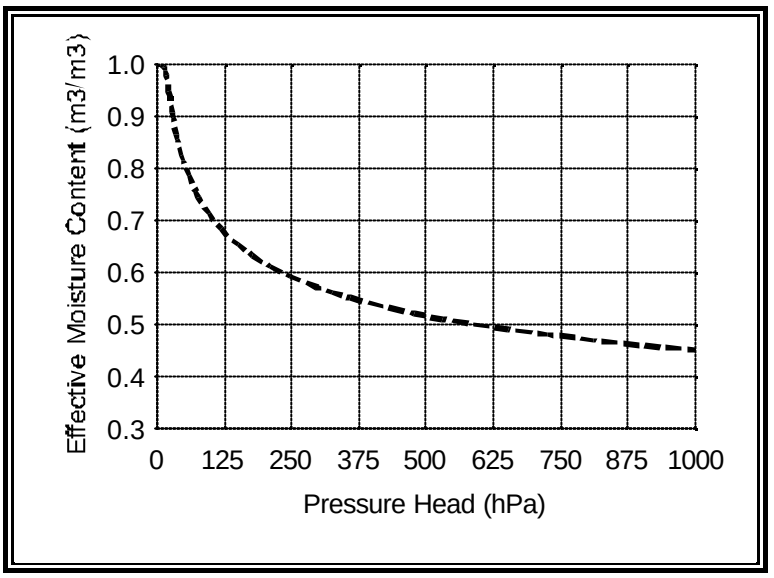

C: Pressure Head vs. Effective Moisture Content

Figure 5.17: Fitted hydraulic characteristics curves for site B based on simultaneously measured soil moisture and tension at 3 depths (30cm, 60cm and 100cm) during the study period.

To describe the hydraulic conductivity function of each site, the effective saturation value was then substituted into the Mualem - van Genuchten (1980) relationship defined as

$$K(q) = K_s K_r(q) = K_s S_e^{0.5}\left[1-(1-S_e^{1/m})^m\right]^2 \qquad (5.2)$$

where K_s and K_r are the saturated and relative conductivity function, respectively. The parameter m=1-1/n is obtained from the retention characteristic, and determines the shape of the conductivity function. Zhu and Mohanty (2003) observed that the Gardner and van Genuchten functions resulted in the most effective parameters amongst the models they compared. To calculate effective hydraulic conductivity $K(q)$, at least one measured value is needed as a matching point for K_s (Kasteel et al., 2000). The arithmetic average of the saturated hydraulic conductivity from measurements on the plot at the different site was used. This resulted in values of 15.8 $mmhr^{-1}$ for site A and 53.6 $mmhr^{-1}$ for site B, thus the hydraulic conductivity ratio between site A and site B is 3.4. This literarily implies that, there should be a scale factor of 3.4 in the difference

of the runoff response to rainfall events from the two sites, if spatial variability of hydraulic properties alone, could explain the observed differences. However, from the result of field observation did not show such scale of difference, and this further necessitates a better understanding of the effect of other factors on hydrological response.

5.5 Soil moisture dynamics

Soil moisture is another state variable for a range of hydrological processes and act over a variety of spatial and temporal scales (Hupet and Vanclooster, 2002). It is key among the factors that influence the partitioning of rainfall into infiltration and runoff. As has been shown in the previous sections, it is critical in the determination of effective parameters that describe the hydrological behavior of various catchments. The measured values of soil moisture, in the first 1000mm depth of soil; where the process of partitioning of rainfall into surface runoff, infiltration and deep percolation takes place is used for this analysis. Figure 5.16a and b presents the fluctuations in soil moisture at the various depths, compared with the rainfall depth in the major rainfall season of year 2002.

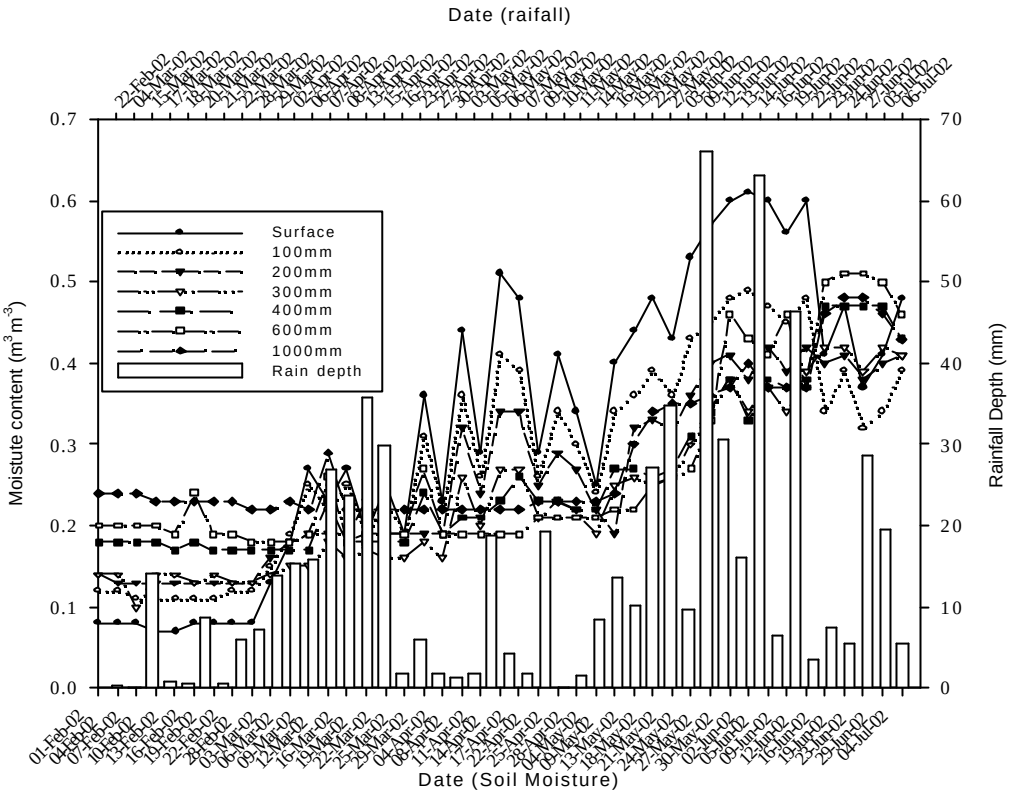

Figure 5.17a Profile soil moisture and rainfall dynamics for site A

The linear variation of moisture at the soil surface and at 100mm depth with the rainfall depth trend is clearly displayed at both sites. However, the deeper portion of the soil, i.e., depth 600mm to 1000mm, did not respond linearly to rainfall events until a sufficient build up of soil moisture around the beginning of June. The consistent fluctuation of moisture content from the surface to the 300mm layer is an indication of the impact of the soil evaporation process on soil water flux in the catchment. Despite the presence of macropores in site B, which have been seen to influence hydrologic behavior in the site, the response of the 600mm to 1000mm layer of soil to input from rainfall event is slower than the response in site A. Also the amount of water held in the top layers of site B is lower relative to the corresponding layers in site A. The moisture regime in the deeper layer are however very close. These observations clearly show that the macropores from earthworms activities in the site are concentrated in the top horizon. It also suggests the secondary effect of macropores enhancing evaporation losses from soil. Results from saturated hydraulic conductivity mapping of the different

sites also show that water movement in the topsoil layer in site B, is enhanced by the effect of macropores.

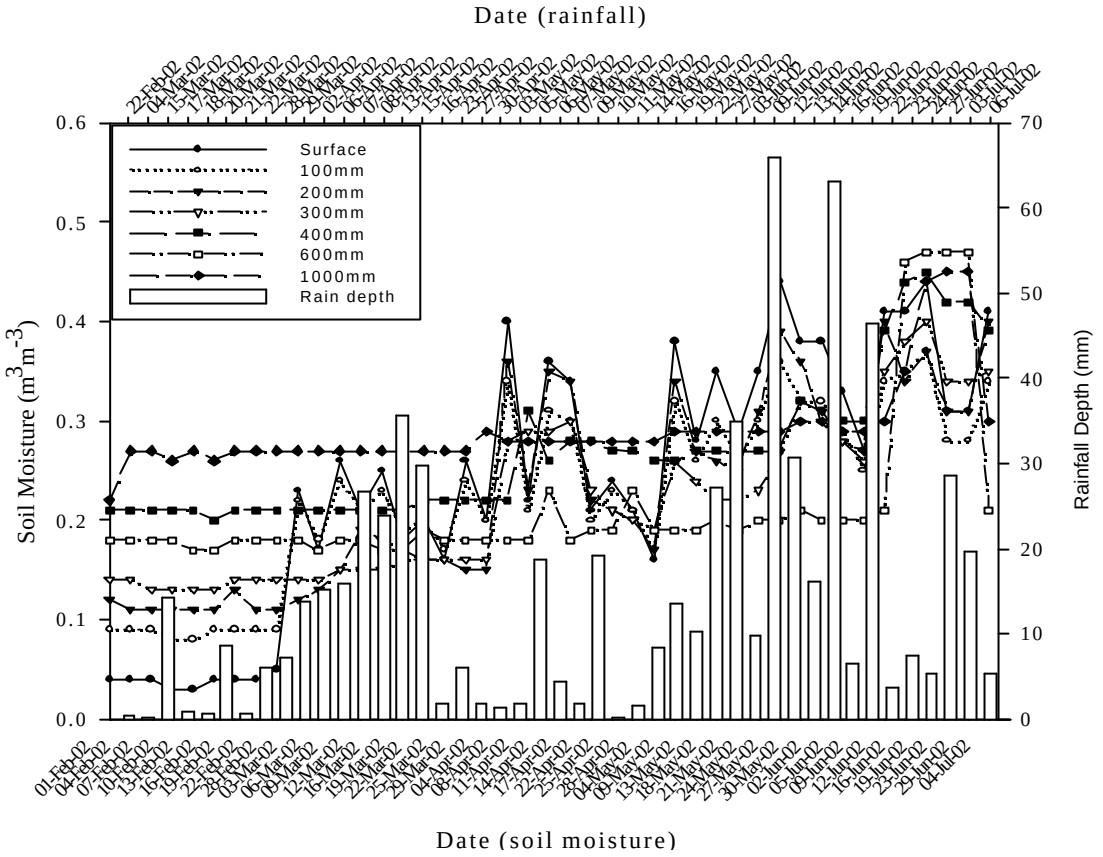

Figure 5.17b Profile soil moisture and rainfall dynamics for site B

Attempts to relate the surface moisture contents to surface runoff volume and the possibility of runoff events did not produce any significant results on both sites. This implies the dominance of the Hortonian rainfall process in the catchment. The initiation of such surface runoff depends more on the rainfall intensity, rather than soil infiltration capability. Fitzjohn et al. (1998) and Campbell (1989) also report similar observations and then concluded that the effect of initial surface moisture content is more important in the saturation excess overland flow where connectivity between source areas and the development of continuous hydrological pathway is critical in determining catchment runoff and erosion. It was, however, observed that the initial surface moisture content at both sites influences the delay period before the observation of runoff at the gutter.

The effect of macropores could also be clearly seen in the reduced volume of runoff discharge at site B. It is clear that due to the increase in infiltration capacity, the

quantity of overland flow percolating in transit increases, thereby reducing the volume of runoff that reaches the gutter. This impact is more pronounced in low and medium intensity rainfall events and in rainfall events with frequent pulses and prolonged recession phase. Léonard and Perrier (2001), in a model and field evaluation of the effect of macropores resulting from earthworm activities in Niger also made similar observations showing that small heterogeneities like macropores can have a high impact on the runoff process. This conclusion also lends credence to the argument of substantial if not domineering effect of temporal dynamics in overland flow routing, in explaining the scale effect in rainfall–runoff response.

5.6 Scale dependence of runoff response

Results from various analyses of the collected field data have revealed the dependence of various factors in the rainfall-runoff response system on the scale of observation. The enclosed area by a runoff plot or a catchment influences runoff coefficient, unit runoff discharge, ponding time, and in a way, the total volume of runoff recorded. Since all eight runoff plots used for the field observation in this study have the equal width, variation in response can be compared with the slope length in each plot. It is often termed scale dependency of scale effects. Scale dependence of runoff response has been varyingly attributed to spatial properties of soil, temporal dynamics of rainfall and temporal dynamics in runoff routing. Possible causes of scale effect in the rainfall runoff transformation process based on the analysis and interpretation of the observed data in this study are discussed in this section.

Scale dependency in rainfall-runoff processes is evaluated by comparing the ratios of runoff coefficient to the length ratio. Another method of evaluating scale effect is to compare the unit runoff discharge, with the ratio of the area the plots. The unit runoff discharge gives an estimate of the maximum yield of the runoff plot per unit area for an event.

In this study, the runoff coefficients (RQA_1, RQA_2, RQB_1, RQB_2) for all the individual events for the long plots (A_1, A_2, B_1, and B_2) and the runoff coefficients (RQA_3 and RQB_3) for the medium plots (A_3 and B_3) is divided by the runoff coefficients (RQA_4 and RQB_4) of the small plot (A_4 and B_4) for the corresponding event. The obtained values are compared with the corresponding length ratio. The

length ratio (LR) is defined as of the length of the short runoff plot (2m) divided by the length of the long runoff plot (18m) or the length of the medium runoff plot (6m). Thus $A_4/A_1 = A_4/A_2 = B_4/B_1 = B_4/B_2 = 0.11$, while $A_4/A_3 = B_4/B_3 = 0.33$. If RQA_1/RQA_4 or RQA_2/RQA_4 or RQB_1/RQB_4 or RQB_2/RQB_4 equals 0.11, or if RQA_3/RQA_4 or $RQB_3/RQB_4 = 0.33$; the different plot lengths generate the same absolute value of runoff. If any of these ratios is higher than the corresponding length ratio, the longer plots generate less runoff compared to the short plot for the event. Furthermore, if RQA_1/RQA_4 or RQA_2/RQA_4 or RQB_1/RQB_4 or RQB_2/RQB_4 or RQA_3/RQA_4 or RQB_3/RQB_4 equals one, there is no scale effect as both the long runoff plots and the short plots runoff the same proportion for the event. Literarily, the 'LR' is the minimum value that would be expected for any event (van de Giesen et al., 2000; Esteves and Lapetite 2003).

The results from both sites used in the study are presented in Figures 5.18a-d. Figure 5.18a and c show the graph of the ratio of the runoff coefficient for the twin-long plots at site, while the two-medium runoff plots are compared in b and d. The ratios of the coefficients are compared with the corresponding rainfall depth for the event in order to see the possible relationship in scale dependency and rainfall magnitude. The results show wide variability in all the four figures.

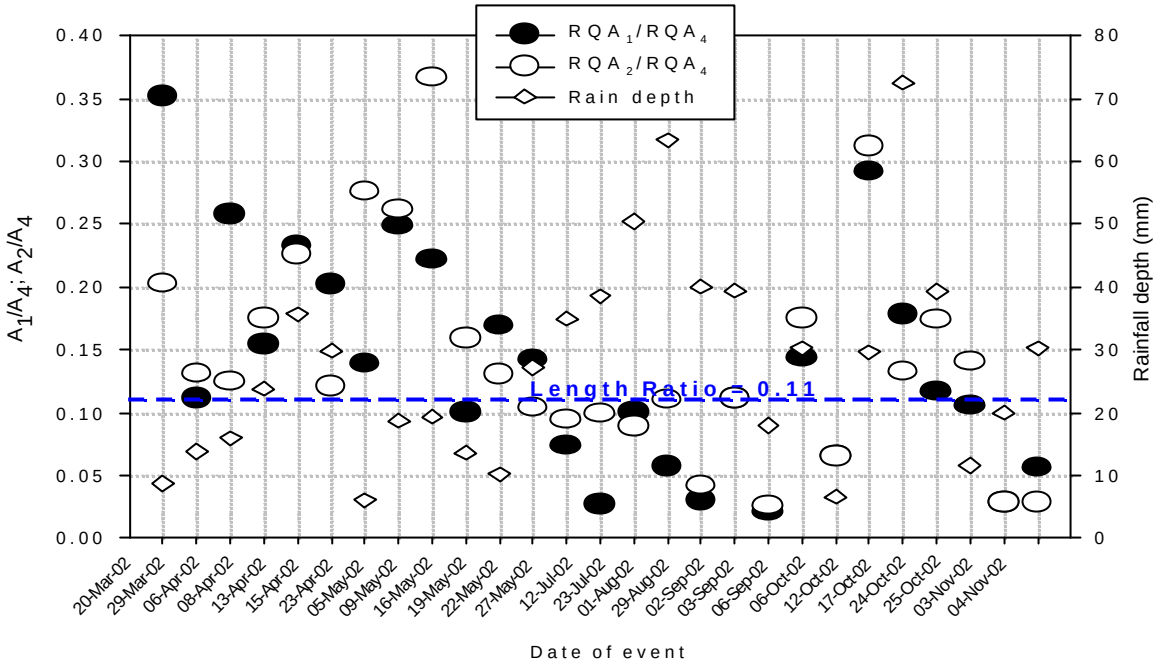

Figure 5.18a: Ratio of runoff coefficient for the long plots A_1, A_2 and A_4 in site A

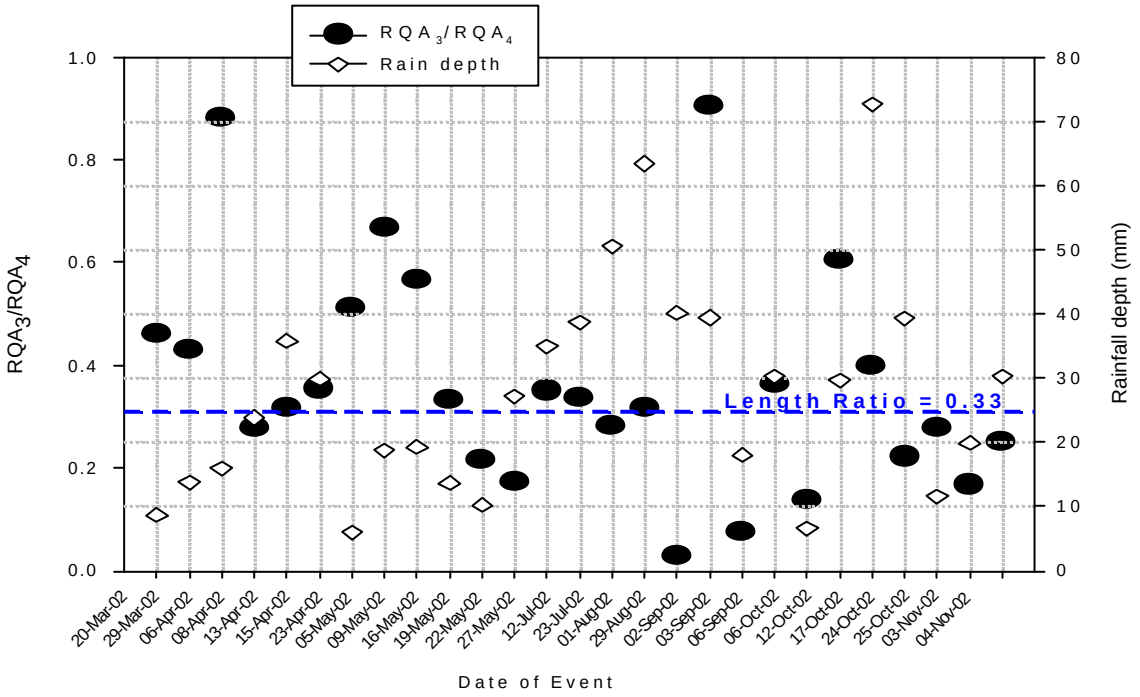

Figure 5.18b Ratio of runoff coefficient for the medium A_3 and short plot A_4 in site A

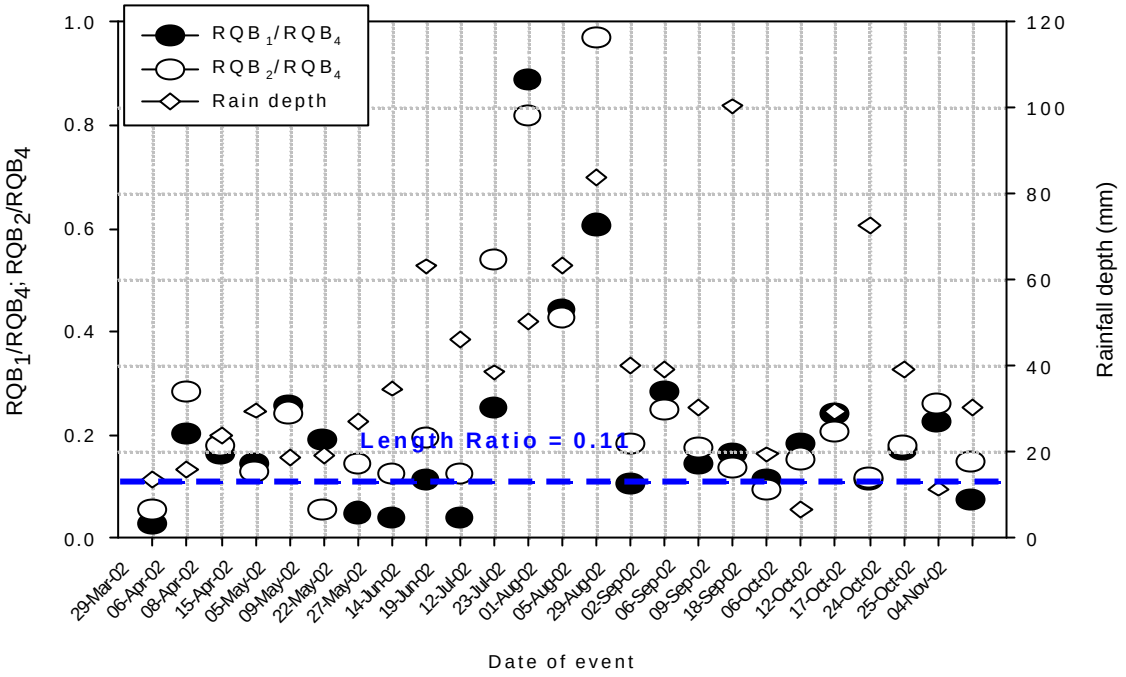

Figure 5.18c Ratio of runoff coefficient for the long plots B_1, B_2 and B_4 in site B

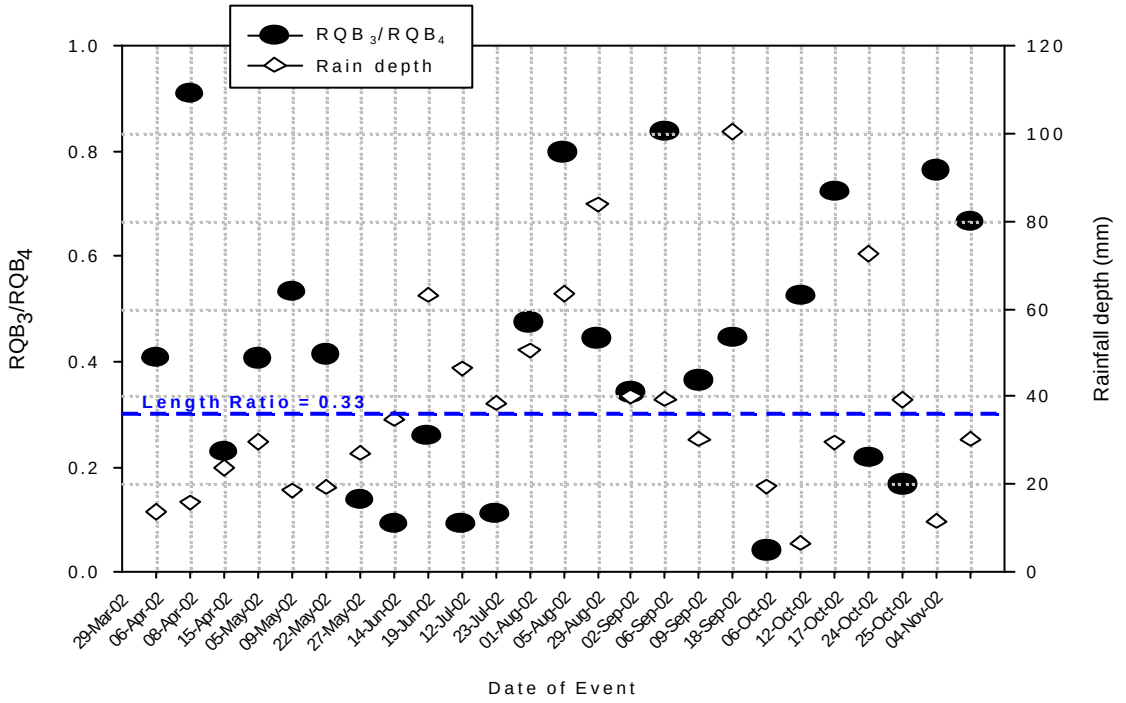

Figure 5.18d Ratio of runoff coefficient for the medium B_3 and short plot B_4 in site B

For all the runoff events in the season, there was no case in which, the proportion of runoff generated in the any of the two different plots sizes is equal;

implying varying degrees of scale effect, in all the runoff events. In a few number of events, the ratios of runoff coefficients are equal to the length ratio. However as observed in the studies by van de Giesen et al. (2000) and Esteves and Lapetite (2003), there were also some substantial number of events, in which the ratios of the runoff coefficients were less than the 'theoretical minimum value' i.e. the length ratio. For the runoff events monitored at site A, about 38% of the events record a coefficient ratio less than 0.11 and 44% of the event records coefficient ratios less than 0.33 (for the long and medium plot respectively). At site B, only 17% of the events return the coefficient ratios less than 0.11 and 38% of the event record a coefficient ratio less than 0.33. This indicates that, as the length ratio increases, there is more probability of recording events with the ratio of the coefficient being less than the length ratio. There is no consistent trend in the effect of the rainfall depth on the quotient of the runoff coefficient. However it is observed that in most of the events, with low rainfall depth, the quotient the runoff coefficients are generally higher than those for events with higher rainfall depths.

Scale effect as observed in this field study is strongly linked to spatial variability in surface storage and hydraulic conductivity in the runoff plots. Comparatively, the degree of variation is wider in long plot than in small runoff plots. The effect of spatial variability in infiltration properties is clearly displayed the site B, and that explain the high ratio of runoff coefficient. Scale effect induced by spatial variability in infiltration properties and surface storage properties are more conspicuous in events with small runoff volume and during low intensity events. As the volume increases, the difference in the ratios reduces. Low intensity event translate to low velocity of travel of surface runoff, since the driving force (rainfall intensity) is minimal, thus in the process of traveling down to the gutter, the differential level of infiltration, results in change in magnitude. The length of slope determines the infiltration opportunity and also determines the possible changes in surface storage. During such event, the unit runoff discharge of the long plot is lower than that of the short plot, because, only a small portion of the long plots close to the gutter directly contributes to runoff collected. Therefore, the effect of spatial variability in infiltration and surface storage changes are only effective because of the temporal dynamics during runoff routing.

Conclusively, the rainfall runoff transformation processes in the Volta basin as in several other tropical catchments exhibit a very weak linearity. This has resulted in a situation, in which results from field observation are inconclusive but rather formulate the basis of further research need, for adequate representation of the process physics. This will facilitate adequate diagnosis of the processes, unlike the lumped effect that always results from field measurements and provide the basin for upscaling of results. In answering some of those questions, a solution was obtained for the full hydrodynamic equation, which has been widely shown to represent the surface runoff process effectively (Fiedler and Ramirez, 2000; Esteves et al., 2000, Zhang and Cundy, 1997). The next chapter presents the validity of the solution in the case of surface runoff process in the Volta basin and investigates the effect of the various components of the rainfall-runoff response system with a view to identifying the optimal parameters that influence scale dependency in the system.

6 MODEL RESULTS AND DISCUSSION

6.1 Model implementation

The model is written as a FORTRAN program. The program requires two types of input parameters. The general input parameters (table 6.1) include the rainfall data file in cumulative format, the sorptivity value depending on soil moisture at the surface and in the first 300mm depth, the saturated hydraulic conductivity data file (allowing the definition of values on all the grid points), the terrain data file (allowing the definition of values on all the grid points) the total event time in seconds, the discretized time interval (including time to summarize the output and write into output files), the initial flow depth, the initial flow velocity in x and y-directions, the diffusion factor, number of points for observation, the coordinates of the observation points (in x and y) and the open / close boundary specifier. The possibility of defining the elevation at all the grids allows for the use of the model on complex terrains. Since it is possible to define the saturated hydraulic conductivity at all the grids, it is easy to study a field with spatially varied hydraulic properties.

The runoff plot or hillslope segment parameters include the plot length and width, slope, the vegetated (canopy) fraction, the type of surface (i.e., rough, flat, or inclined), and the friction factor (depending on average rainfall intensity, surface characteristics and vegetation type and age). By specifying the grid spacing (equal for x and y), and the number of grid points in the x and y directions, a user is able to change the runoff plot (hillslope) length and width.

The model output for each runoff plot (hillslope) segments includes the velocity of flow in the x and y-direction, the depth of flow, the infiltration rate, the net inflow rate. All these values are averaged over the user-defined time step; therefore a small time step will ensure the observation of very minute detail. The output variables are used to generate graphical outputs of discharge in $cm^2 sec^{-1}$, depth of overland flow in cm, interactive infiltration during the event in $mmhr^{-1}$ and, the rainfall intensity in $mmhr^{-1}$. Other graphical outputs of the model are, the hillslope (runoff plot) terrain, the flow vector and its values in contour, the flow vector over the terrain, the velocity vector and the speed contour and the flow vector along a single column (grid interval) and across the selected observation points. The graphical outputs are produced with

MATLAB software (Mathworks, 2000) using the plotter programs, written for the study purpose.

Initial infiltration into soil during a rainfall event is regulated by the prevailing moisture conditions among other factors. In reality, the antecedent moisture conditions in a hillslope represent a sequence of rainfall, drainage, and redistribution conditions, and therefore it is extremely difficult to generalize. However, moisture content is known to fluctuate more at the surface and in the first 300mm profile. Consequently, the sorptivity value is defined based on the measured soil moisture content at the surface and in the 300mm profile. In simulation cases with uniform hydraulic conductivity, a value between the range of the effective hydraulic conductivity for the two sites, determined from the van Genuchten-Mualem model (see 5.4) is used. The use of a constant hydraulic conductivity eliminates spatial variability in hydraulic properties. Such scenarios facilitate the comparison of the effect of temporal factors.

In accounting for vegetation interception, the rainfall volume per tip from the tipping bucket rain gauge is reduced by the canopy cover fraction, which depends on the vegetation density. Vegetation density is obtained from the average leaf area index (LAI) measurements of representative vegetation in the catchment. It is well correlated to the period since the onset of the rainy season, since the active vegetation pattern in the catchment and other parts of the Volta basin has a well-defined cycle. The cycle is regulated by the widely practiced bush burning in the dry season (December through February) and the characteristic-cropping pattern. The reduction factor is selected based on the modified Gash model for multiple cropping (van Dijk et al., 2000).

6.2 Model evaluation and testing

The model's performance was evaluated in two ways. In the first method, we compared the model output with observed measurement for a selected event. Two performance criteria were defined as used in the study by Esteves et al. (2000) for the evaluation. The accuracy or otherwise of the runoff volume is quantified, using the relative error (R_e) calculated from the relationship:

$$R_e = \frac{V_{sim} - V_{observed}}{V_{observed}} \times 100\% \qquad (6.1)$$

A low value of the percent relative error indicates that the simulated and observed volume is close. A negative value of R_e indicates that the runoff volume predicted by the model is lower than the observed and vice-versa. Also the ability to reproduce the observed runoff hydrograph is evaluated using the coefficient of efficiency (C_e) defined by Nash and Sutcliffe (1970) as:

$$C_e = 1 - \frac{\sum_{i=1}^{n} (Q_i - \hat{Q}_i)^2}{\sum_{i=1}^{n} (Q_i - \bar{Q})^2} \qquad (6.2)$$

where Q_i is the observed runoff discharge at time i; $\bar{Q}$ is the mean runoff rate of the particular rainfall-runoff event; $\hat{Q}_i$ is the runoff discharge predicted by the model at time i; and n is the number of time step in the computation. C_e =1, indicates a perfect agreement between the model predicted hydrograph and the observed hydrograph for the event under consideration. It must however be mentioned that this is rarely possible in view of certain assumptions often used in model simulation runs which often do not adequately represent field conditions. The more the value of C_e slides away from 1, the lesser the goodness of fit, and a negative value implies that the observed mean is a better estimate than the simulated value (Esteves et al, 2000).

One high intensity event was selected for this validation. Simulations experiment using the rainfall intensity data for the event was conducted on a long (18m x 2m) and a short (2m x 2m) runoff plot. The bed slope and the friction slope are calculated from the microtopography data, while the Darcy–Weisbach formula was used to estimate the friction slope. A time interval 0.005s was used for the simulation. A uniform vertical (downslope) and horizontal (cross-slope) grid spacing of 10cm was used. The 10cm grid spacing is selected to conform with the measured terrain data resolution for the runoff plots. Consequently, the small runoff plot is discretized into 400 girds, and the long plot to 3600 grids. The surface terrain configuration of the runoff plots for the simulation is based on the field measurement of the surface microtopography described earlier. The measured data were transformed with some limited smoothing into digital terrain models for the corresponding plots, using the contouring features of the Surfer package (Golden software, Inc. 2000). This limited smoothening was necessary to eliminate spikes capable of inducing instability in the

numerical process (Tayfur et al., 1993; Fiedler, 1997). The terrain model (surface plot) of the measured soil surface and the statistical properties are presented in figures 6.1 and in Table 6.2.

Table 6.1 General input parameters for surface runoff simulation model

Parameter	**Description**	**Value**
Rainfall	Temporally dynamic events	Based on Tipping bucket measurement
Hydraulic conductivity	Can be defined at all grid in a runoff plot or hillslope	Constant of Spatially varied
Sorptivity	Determined based on initial moisture content	90mm/hr used in most simulation
Slope angle	Field inclination	Based on plot geometry, but 0.05 was used for inclined terrain
f (based of rainfall intensity range and surface condition)	Account for friction effect of surface and raindrop	Based on modified DW equation
Rainfall duration	Total time of rain event	Event based
Rainfall volume per tip	Reduced volume determined after the Gash model has been applied	Vale depends on vegetation density
Initial flow depth	Necessary to prevent collapse of simulation	0.001cm used in all simulations
Initial velocity	Flow velocity in both directions	0.0 used in all simulations
Terrain condition	To define the type of surface for simulation i.e., Smooth (flat), Smooth (inclined) or rough	Based on experiment

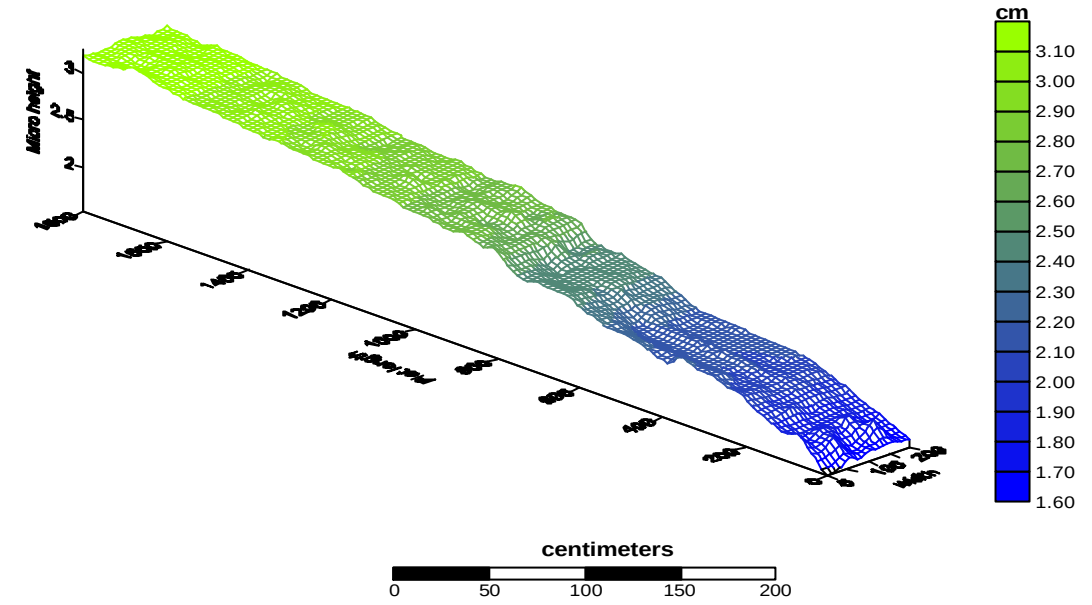

a) Long plot (LP)

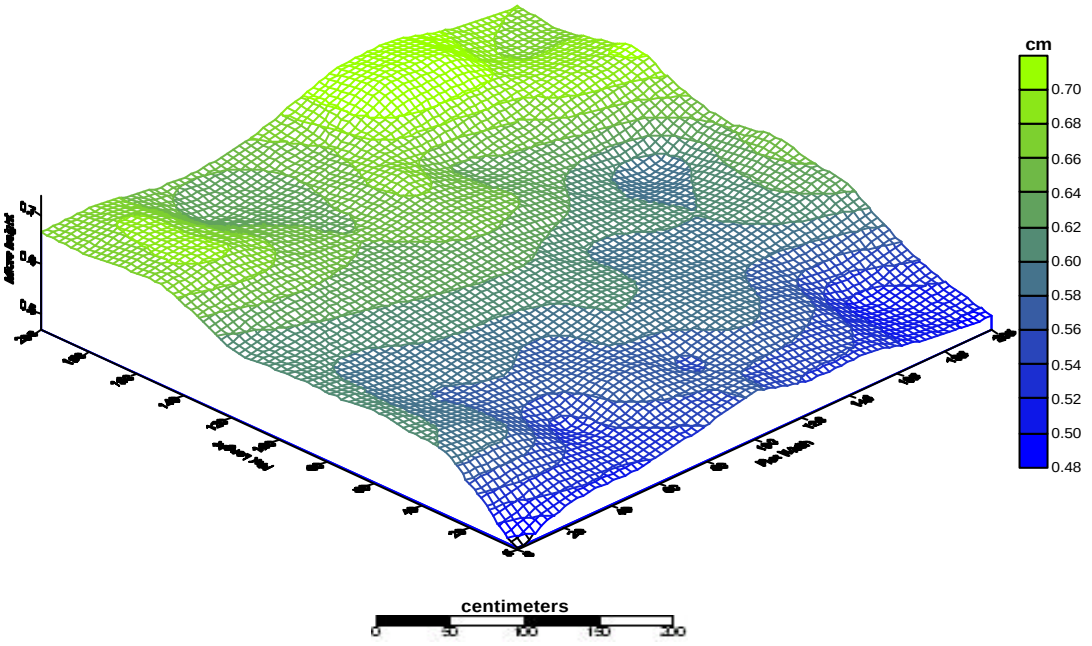

b) Small plot (SP)

Figure 6.1 Measured microtopographic ground surface of the long and short runoff plots used for simulation

Table 6.2 Statistical properties of the plot microtopography

	Z_{min}	Z_{max}	Z_{mean}	Z_{med}	Z_{STD}	Z_{cv}	Z_{skew}	ZX_{slope}	ZY_{slope}
LP	1.549	3.244	2.593	2.720	0.442	0.171	-0.394	1.0°	5.1°
SP	0.466	0.736	0.615	0.613	0.053	0.085	-0.088	2.8°	5.4°

Note ZX = slope in x-direction; ZY = slope in y-direction.

Figure 6.2a and b present the rainfall hyetograph, the simulated and the observed runoff on two plot sizes, for the event used for validation. The agreement in trend with data points indicates that the developed equation in chapter 4 can describe the surface runoff process observation very well. Comparison of the hydrographs suggests that the magnitude of simulated discharge is slightly lower during the pulse period in the event, and also in the falling limb during the second cycle of the rainfall event. This was, however, evened out by the slight overestimation in the rising limb and at the peak periods. Detail inspection of the time before the onset of runoff in both plots sizes also showed that the simulated time before the onset of runoff is consistently less than the observed. This consistence difference possibly emanate from the use of an average effective saturated hydraulic conductivity value in the simulation. The average effective saturated hydraulic conductivity is obviously less than the actual saturated hydraulic conductivity from the field measurement. The assumed value of sorptivity may also influence the delay time in the simulation. A detailed analysis of the performance based on the defined criteria relative error *(R_e)* and coefficient of efficiency *(C_e)*, show that the model performance is satisfactory and efficient. With an absolute value of less than 12% for the two plot sizes; the model predictions could be described as a very good representation of the observed process. The summary of simulated and measured values of maximum runoff intensity, total runoff duration, and relative error and efficiency for the different plot sizes, are presented in Table 6.3. This is representative of the model performance for complex (high intensity over short period) rainfall events commonly associated with tropical rainstorms. It also provides the platform upon which the understanding of the various complex process associated with the rainfall-runoff transformation process in the tropics can be evaluated based of the developed model and its solution.

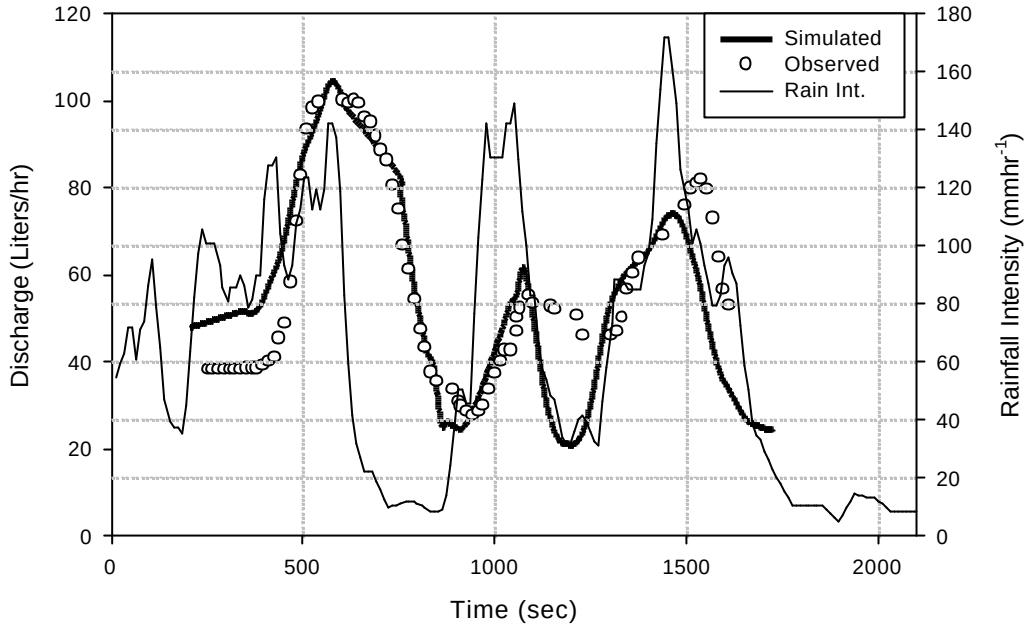

Figure 6.2a Comparison of observed and simulated discharge on the short plot (SP)

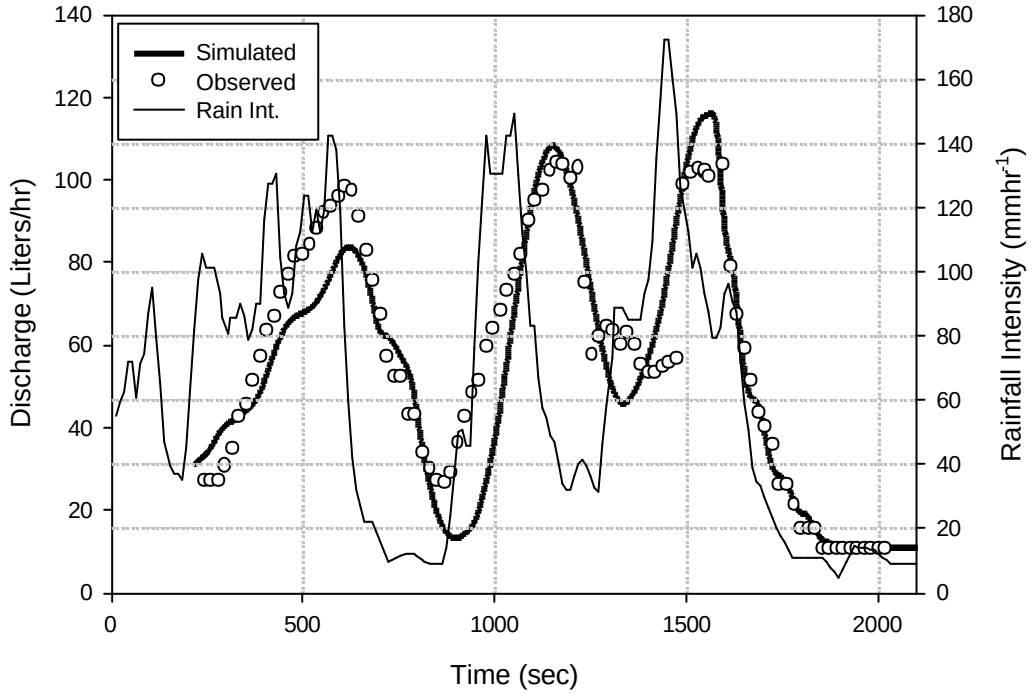

Figure 6.2b Comparison of observed and simulated discharge on the long plot (LP)

The second way that the model was evaluated was to compare in a scatter plot, the simulated and observed runoff intensity at some selected equivalent times (a time

simultaneously or very closely recorded in both the simulated and observed hydrograph) in the event hydrographs. For the hydrograph of the short plot (2m x 2m), Eighteen equivalent times were randomly selected, while for the hydrograph of the long plot (18m x 2m), Thirty-two points were randomly selected. Figure 6.3a and b present the resulting scatter plot, which was fitted with the linear equation appropriately displayed. For the short runoff plot, the coefficient of determination is 0.85, while for the long runoff plot; the coefficient of determination is 0.89. The value of r^2 in both hydrographs also reflect the match in both simulated and observed hydrograph and show good agreement of the observed and simulated hydrographs for an individual event. This agreement indicates that reasonable inferences could be drawn from the model outputs.

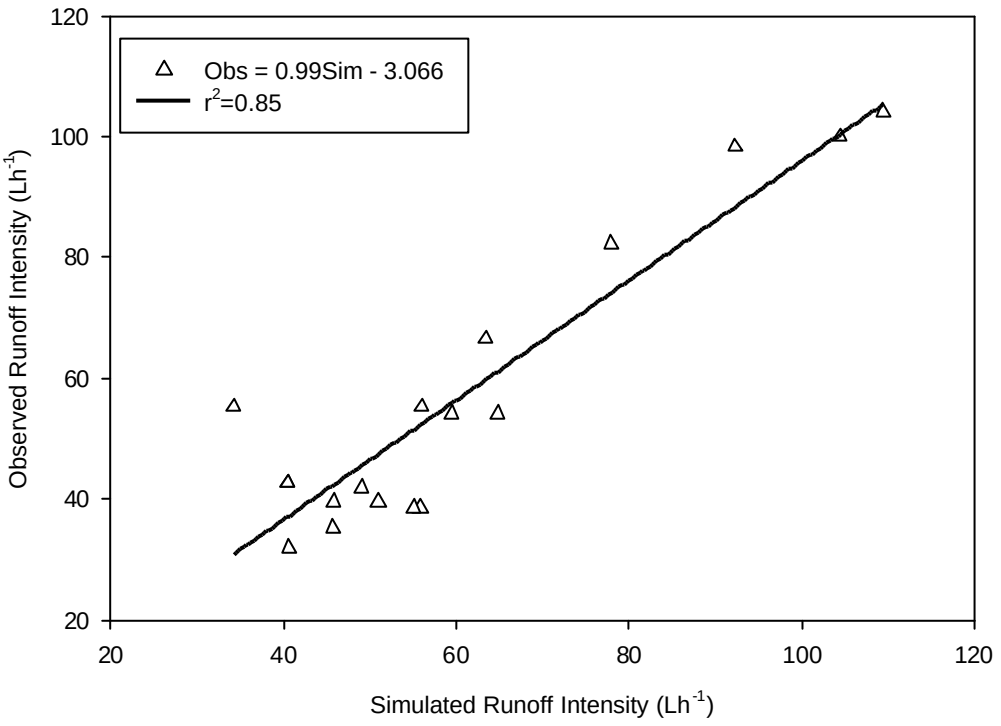

Figure 6.3a Relationship between observed and simulated runoff intensity at 18 randomly selected equivalent times for the short plot (SP)

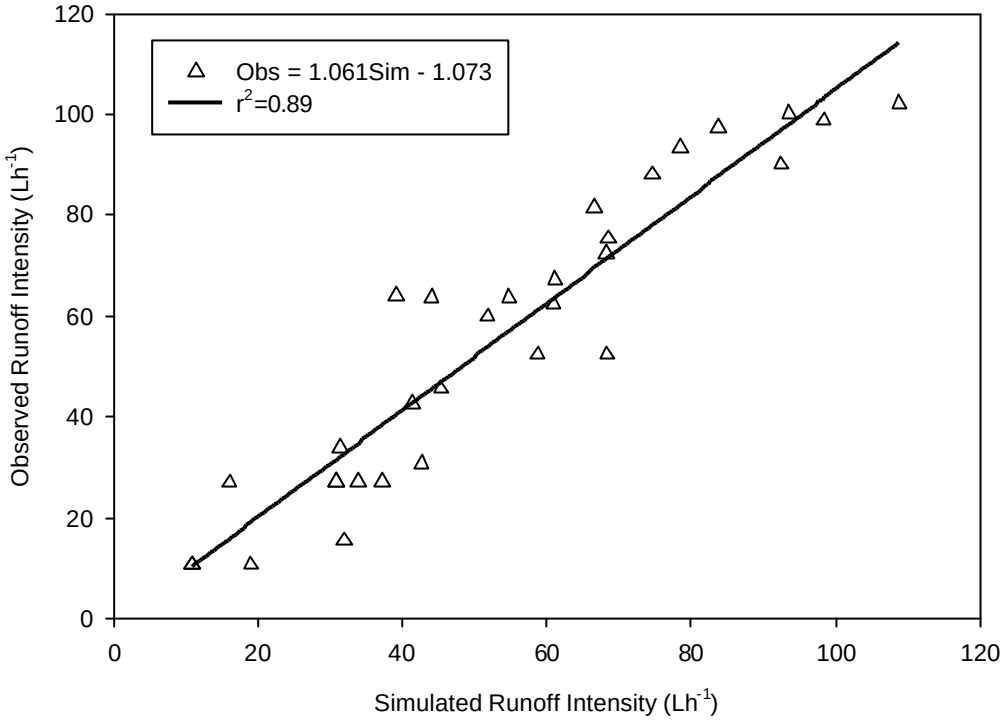

Figure 6.3b Relationship between observed and simulated runoff intensity at 32 randomly selected equivalent times for the long plot (LP)

Table 6.3 Summary results of validation event for the two plot sizes

	Q_{sim} max	Q_{sim} mean	Q_{obs} max	Q_{obs} mean	N	R_e	C_e
SP	110	56	104	59	14	-11.5	0.89
LP	119	54	104	57	28	4.76	0.88

Summarily, the model outputs mimic the relationships observed in the field study adequately. The complex shape of the observed hydrographs is well represented by the model, and the different timings (time before the onset of runoff; recession time at the end of rainfall event; the runoff duration) are fairly described. The rising limbs, recession limbs and the pulse (transient) moments of the observed runoff hydrographs have been well replicated by the model. The model equally captures the effects of pulse moment of rainfall on runoff response. The dynamics of rainfall intensity during an event are well reflected in the observed and simulated runoff hydrograph. Therefore it is suffice to use the model result for further investigations of the rainfall-runoff process in the Volta basin and other tropical climate with similar catchment properties.

6.3 Simulation experiments

Following the satisfactory performance of the model in reproducing close to the field observations, several numerical experiments were performed in line with the overall project objectives of evaluating the effect of various hydrological state variables on the runoff response to selected rainfall events. The different scenarios simulated were selected to reflect possible field conditions, but some scenarios are only hypothetical, but are necessary for detail understanding of certain critical parameters in the rainfall-runoff process. It should, however, be noted that in such hypothetical cases, the model parameters are selected based on observed values.

It is also important to emphasize here that the purpose of applying a physically based numerical model in this simulations study is to gain insights into the interactions between heterogeneities in catchment structure and hydrologic processes, rather than to make precise predictions of runoff discharge from the plots. The distributed-parameter approach permits several structural attributes to be varied in a controlled fashion, including the distribution of soil hydraulic properties, surface feature and slope geometry.

Generally, the discharge rate and magnitude of surface runoff intensity are most sensitive to rainfall rate; therefore two contrasting rainfall intensity events were used in the model simulation. The events were chosen to represent two of the possible rainfall event scenarios, i.e., high intensity (henceforth referred to as event A), and low to medium intensity (henceforth referred to as event B) based on the observation from the record of rainfall intensity in the basin for the 2002 season. The average slope angle for all the runoff plots from the measured topographic data was 5°, therefore inclined terrains used in the simulations trials were oriented to that same angle, to establish a basis for comparison.

Most simulations on rough terrain configurations are performed with the medium runoff plot (figure 6.4). The statistical properties of the medium plot microtopography are presented in the table 6.4. Some other simulations are implemented on the small runoff plot sizes and long runoff earlier described (figure 6.1 and table 6.3), since the responses from all the plots sizes are analogous. A common point close to the gutter was used to monitor point interactive infiltration, flow depth and the discharge in most of the simulation, and exceptions are clearly stated. There is

also a possibility to view the predicted flux of all of these parameters at any selected time, along and across the observation point column and row. In all the simulation experiments, a uniform depth of 1mm was used as will be noted in the output contribute to flow depth and discharge even at the moment when there is no flow. The following sections discuss the results from the various simulation experiments and provide some basis for better understanding and appreciation of the field experiment results, enhancing a detail discussion and conclusions from this study.

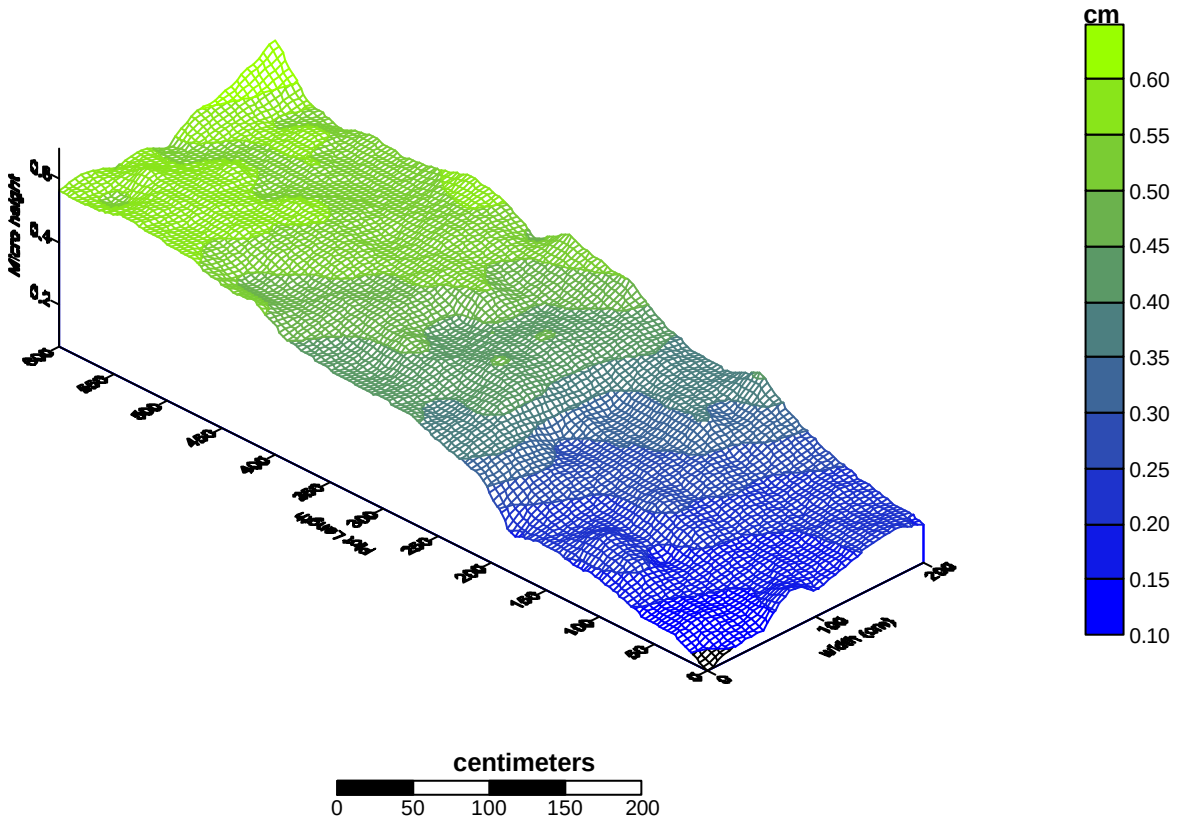

Figure 6.4 Measured microtopographic ground surface of the medium runoff plot used for simulation

Table 6.4 Statistical properties of the the medium runoff plot microtopography

	Z_{min}	Z_{max}	Z_{mean}	Z_{med}	Z_{STD}	Z_{cv}	Z_{skew}	ZX_{slope}	ZY_{slope}
MP	0.066	0.699	0.408	0.442	0.141	0.345	-0.479	3.8°	4.8°

6.4 Scale effect

The analysis of runoff coefficient and the unit runoff discharges from the field data showed consistent trend of decreasing coefficient and unit runoff discharge with

increasing plot sizes or better still, with increasing slope length (since all the plots have uniform width). Consequently, simulation experiments with the different plot sizes (slope length) were implemented to investigate a possible repeat of the trend and possibly isolate the causative factor(s). Alongside with the three slope lengths used for in the field observation, i.e., 2m, 6m and 18m, a simulation run using a slope length of 200m was implemented, for event A to appraise the trend with increasing length of slope. Both the high intensity and low-medium intensity events were used for the evaluation.

Figure 6.4a and b present the cumulative discharge per unit plot length, for the four plot sizes (slope length), under the two rainfall events. The figures clearly reveal the effect of slope length and rainfall pattern on the runoff discharge. Cumulative discharge increases with plot size, but the discharge per unit length decreases exponentially. The shape of the cumulative discharge curves is influenced by the pattern of the rainfall. For example in event A, the number of flattened portions (constant or no discharge) is dependent on the number of pulses recorded in the event (no of peaks). At such pulse moments, the slope length actively partitions infiltration, run-on and runoff depending of the microtopography.

The responses under event B accentuate the effect of the magnitude of rainfall on runoff processes. For most part of event B, there was no discharge due to the low value of rainfall intensity. During low intensity events, the discharge volume and rate is reduced by the increased redistribution and infiltration opportunity for overland flow. The velocity of flow depends among other factors on the kinetic energy, which linearly varies with the rainfall intensity. Since the intensity is low, most of the rainfall will infiltrate, and a large proportion of overland flow also percolates because of the low travel velocity. During low intensity rainfall event, there are always unconnected patches of runoff, and only patches connected to the channel contribute to discharge. However, during high intensity event, there is an increase in opportunities for the patches to be connected, hence the path length of runoff increases, and consequently the volume of runoff is increased.

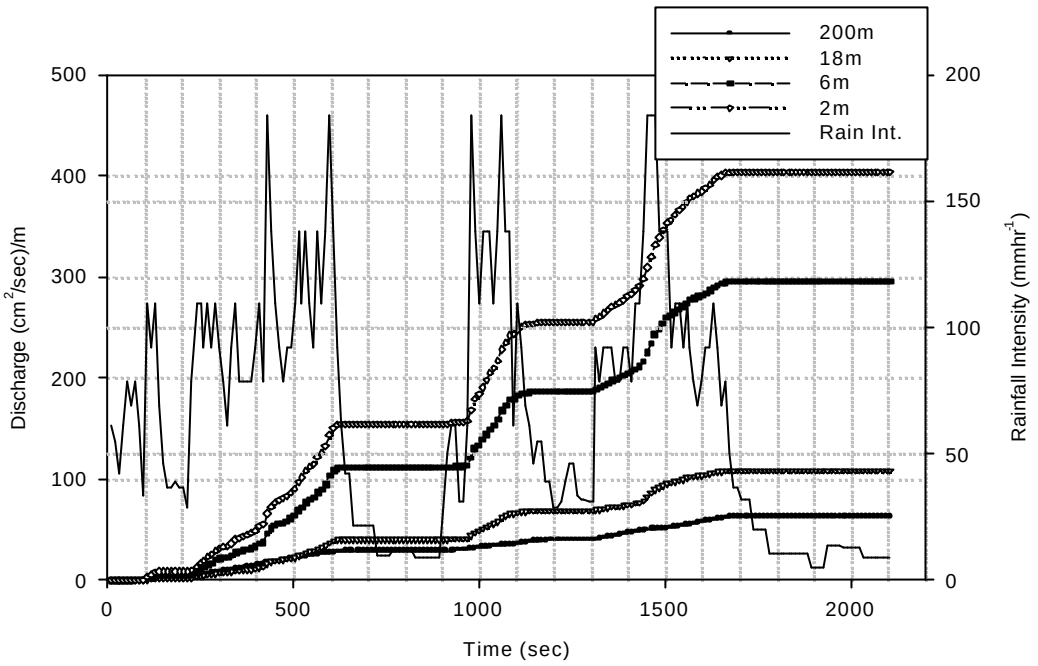

Figure 6.4a Cumulative discharge per slope length for event A (high intensity)

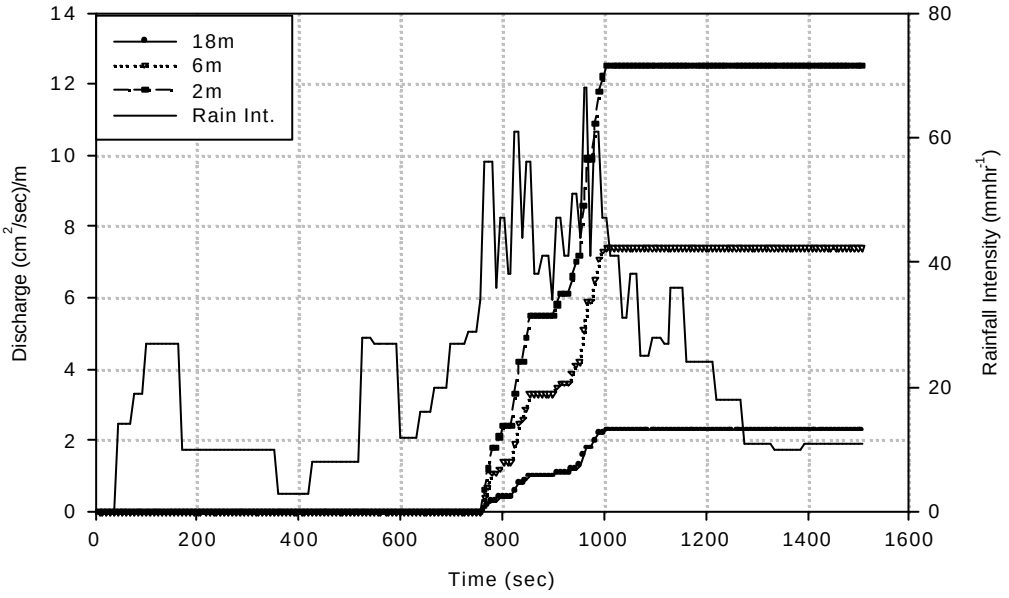

Figure 6.4b Cumulative discharge per slope length for event B (low intensity)

Despite the low volume of discharge, the effect of slope length is evident with the low intensity event similar to the observation with high intensity rainfall. Inspection of the figures show that the slope of the cumulative discharges are steeper during low intensity event, and is drastically reduced as the slope length increases. This observation

is explained by the redistribution of runoff on long slope length during low intensity event. The redistribution affects the discharge rate during low intensity events and also at the pulse moment in an event, particularly on plots with rough surface (microtopography). On short slopes, most of the runoff paths have a better chance to link up with the gutter, due to their proximity, and will therefore contribute to the outflow, which increase the discharge per unit length.

Table 6.4 presents the runoff coefficient under the different plot lengths for the two events. The high intensity event consistently have higher runoff coefficient than the low intensity event on all the plot sizes. Figure 6.5 shows the plot and fitting of the runoff coefficient with power equations. It is interesting that for both events; the runoff coefficient decreases with slope length exponentially, similar to the observation in the field experiment. The simulation results corroborate the results from the field observation in agreement with other previous studies (Kirkby et al., 2002; Yair and Kossovsky, 2002; Joel et al., 2000; van de Giesen et al., 2000). The graph also showed that the combination of the two different intensity ranges significantly reduces the coefficient of determination of the power equation, implying that rainfall factor could explain the difference in magnitude of scale effect reported in several studies. This is apparent since all hydraulic variables were kept uniform; as such effect of spatial variability of soil hydraulic properties is eliminated. It also reveals very clearly, that the difference in response by different plot sizes is closely related to the temporal pattern of rainfall intensity and slope length. Runoff coefficient is proportional to the rainfall magnitude. Close examination of the within storm (event) dynamics of the runoff coefficient shows marked fluctuation. The runoff coefficient dynamically changes with rainfall intensity and rainfall duration. However, the fraction of the difference from smaller to longer plot length is more obvious than at lower rainfall intensity. Several factors as have been observed could have in one way contributed to this observation, but a very dominant factor is the loss in momentum of the runoff, during travel time from upslope to the outlet. This is clear, since setting the saturated conductivity at all grid points to the same value in all the simulation eliminates all spatial variability in hydraulic properties.

Table 6.5 Runoff Coefficient for the two-events with different slope lengths

Slope Length	Event A	Event B
200m	0.069	0.017
18m	0.095	0.023
6m	0.271	0.084
2m	0.412	0.193

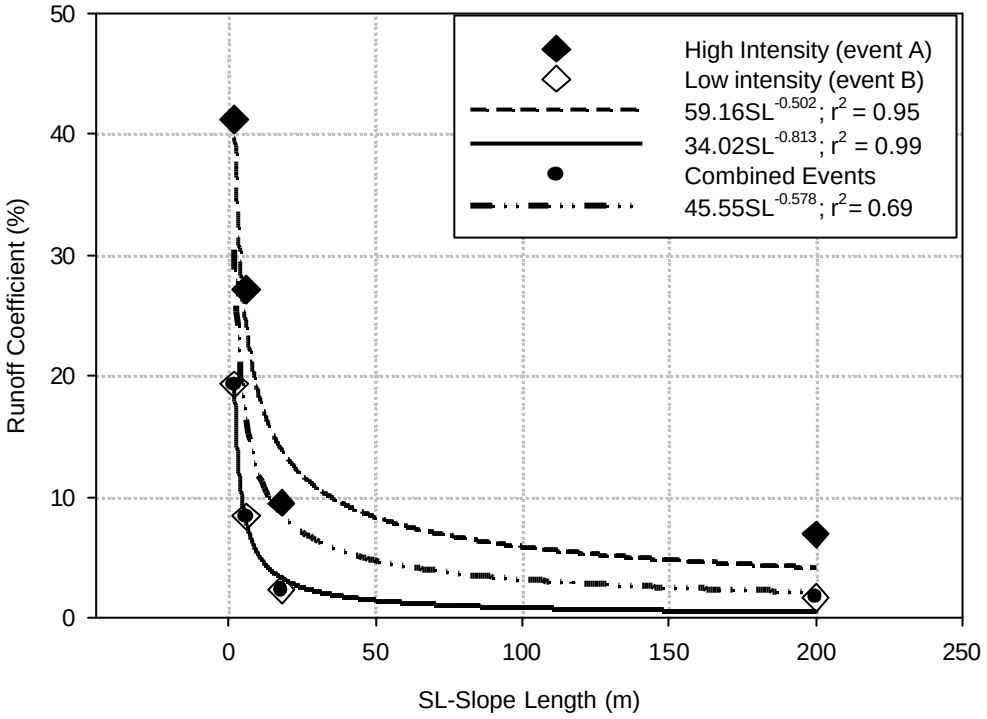

Figure 6.5 Relationship between runoff coefficients and slope length

To elucidate on momentum change during travel, a second series of simulations using the flat plane terrain and the inclined surface were implemented. The use of a flat surface ensure that the effect of slope will be completely eliminated, while the use of inclined terrain is to determine the response on the slope used for runoff studies, but with a plane surface. This eliminates any influence of surface microtopography. Figure 6.6 presents the result on a smooth-plane terrain. The figure show that the length of slope affect runoff coefficient, even on flat terrain. Scale effect is more conspicuous on such terrain, since the velocity of flow is significantly reduced. It also shows that the response is affected by the rainfall intensity pattern. The results

for the inclined surface also concur with the observation on both rough and flat-plane terrain.

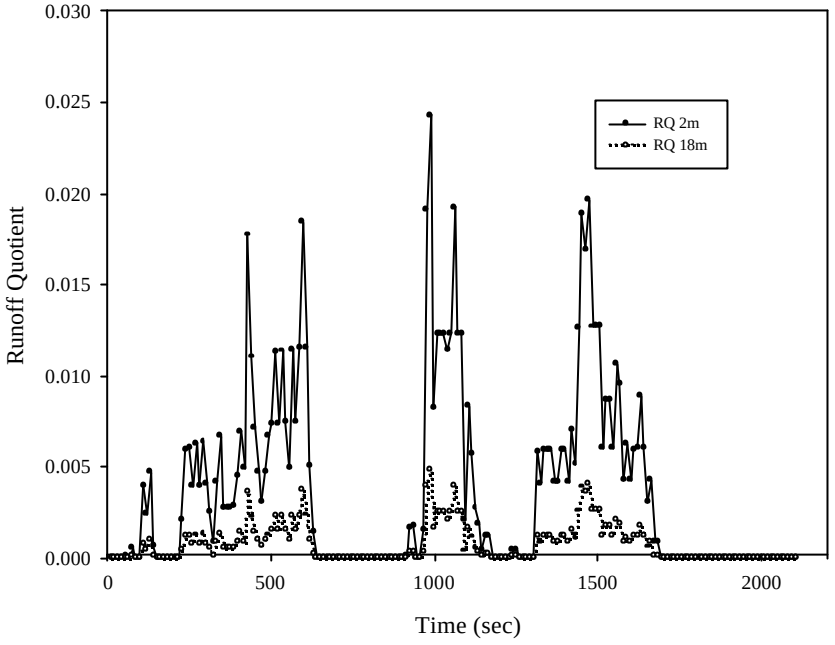

Figure 6.6 Variation in runoff coefficient on a flat plane for two-slope length

6.5 Spatial variability of soil hydraulic properties and surface runoff process

Spatial variability of soil hydraulic properties has been cited in a number of studies as the basis of the observed differences in runoff response using analytical or model-based evaluation. But as noted by Woolhiser et al. (1996), the different process of simplification of the routing model has limited the application of the results. Another limitation of most of the model used for such analysis is the failure to couple infiltration process. Since the developed model in this study can better take care of most, if not all, of observed limitations in previous studies, it is imperative to investigate the effect of spatial variability of infiltration and other hydraulic properties on runoff discharge. Three possible scenarios were simulated on the medium size plot, using both high and low intensity events data. In the first experiment (**case A**), a linear increase in saturated hydraulic conductivity downslope was simulated. In this scenario, the K_{sat} value is increased by 3% at every grid point along the flow direction (downslope), such that, at the end of the plot, where discharge is monitored, the final value of K_{sat} is 171.6mm/hr. Thus, the average hydraulic conductivity is 81.5mm/hr while the standard deviation is

41mm/hr. An inverse of this linear variation was used for the second experiment (**case B**), such that, the K_{sat} reduces downslope from a maximum of 171.6mm/hr at the plot upslope.

For the third scenario (**case C**), the measured saturated conductivity data for the medium plot at site B i.e., (B_3) is used to represent random variation in K_{sat} value within a plot. The contour map of the different distributions of K_{sat} is presented in Figure 6.7. The contour map shows that the upper and the lower limits of the hypothetical linear variations in the study could be observed within the plot. The three cases were used to study the dynamic effect of infiltration opportunity, as limited by a shrinking or expanding area from which infiltration can occur.

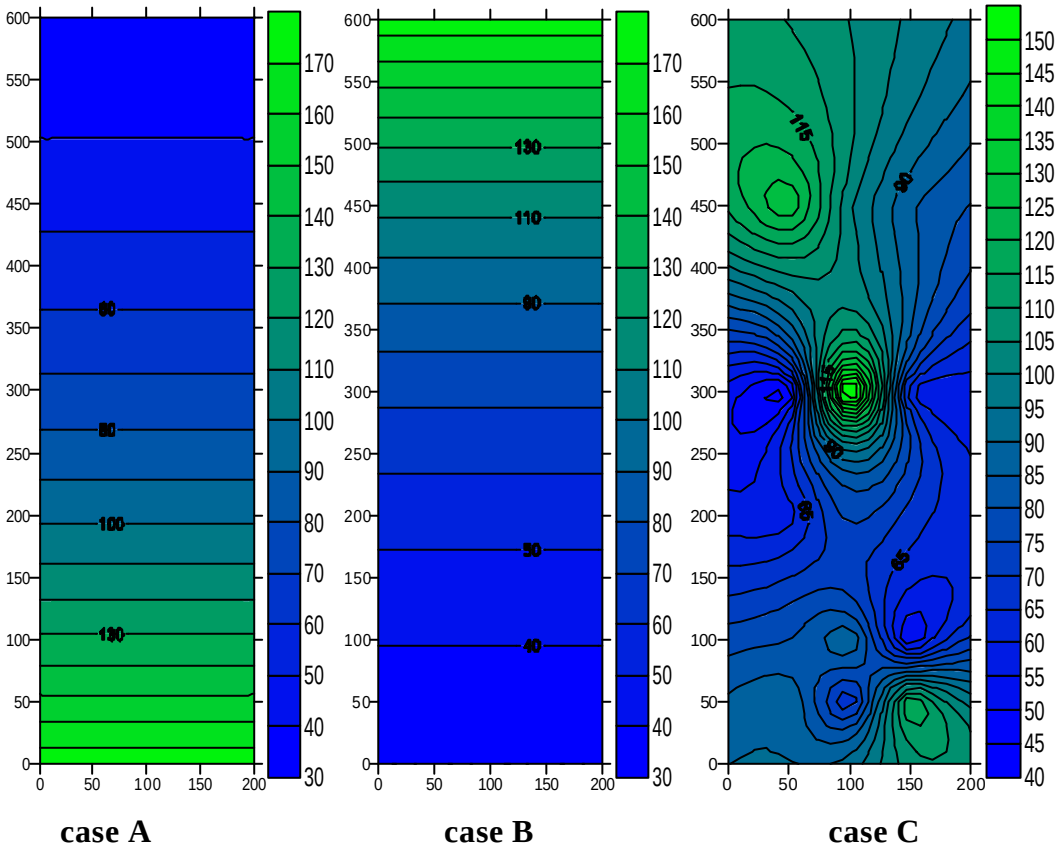

Figure 6.7 Contour map of saturated conductivity (K_{sat}) for the different distribution used in the simulation experiment.

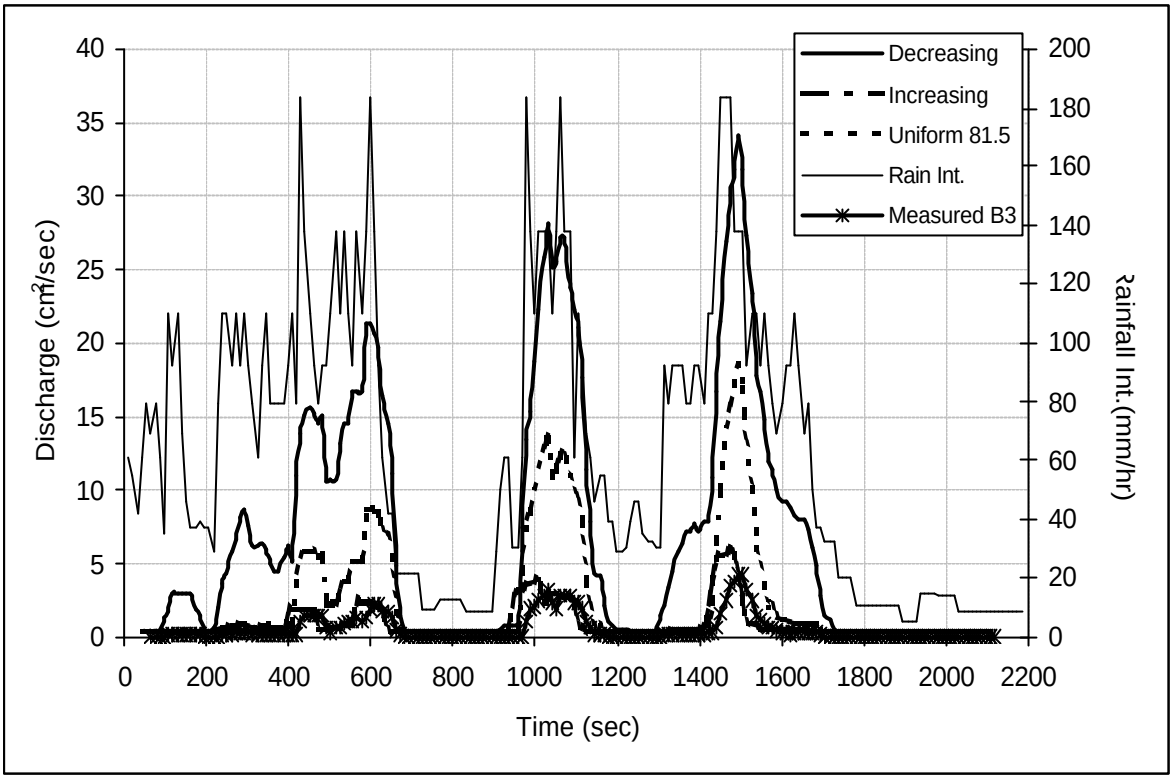

Figure 6.8a. Comparison of simulated outflow hydrograph showing the effect variations in the distribution of K_{sat} for event A

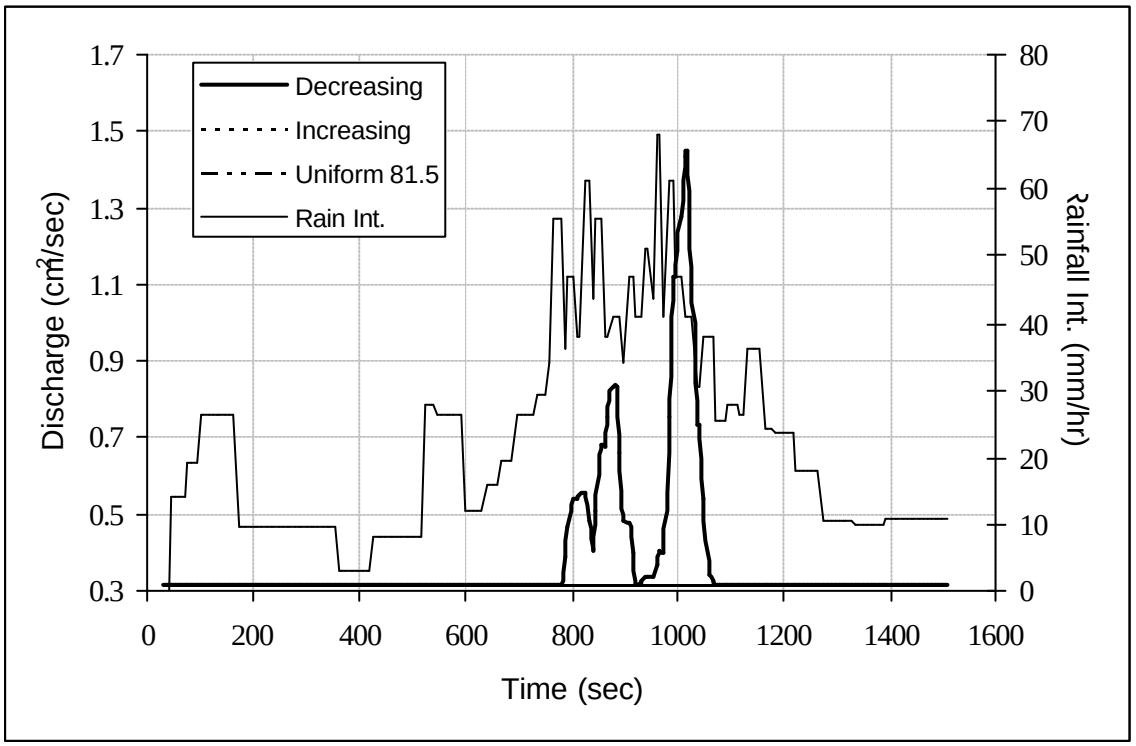

Figure 6.8b. Comparison of simulated outflow hydrograph showing the effect variations in the distribution of K_{sat} for event B

Figures 6.8a and b indicate that the magnitude and spatial pattern of K_{sat} within a plot or on a hillslope could significantly affect the observed discharge in a runoff event. Increasing saturated conductivity downslope allow more of the overland flow traveling towards the gutter to be lost due to increasing infiltration opportunity. This results in a significant reduction in discharge and peak rates. The high value of saturated hydraulic conductivity also induces a substantial reduction in flow depth and this is clearly displayed in the asymmetric pattern of the flow depths at about 500 sec into the event. When the conductivity decreases in the downslope direction, flow depth, discharge, and peak rate increases. Overland flow apparently emanating from the downslope regions with low saturated conductivity values, and, which only has a short distance from the gutter to overcome results in the sharp increase in discharge, in this scenario. With the low intensity events (figure 6.8b), the downslope increase, the random variation and uniform conductivity of $81.5 mmhr^{-1}$ produce no surface runoff. This apparently results from the high infiltration rate compared with the rainfall intensity in the two cases. Case B produces small quantity of surface runoff and this explains why the effect of scales in runoff response is often more pronounced with low rainfall intensity events. In those cases, the differences in runoff appear to be attributable to increased opportunity for infiltration with increasing slope length. In all the three different cases, and in both high and low intensity events, the flow pattern is considerably influenced by the microtopography (Figure 6.9). The magnitude of the difference between the hydrograph for the downslope-decreasing trend also shows that most of the runoff that arrives at the gutter emanates from regions not too far from the point of discharge. There is a marked similarity in the outflow hydrographs of random variation (measured values) and an average of the K_{sat} in the varied scenarios. This indicates that, appropriately selected average Ksat value could be used for investigation without too much loss of accuracy. At 1750 sec, which corresponds to the tailing part of the rain for event A, flow pattern and all other parameters are uniform in the three cases. This also explains why the difference in scale effect is reduced in rainfall event with extended recession phase or with prolonged pulse moments.

The differences in the outflow hydrograph in the various cases considered provide an avenue to evaluate the importance of spatial variability of soil hydraulic

properties in the Hortonian runoff process. The trend of spatial variation of infiltration properties influences the discharge from runoff plots or hillslope.

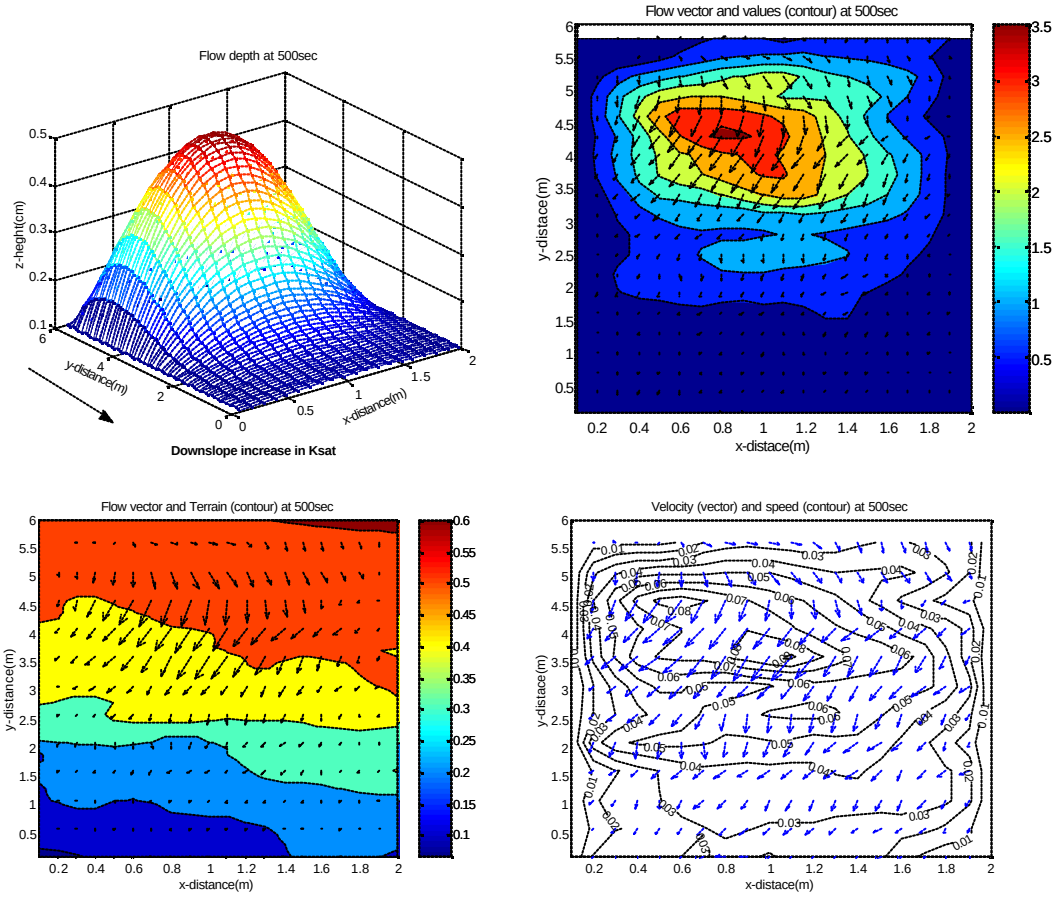

Downslope increase

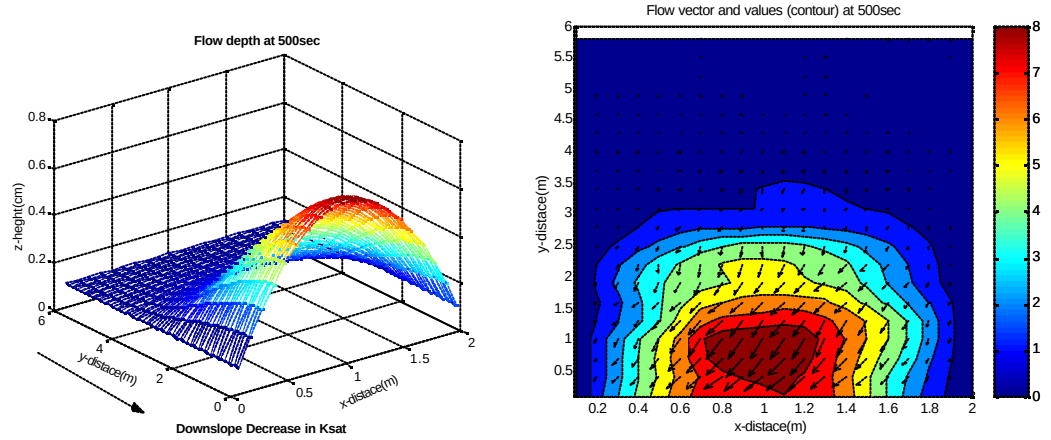

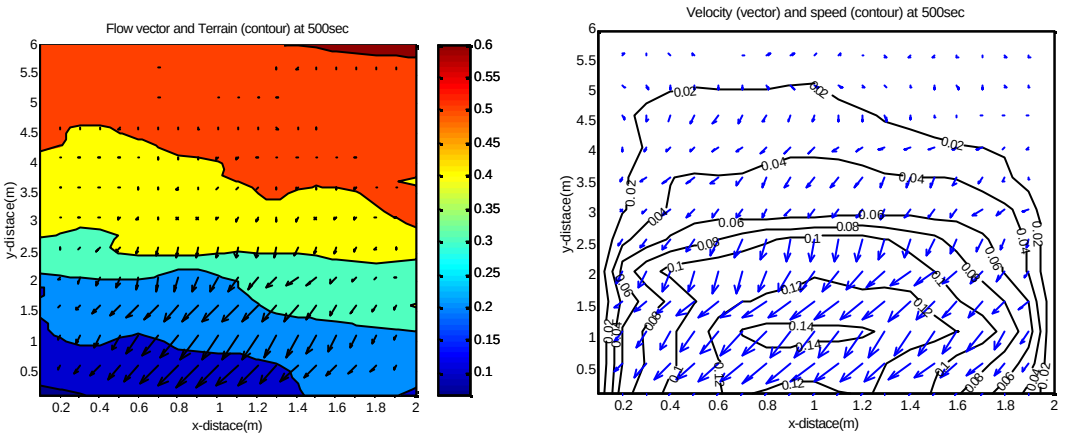

Downslope decrease

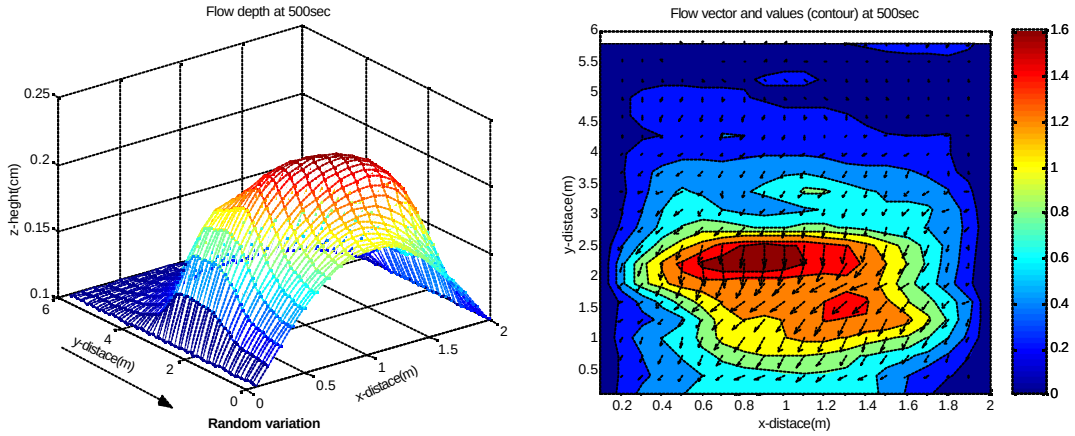

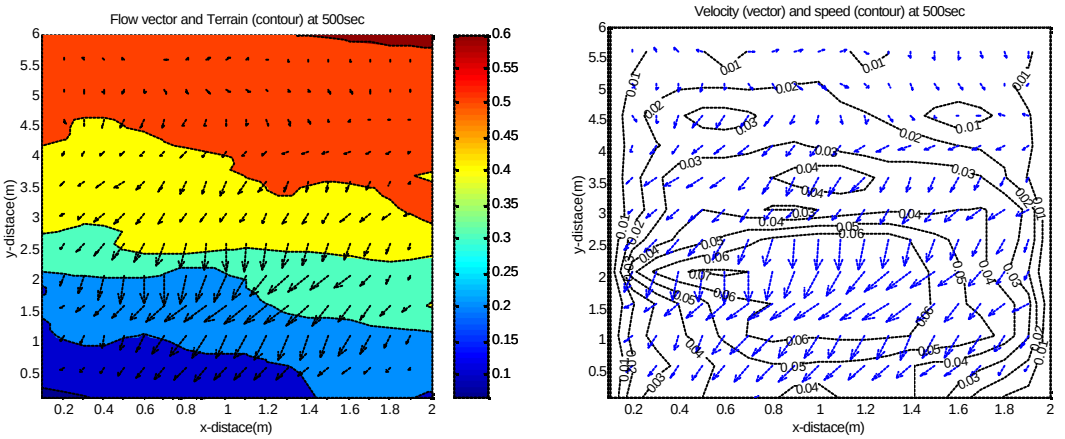

Measured value

Figure 6.9 Overland flow characteristics with linear increase, decrease and measured (random) variation in K_{sat}

However the effect can only be explained in the context of the temporal related changes that occur during the time required for the overland flow to move from the point of initiations, to the point of collection. The required time depends on the rainfall intensity, which determines the available kinetic energy, the microtopographic forms which moderate depression storage and slope of the field. All the three factors affect the velocity of flow. This observation explains why Wainwright and Parson (2002) advocated for the use of variable intensity rainfall data in appropriate resolution (preferably tipping bucket) in better understanding of scale effect. The study has gone further to enhance the understanding of rainfall runoff dynamics in the face spatially variable infiltration opportunities, which Woolhiser et al., (1996), admitted was not possible in their study because of the inability of their model to accommodate heterogeneity in rainfall intensity as well as incomplete knowledge of field conditions.

6.6 Effect of microtopography on surface runoff process

The significant effect of microtopography in the Hortonian runoff is briefly depicted in the previous section on spatial variability. In attaining a better understanding of the effect on surface runoff initiation, flow and discharge, a series of simulation experiments were implemented. The two selected characteristic rainfall patterns was simulated over (i) flat (plane) surface (as used in basin irrigation scheme); (ii) plane surface inclined at 5° (similar to field slope); and (iii) rough terrain based on the digital elevation model from measurement in the runoff plot. A uniform saturated conductivity of 30mmhr^{-1} was used on all the grids, and the sorptivity of 90mmhr^{-1}. Flow depth and discharges were monitored at the same point in all the experiments in a small plot (2m x 2m). All input parameters are kept uniform, such that the surface and rainfall pattern are the only variables. The rainfall events duration were discretized in a way to monitor the detail the responses at short time intervals. For example, event A lasting 2160 seconds is monitored every 11sec, while event B lasting about 1600 seconds is monitored every 7 seconds.

Figures 6.10a and b compare the cumulative discharge for both events on the different surfaces, and figure 6.11a and b compare the depth of flow on the three different surfaces for the two events. The cumulative discharges curves show that microtopography reduces discharge in both events. This consistent observation in both

high and low intensity events result from interaction of several factors. In the first instance, the shape and form of microtopography determine the available surface depression storage. These depression storages delay the process of connections between the various runoff-forming patches during an event, resulting in an increase, in the time required for the flow path to link up to the gutter, thereby increasing the time before discharge is recorded in the rough-surfaced plot, relative to the inclined plane surface. The delay accounts for the slow rise of the hydrograph of the plane inclined surface. Moments after the surface depression have been ponded or inundated, signifying the connections of most of the different flow paths to the gutter, surface roughness continues to reduce the velocity of flow, when compared to the smooth-surfaced inclined terrain and flat terrain (figure 6.11). Although both inclined and rough surfaces have the same range of flow velocities ($0.05 cms^{-1}$ to $0.25 cms^{-1}$), the proportion of the runoff plot under the higher velocity range is higher on the inclined plane surface compared to the rough terrain.

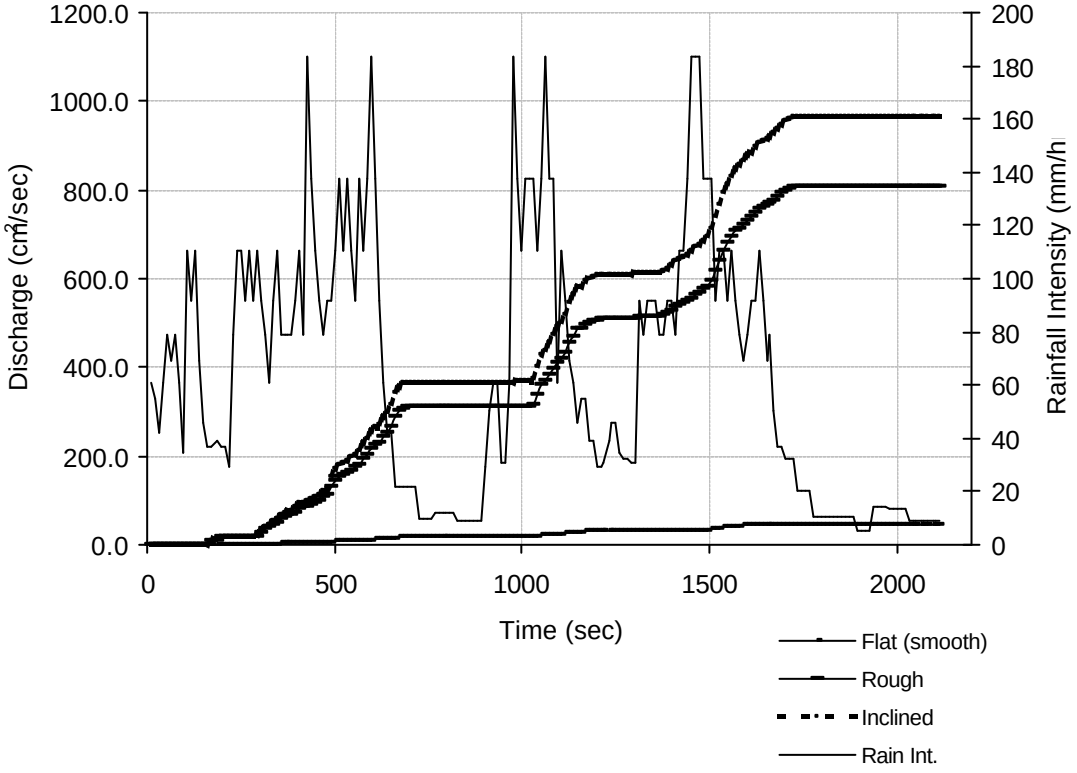

Figure 6.10a Comparison of cumulative discharge of the 3 different surfaces for event A

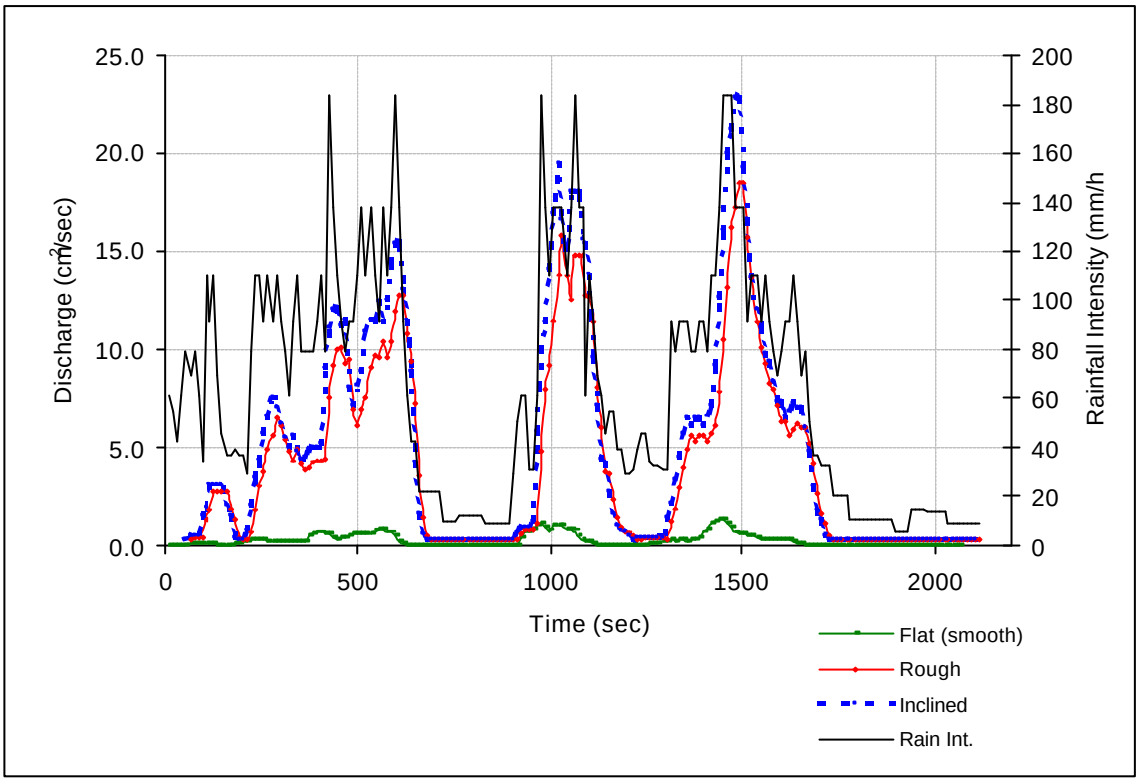

Figure 6.10b Simulated hydrograph of the 3 different surfaces for event A

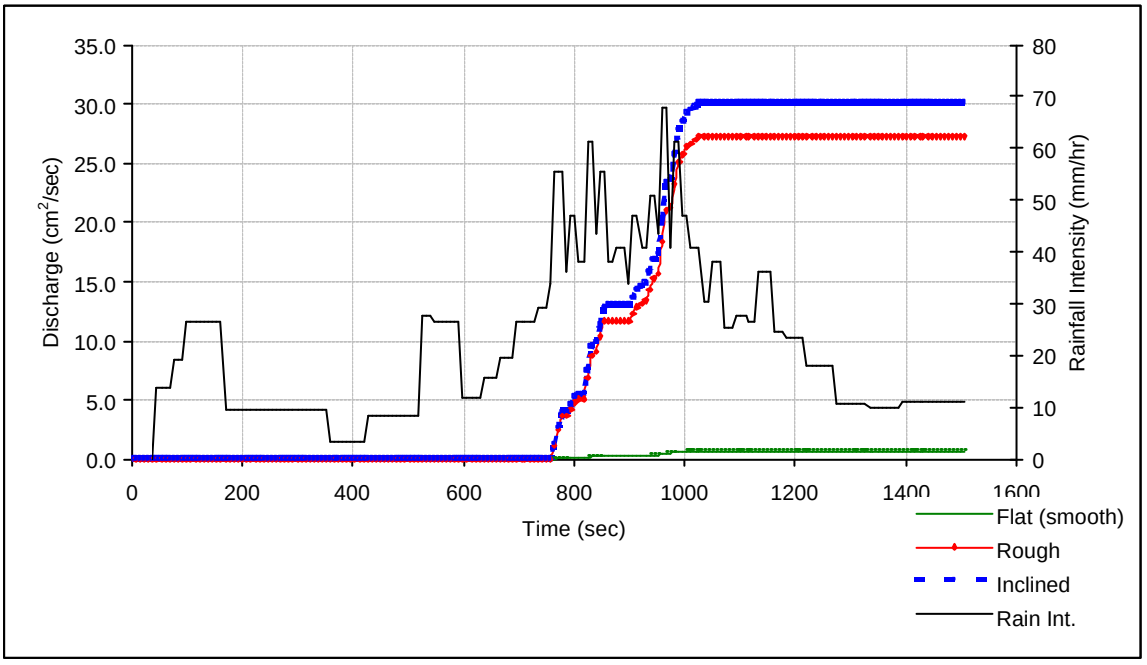

Figure 6.10c Comparison of cumulative discharge from the different surfaces for event B

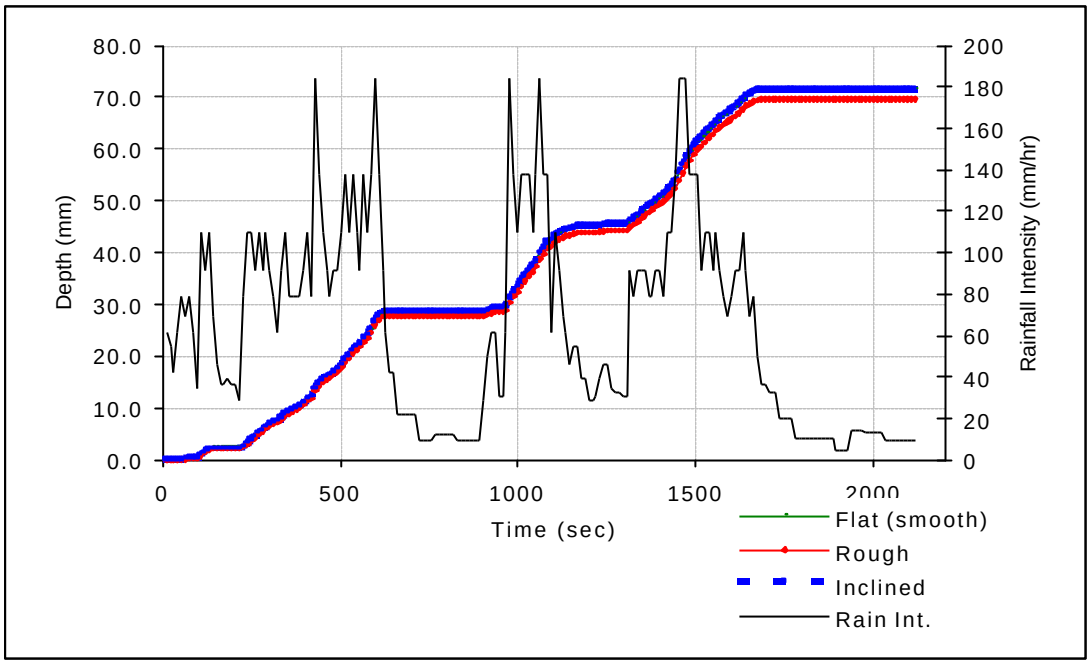

Figure 6.11a Cumulative flow depth on different surfaces for event A

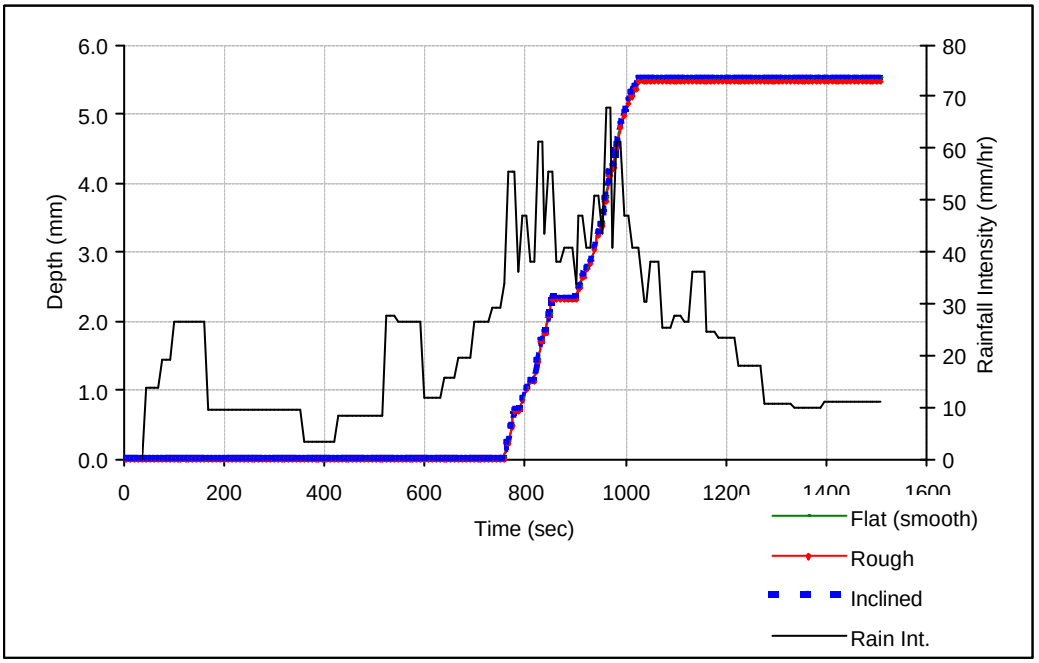

Figure 6.11b Cumulative flow depth on 3 the different surfaces for event B

Roughness due to the microtopography also increases the friction between overland flow and the surfaces, inducing considerable reduction in the flow velocity. Similarly, the depression storages increase the residence time, thus allowing significant

poststorm infiltration, which reduces surface runoff volume. This was similarly observed by Dunne and Dietrich (1980) with vegetated microtopography.

Figure 6.12a and b indicate that microtopography reduces the cumulative flow depth. Both flat-smooth terrain and inclined-smooth terrain is seen to maintain equal flow depths throughout the two events, inspite of the very clear difference in slope angle and discharge rate (Figure 6.12). The magnitude of the difference is reduced in the low intensity event, apparently due to the substantial reduction in runoff volume. The influence of surface roughness on flow velocity, flow depth and discharge volume is observed to increase with increasing slope length and increase duration of the event.

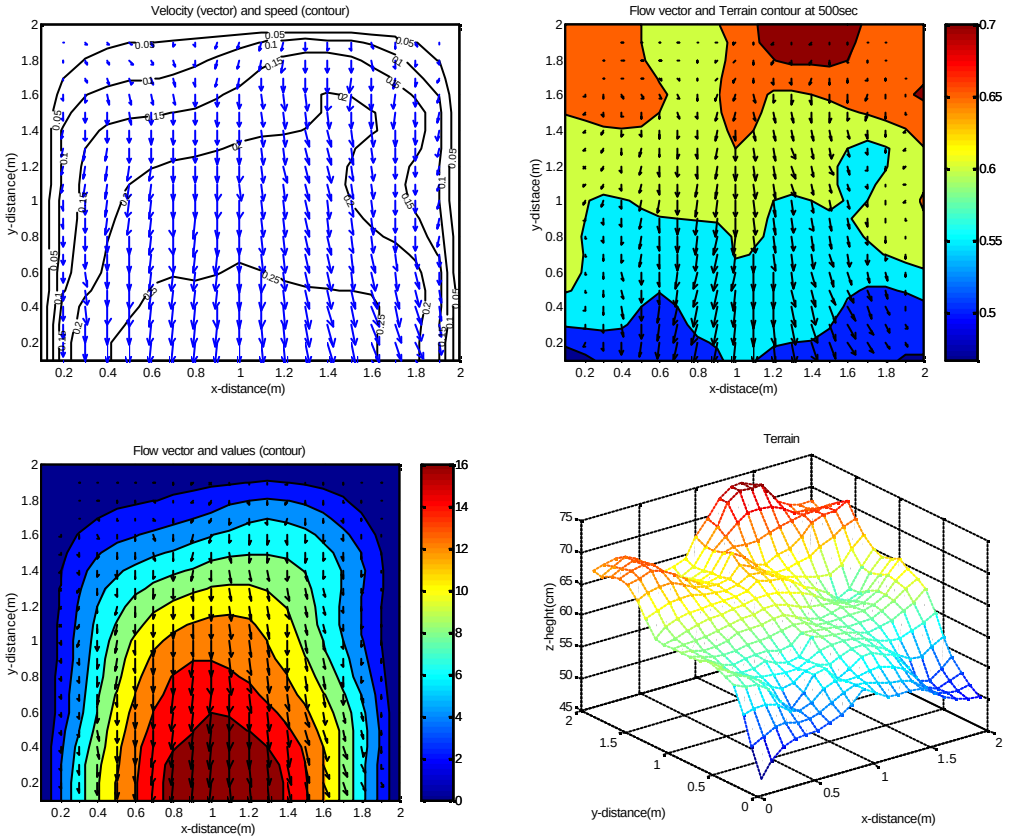

(a). Rough Terrain

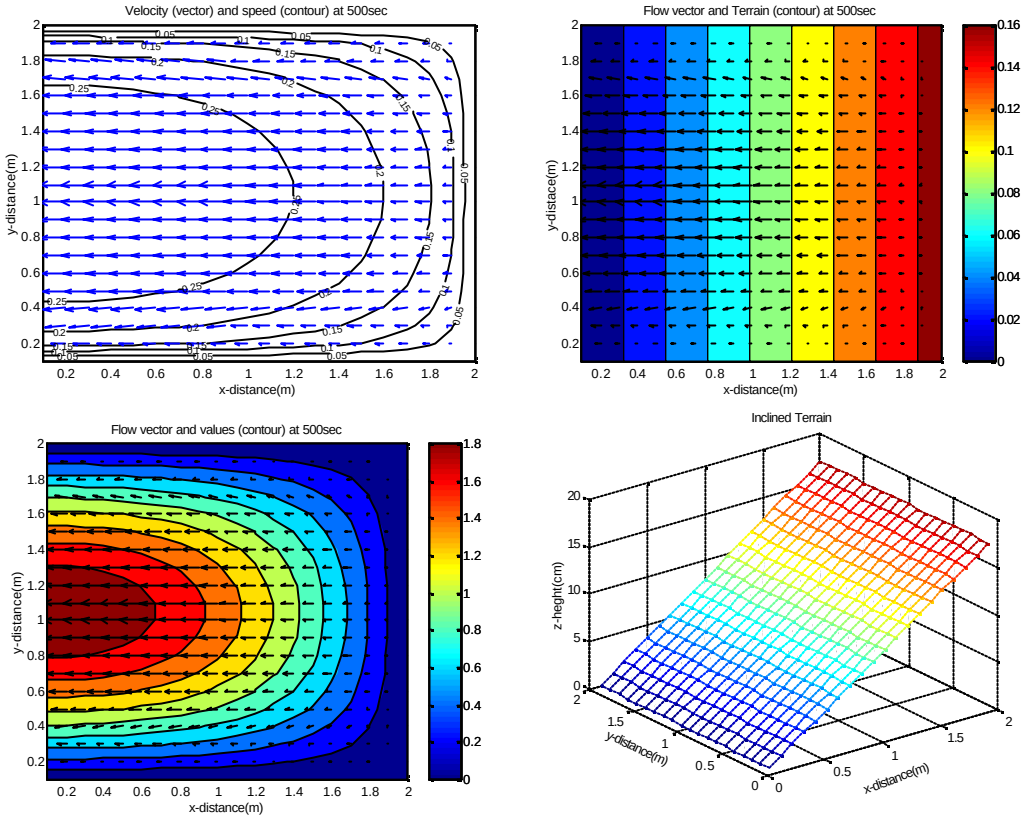

(b) Inclined Terrain

Figure 6.11 Flow vector, speed and depth on different terrain at 500sec for event A

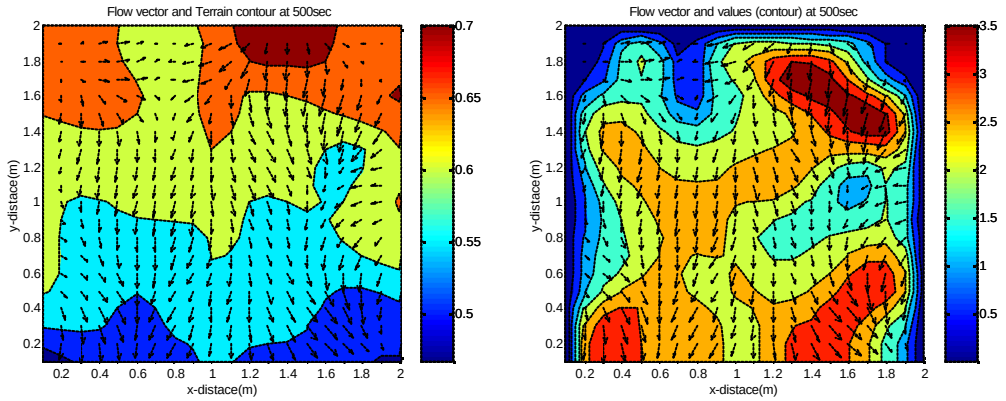

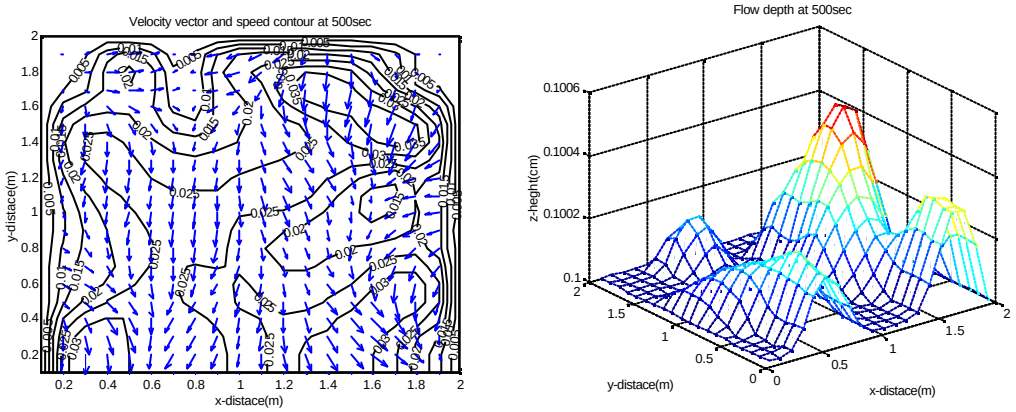

(a) Rough terrain

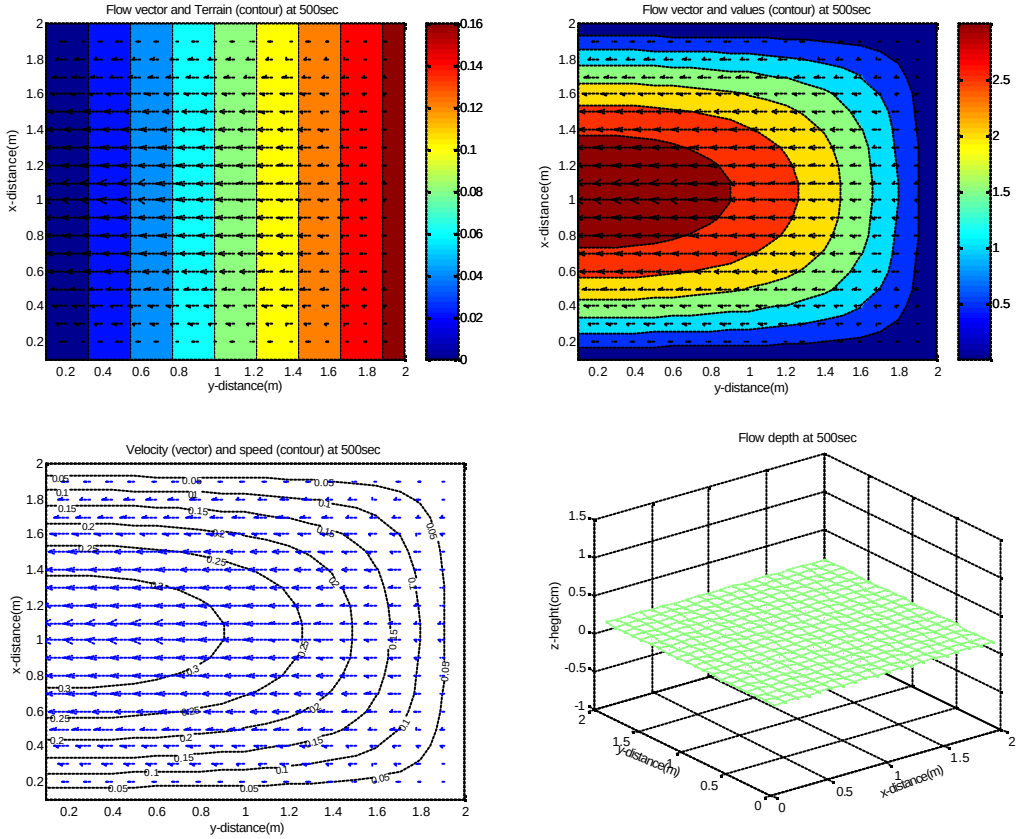

(b) Inclined Terrain

Figure 6.13 Flow vector, speed and depth on different terrain at 500sec for event B

In both events, microtopography clearly dictates the flow direction and influences the distribution of flow depth, especially during the pulse moments of rainfall events and during the recession stages. This explains why the influence of microtopography is more pronounced during low intensity events, resulting in higher

infiltration capability. Figure 6.13a depicting the flow conditions at 500seconds into event B show that the spatial distribution of flow depth and the flow pattern and direction are distinctly influenced by the microtopography as was similarly observed by Esteves et al. (2000). This contrast the observation by Zhang and Cundy (1989) who concluded that microtopography did not significantly alter flow direction. It could however, be understood that the effect of microtopography in their simulation experiments were clouded by the relatively large grid spacing of 1.0m in the simulation.

Changes in surface microtopography are widely influenced by land use at small scale and catchment morphology at large scale. Small-scale microtopography results from field cultivation and vegetation changes and has been shown in the model simulation to be significant in influencing runoff process. Observations like the one depicted in figure 6.14b are similarly recorded in the tailing period of event A. This trend of fluctuation between high and low intensity over short time form part of the distinguishing features characterizing tropical rainstorm patterns and will be very helpful in the study of the environment related impact of surface runoff processes in the tropics. It is evident as postulated by Zhang and Cundy, (1989) that, a spatially varying flow field cannot be obtained by assuming a uniform roughness surface.

It is apparent that rainfall events with prolonged recessions, or more frequent pulse moments (multiple peak), will behave very differently when compared to a single peak event with the same depth, in terms of runoff response even when they have equal duration. It is therefore expedient to agree with the conclusion of Wainwright and Parson, (2002) that a better understanding of the temporal variability of rainfall intensity is important in both understanding field measurements and developing robust models of overland flow. A single peak event will reduce the scale of the difference in discharge among the three surface conditions.

The low values of discharge on a flat plane surface accentuate the importance of slope angle in the transformation of ponded water into surface runoff and also lend credence to the choice of diffusion process in the model operation. The uniformity in flow depth over the smooth-plane terrain and smooth-inclined plane has been shown earlier. The low discharge shows that the water only ponded and did not flow, but is redistributed over the whole plot in manner similar to the application of irrigation water; with the maximum velocity recorded in the center of the plot. This clearly shows the

ability of the model to monitor the advance and trajectory of applied water in irrigation schemes similar to the work of Playan et al. (1994). This observation provides a tool that can aid decision process in soil management techniques aimed at managing surface runoff and soil erosion

Simulation on different plane surface with different slope angle showed that the volume of runoff increases proportionately with increase in slope angle, but the proportionality is not observed when a rough terrain inclined at similarly different angles was used. This suggests that scale effect in runoff process also depend on the microtopography.

7 CONCLUSIONS AND RECOMMENDATIONS

This study was designed to answer some basic questions about runoff generation and transmission processes in the Volta river basin, west Africa, such as what proportion of rain is lost to surface runoff, what is the influence of scale, what are the factors that determine scale effect and under what conditions it occurs, a concise summary of the major findings of this research in the light of the research objective and questions are outlined here:

The dominant runoff generating mechanism in the catchment in the study area and presumably in the Volta Basin is the infiltration-excess process. This does not foreclose the pseudo-saturation excess runoff process in the valley area close to the rivers and in the parts of the basin with very shallow soil depth. The prevalence of high intensity storm in the catchment combined with poor infiltration properties of the soil initiate surface runoff flow process.

The diverse nature of response to the same rain event at the two sites within the same catchment further reflects the importance of heterogeneous soil and hydraulic properties as they affect storm runoff responses. A study of the profile soil moisture indicates very high variability in soil moisture content in the first 300mm layer of soil. The occurrences of rainfall influence the moisture status, at the surface and in the 100mm depth. Possibly due to the high sand content, the temporal analysis of soil moisture shows that, the stored moisture are quickly depleted. This explains runoff yield is often not correlated with rainfall amount, or peak rainfall intensities, particularly for the low intensity events. The moisture gradient always increases sorptivity and increase time required for ponding. Results from both field and model simulation also show that vegetation and vegetation changes can significantly influences total runoff observed, due to the varying interception losses and the reduction of flow velocity.

In both field observations and simulation experiments, an exponential trend of reduction in runoff coefficient and unit runoff discharge with increasing slope length was observed, suggesting the import of observation scales in the surface runoff process. The observed scale effect is mainly caused by spatial variability in infiltration opportunities. The study also showed that the infiltration opportunities vary with slope length and the pattern of the distribution of hydraulic conductivity. The difference in

infiltration opportunities result in differences in transmission losses potential, during surface runoff routing downslope. It can also be concluded that the vegetated and surface microtopography, which become more varied with increase in slope length determined surface depression storage shape and network, consequently influencing runoff initiation and flow rate. However, the effect of the two factor of spatial variability is influenced by the time required to move from point of runoff initiation to the trough, which also depend on the rainfall intensity and field slope. Thus, the temporal pattern of rainfall can influence runoff response. Temporal patterns of rainfall intensity; particularly the distribution in terms of numbers of peaks in the event, the duration of the pulses, the length of time for recession, and magnitude of rainfall intensity coupled with temporal variation in travel largely determine the response to high intensity events while, soil related effect in terms of spatial variability in hydraulic properties mainly influences low intensity event. The dominance of temporally induced factors in the basin could be related to the high intensity events synonymous with tropical storm, which often do not allow the spatial factors to manifest. The other factor of soil that could significantly influence runoff response is the initial moisture status of the soil. However, the high intensity rainfall predominant in the Volta basin limits its influence. In low intensity events, high initial moisture content increases runoff volume.

Analysis of the hydrograph from simulation experiment with different microtopography shape indicates that, runoff volume can be widely varied from runoff plot of the same size. This apparently results form the different shape and density of depression storage created by the microtopography shape, thereby showing that soil surface microtopography will significantly influences the rainfall-runoff process. In comparison with smooth terrain of similar inclination, microtopography reduces runoff discharge. The low values of discharge on a flat plane terrain accentuate the importance of slope angle in the transformation of ponded water into surface runoff. Another significant effect of soil surface microtopography is that it influences flow direction of surface runoff throughout the event even when the surface ought to have been submerged by increased flow depth. The period of effective influence of microtopography under less intensive events is more pronounced compared to high intensity events. This indicates that microtopography plays very determining role in

directing flow, creating rill and micro-channel path, and determining flow velocity under low intensity rainfall.

Results from the model showed that it is possible to predict hydrologic response, if the model structure is designed to accommodate variability in K_{sat} or precipitation as observed in the field. If, however, the model fails to recognize this variability, we can expect that agreement with observation will be poor. This study as has also demonstrated that with the inclusion of condition similar to the one obtainable on the field and the selection of appropriate model, it is possible to capture rain-runoff transformation in tropical environments. The developed model will be useful in studying the dynamics of surface runoff, water erosion, and nutrients dynamics under complex microtopographic condition and spatially varying soil hydraulic characteristic and temporally dynamic rainfall intensity obtainable in many tropical catchments. It also provides practical tool for facilitating decision processes in soil management techniques aimed at managing surface runoff and soil erosion and provide the basis for upscaling to monitor the basin runoff process.

RECOMMENDATIONS

In the light of the results from both field observations and modeling techniques used in this study, the following recommendations in terms field experimentation and possible applications and further extension of the modeling are proposed:

Sustained long term studies on surface runoff process in the basin. The result from the single season studies will be better validated if it is compared with results from the same plot over 3-5 seasons. Repeating the field trials ensures that more data will also be available for comparism with the model simulations.

In carrying out such studies, it will be very good to further improve on the developed the tipping bucket runoff meter, to handle lower volume of runoff per tip. Such development will increase the sensitivity of the tipping bucket and will facilitate better comparism.

The results had indicated that, frictional resistance differs according to plant structure, which depends on the age and type of vegetation. It would be a good idea, if further research is carried out on the estimation of frictional resistance by the different configurations of surface and vegetation microtopography in surface runoff processes.

Such estimation will enhance the large scale application of the model, as the derived factors could be used explicitly to account for microtopography in large scale i.e. basin-wide applications-

It will also be a good idea to explore the possibility of integration of the developed model with mesoscale model like MM5 for large scale application and climate impact studies;

Finally, it will be a good idea to apply the developed model in the area of Solute Transport studies e.g. erosion, pesticides movement etc. with necessary subroutine and models incorporated.

8 REFERENCES

Abbott M.B. and Basco D.R. 1989. Computational fluid dynamics, Longman, London.

Abbott M.B. and Minns A. 1998. Computational Hydraulics 1st ed., Pitman, London/Longman, London, and Wiley, New York/2nd edition, Ashgate, Aldershot, UK, and Brookfield, USA.

Abiodun B.J. 2003. Numerical modeling of mesoscale convective systems over West Africa. Ph.D. dissertation, Department of Meteorology, Federal University of Technology Akure, Nigeria. 120 pp

Abrahams A.D., Parsons A.J., and Wainwright J. 2003 Disposition of rainwater under creosote bush. Hydrological Processes 17 (13) pp. 2555-2566.

Agyare W.A. 2004. Soil characterization and modeling of spatial distribution of saturated conductivity at two sites in the Volta Basin of Ghana. Ecology and Development series No. 17

Akan A.O. and Yen B. C. 1981. Diffusion-wave flood routing in channel networks. J. Hydr. Div., ASCE, 107 (6): 719-731.

Akanbi A.A. and Katapodes 1988. Model for flood propagation on initially dry land. J. Hydr. Engrg. ASCE 114 (7) pp. 689-706

Angermann T., Wallender W.W., Wilson B.W., Werner I., Hinton D.E., Oliver M.N., Zalom F.G., Henderson J.D., Oliveira G.H., Deanovic L.A., Osterli P., Kruegerb W. 2002 Runoff from orchard floors-micro-plot field experiments and modeling. J. Hydrology 265: 178–194

Arnaud P., Bouvier C., Cisneros L. and Dominguez R. 2002. Influence of rainfall spatial variability on flood prediction. J. Hydrology 260 (1-4): 216-230

Asselin R. 1972. Frequency filter for time integrations. Mth. Wea. Rev., 100:487-490.

Auzet A.V., Boiffin J. and Ludwig B. 1995. Concentrated flow erosion in cultivated catchments: Influence of soil surface state. Earth Surface Processes and Landforms 20 (8): 759-767

Bellos C., Soulis J. and Sakkas J. 1991. Computation of two-dimensional dam break induced flow. Adv. in Water Resour. 14(1): 31-41.

Bergkamp G. 1998. A hierarchical view if the interaction of runoff and infiltration with vegetation and microtopography in semiarid shrublands. Catena 33:201-220.

Beven K.J., Wood E.F. and Murugesu S. 1988. On hydrological heterogeneity-catchment morphology and catchment response. J. Hydrol. 100: 353-375.

Borah D.K., Prassas S.N. and Alonso C.V. 1980. Kinematic wave routing incorporating shock fitting. Water Resour. Res., 16: 529–541

Braud I., Vich A.I.J., Zuluaga J., Fornero L. and Pedrani A. 2001. Vegetation influence on runoff and sediment yield in the Andes region: observation and modeling. J. Hydrology 254 (1-4): 124-144

Brown D.L. 1995. An analysis of transient flow in upland watersheds: interactions between structure and process. Ph.D. Dissertation, University of California at Berkeley.

Campbell I.A. 1989. Badlands and badland gullies. In: Thomas SG (eds), Arid zone geomorphology. Belhaven Press, London. pp. 159-183.

Campling P., Gobin A., Beven K. and Feyen J. 2002. Rainfall-runoff modelling of a humid tropical catchment: the TOPMODEL approach. Hydro. Processes 16 (2): 231-253.

Carsel R.F. and Parrish R.S. 1988. Developing joint probability distributions of soil water retention characteristics. Water Resour. Res. 24: 755-769.

Chaplot V.A.M. and Le Bissonnais Y. 2003. Runoff features for interrill erosion at different rainfall intensities, slope lengths, and gradients in an agricultural loessial hillslope. SSSA J. 67 (3): 844-851

Chevallier P. and Planchon O. 1993. Hydrological process in a small humid savannah basin (Ivory Coast). J. Hydro.151: 173-191.

Chilés J.P. Delfiner P. and Delfiner P. 1999. Geostatistics: Modelling spatial uncertainty. Wiley Joohn and sons. 720pp.

Chow V.T. 1964. Runoff: Section 14 in handbook of applied hydrology. Edited by Chow V.T. McGraw-Hill, New York.

Chow V.T. and Ben-Zvi A. 1973. Hydrodynamic modeling of two-dimensional watershed flow J. Hydr. Div., ASCE 99(11): 2023-2040.

Cunge J.A, Holly F.M. Jr. and Verwey A. 1980. Practical aspects of computational rivers hydraulics. Pitman Publishers, Boston Mass.

Darboux F., Davy P., Gascuel-Odoux C. and Huang C. 2002. Evolution of soil surface roughness and flow path connectivity in overland flow experiments. Catena 46 (2-3): 125-139.

Darboux F., Gascuel-Odoux C. and Davy P. 2002. Effect of surface water storage by soil roughness on overland flow generation. Earth surface processes and landforms 27 (3): 223-233.

de Lima J.L.M.P. and Singh V.P. 2002. The influence of the pattern of moving rainstorms on overland flow Adv. in Water Resou. 25 (7): 817-828.

de Lima J.L.M.P. Singh V.P. and de Lima M.I.P. 2003. The influence of storm movement on water erosion: storm direction and velocity effects Catene 52 (1): 39-56

Diamond J. and Shanley T. 1998. Infiltration rate assessment of some major soils. End of Project Report, Armis 4102, Teagasc, Dublin.

Dibike Y.B. 2002. Developing generic hydrodynamic models using artificial neural networks. J. Hydraulic Res. 40:2

Dickson K.B. and Benneh G. 1995. A New Geography of Ghana. London: Longman

Dikau R. and Schmidt J. 1999. Extracting geomorphometric attributes and objects from digital elevation models-semantics, methods, future needs. In GIS for Earth Surface Systems- Analysis and modeling of the Natural environments, Dikau R Saurer H (eds). Schweizbart'sche Verlagsbuchhandlung: Berlin, Stuttgart; 153-173

Dunne T. 1978. Field studies of hillslope flow processes. In: Hillslope hydrology, Kirkby, M.J., ed., John Wiley & Sons, New York, NY, pp. 227-293.

Dunne T. and Black R.D. 1970a. An experimental investigation of runoff production in permeable soils. Water Resources Res. 6, pp. 478-490.

Dunne T. and Black R.D. 1970b Partial area contributions to storm runoff in a small New England watershed, Water Resour. Res. 6: 1296-1311.

Dunne T. and Dietrich W.E. 1980a. Experimental investigation of Horton overland flow on tropical hillslopes: 1. Soil conditions, infiltration, and frequency of runoff, Z. Geornorph. N.F., Suppl.-Bd. 35: 40-59.

Dunne T., Zhang W. and Aubry B.F. 1991. Effects of rainfall, vegetation and microtopography on infiltration and runoff. Water Resour. Res. 27, 2271–2285

Erbes G. 1994. A study of finr scale atmospheric dynamics and numerical advection methods. PhD thesis, dept. of meteorology, Stockholm University. (

Esteves M Faucher X Galle S and Vauclin M 2000 Overland flow and infiltration modelling for small plots during unsteady rain: numerical results versus observed values. J. Hydrology, 228: 265–282

Esteves M. and Lapetite J.M. 2003. A multi-scale approach of runoff generation in a Sahelian gully catchment: a case study in Niger Catena 50 (2-4): 255-271

FAO 1995 World agriculture: Towards 2010, An FAO study. N. Alexandratos (Editors) FAO, Rome. pp 210.

Fennema R.J. and Chaudhry M.H. 1986. Explicit numerical schemes for unsteady free-surface flows with shocks. Water Resour. Res. 22: 1923–1930.

Fiedler F.R. 1997. Hydrodynamic simulation of overland flow with spatially variable infiltration and microtopography. Ph.D. thesis, Colorado State University.

Fiedler F.R. and Ramirez J.A. 2000. A numerical method for simulating discontinuous shallow flow over an infiltrating surface. Inter. J. Numerical Methods in Fluids 32 (2): 219-240

Fiedler F.R., Gary P.E., Ramirez J.A. and Ahuja L.R. 2002. Hydrologic response of grasslands: effect of grazing, interactive infiltration and scale.

Fitzjohn C., Ternan J.L. and William A.G. 1998. Soil moisture variability in a semi-arid gully catchment: implication for runoff and erosion control. Catena 32: 55-70

Foreman M.G.G. 1984. A two-dimensional dispersion analysis of selected methods for solving the linearised shallow water equation. J. Computational Physics 56:287-323.

Friesen J. 2002. Spatio-temporal rainfall patterns in Northern Ghana. Diplom Thesis, Geographische Institute der Rheinischen Friedrich-Wilhelms, Universität Bonn

Garcia R. and Kahawita R.A. 1986. Numerical solution of the St. Venant Equations with the MacCormack finite difference scheme. Inter. J. Numerical Methods in Fluids. 6: 507-527.

Gaur M.L. and Mathur B.S. 2003. Modeling event-based temporal variability of flow resistance coefficient. J. Hydrologic Engng 8 (5): 266-277

Golden Software, Inc 2000. Surfer(R) Version 7. Golden Software, Inc. 809 14th Street Golden, CO 80401-1866 USA. http://www.goldensoftware.com

Gomez J.A., Orgaz F., Villalobos F.J. and Fereres E. 2002. Analysis of the effects of soil management on runoff generation in olive orchards using a physically based model. Soil use and management 18 (3):191-198.

Govindaraju R.S., Jones S.E. and Kavvas M.L. 1988. On the diffusion wave model for overland flow 1- Solution for the steep slopes. Water Resor. Res. 24(5): 734-744.

Haltiner G.J. and Williams R.T. 1980. Numerical prediction and dynamic meteorology. John Wiley and Sons

Horton R.E. 1933. The role of infiltration in the hydrologic cycle. Trans. Am. Geophys. Union, 14: 446-460.

Hromadka T.V. II., McCuen R.H. and Yen C.C. 1987. Comparison of overland flow hydrograph models. J. Hydraulic Engng (ASCE) 113(11): 1422-1440.

Hudson N. 1995. Soil conservation. 3rd Edition B.T. Batsford, London 391pp

Hupet F. and Vanclooster M. 2002. Intraseasonal dynamics of soil moisture variability within a small agricultural maize cropped field. J. Hydrology 261 (1-4): 86-101

Hursh C.R. 1936. Storm-water and absorption. In: Discussion on list of terms with definitions; Report of the Committee on Absorption and Transpiration, Trans. Am. Geophys. Union, 17: 301-302.

Iwasa Y. and Inoue K. 1982. Mathematical simulation of channel and overland flows in view of flood disaster engineering. Natural Disaster Science 41(1): 1-30.

Jetten V., de Roo A. and Favis-Mortlock D. 1999. Evaluation of field-scale and catchment-scale soil erosion models. Catena 37 (3-4): 521-541

Jha A.K., Akiyama J. and Ura M. 1995. First and second-order flux difference schemes for dam break problem. J. Hydraul. Engng., 121: 877–884.

Jhorar R.K., van Dam J.C., Bastiaanssen W.G.M. and Feddes R.A. 2004. Calibration of effective soil hydraulic parameters of heterogeneous soil profiles J. Hydro. 285 (1-4): 233-247.

Joel A., Messing I., Seguel O. and Casanova M. 2002. Measurement of surface runoff from plots of two different sizes. Hydrological Processes 16:1467-1478.

Jolánkai G. and Rast W. 1999. The hydrologic cycle and factors affecting the generation, transport and transformation of nonpoint source pollutants. In: Assessment and control of nonpoint source pollution of aquatic ecosystems: a practical approach. UNESCO and The Parthenon Publishing Group, USA.

Julien P.Y. and Moglen G.E. 1990. Similarity and length scale for spatially varied overland flow. Water Reso. Res. 26: 1819–1832.

Kang S.Z., Zhang L., Song X.Y. Zhang S.H., Liu X.Z., Liang Y.L. and Zheng S.Q. 2001. Runoff and sediment loss responses to rainfall and land use in two agricultural catchments on the Loess Plateau of China Hydrological processes 15 (6): 977-988

Kasteel R., Vogel H.J. and Roth K. 2000. From local hydraulic properties to effective transport in soil. European J. Soil Science 51 (1): 81-91.

Katapodes N.D. and Strelkoff T. 1979. Two-dimensional shallow water-wave model. J. Eng. Mech. Div. Am. Soc. Civ. Eng., 105 (EM2): pp 317-334.

Katopodes N.D. and Strelkoff T. 1978. Computing two-dimensional dam-break flood waves. J. Hydra. Division, ASCE, 104(9): 1269-1288.

Kawahara M. and Yokoyama T. 1980. Finite element method for direct runoff flow. J. hydra. Div. ASCE, 106(4): 519-533.

Kirkby M. 2002. Modeling the interaction between soil surface properties and water erosion. Catena 46 (2-3): 89-102.

Kirkby M., Bracken L., and Reaney S. 2002. The influence of land use, soils and topography on the delivery of hillslope runoff to channels in SE Spain. *Earth surf. Process. Landforms* 27, 1459–1473.

Lal R. 1997. Soil degradative effects of slope length and tillage methods on alfisols in Western Nigeria, I, Runoff, erosion and crop response. Land Degradation Dev., 8(3): 201–219.

Lane L., Hernandez M. and Nichols M. 1997. Processes controlling sediment yield from watersheds as functions of spatial scale. Environmental Modeling and Software, 12, 355–369.

Le Barbé L. and Lebel T. 1997. Rainfall climatology of the HAPEX-Sahel region during the years 1950-1990. J. Hydro.188-189: 43-73.

Léonard J. and Perrier E. 2001. A model for simulating the influence of a spatial distribution of large circular macropores on surface runoff. Water Resou. Res. 37 (12): 3217-3225.

Lidén R. and Harlin J. 2000. Analysis of conceptual rainfall modelling performance in different climates. J. Hydro. 238:231-247.

Liggett J.A. and Woolhiser D.A. 1967. Finite-difference solutions of the shallow water equations, Proc. ASCE J. Mech. Div., 93:39–71.

Littleboy M., Cogle A,L., Smith G.D., Rao K.P.C. and Yule D.F. 1996. Soil management and production of Alfisols in the semi-arid tropics .4. Simulation of decline in productivity caused by soil erosion. Australian J. Soil Res. 34 (1): 127-138.

Logsdon S.D. Jordahl J. and Karlen D.L. 1993. Tillage and crop effects on ponded and tension infiltration rates. Soil & Tillage Res. 28 (2): 179-189.

Mah M.G.C., Douglas L.A. and Rigrose-voase A.J. 1992. Effect of crust development and surface slope on erosion by rainfall. Soil Science 154:37-43.

Malet J.P., Auzet A.V., Maquaire O., Ambroise B., Descroix L., Esteves M., Vandervaere J.P. and Truchet E. 2003. Soil surface characteristics influence on infiltration in black marls: Application to the Super-Sauze earthflow (southern Alps, France) Earth Surface Processes and Landforms 28 (5): 547-564

Mallants D., Mohanty B.P., Jacques D. and Feyen J. 1996. Spatial variability of hydraulic properties in a multi-layered soil profile. Soil Sci. 161(3): 167-181.

Masiyandima M.C., van de Giesen N., Diatta S., Windmeijer P.N. and Steenhuis T.S. 2003. The hydrology of inland valleys in the sub-humid zone of West Africa: rainfall-runoff processes in the M'be experimental watershed. Hydrological Processes 17 (6): 1213-1225.

Mathwork Inc (2000). MATLAB The language of Technical computing. Version 6.0.0.88 Release 12.

Matula S. 2003. The influence of tillage treatments on water infiltration into soil profile Plant Soil and Environment 49 (7): 298-306.

Mohanty B.P. and Mousli Z. 2000. Saturated hydraulic conductivity and soil water retention properties across a soil-slope transition. Water Resou. Res. 36 (11): 3311-3324

Nash J.E. and Sutcliffe J.V. 1970. River flow forecasting through conceptual models, 1, a discussion of principles. J. Hydrol. 10 (1): 282–290.

Návar J. and Synnott J.T. 2000. Surface runoff, soil erosion, and land use in Northeastern Mexico Terra Volumen 18 (3).

Ogden L. F. and Julien Y. P. 1993. Runoff sensitivity to temporal and spatial rainfall variability at runoff plane and small basin scales. Water Resou. Res., 29 (8): 2589-2597.

Osei-Bonsu P. Asibuo J.Y. 1998. Using polythene bags to control the growth of *Mucuna* vines http://www.idrc.ca/books/focus/852/14-sec11.html cited April10, 2003.

Parlange J.Y., Hogarth W., Ross P., Parlange M.B., Sivapalan M., Sander G.C.and Liu M.C. 2000. A note on the error analysis of time compression approximations Water Resource Res. 36 (8): 2401-2406.

Parlange J.Y., Rose C.W. and Sander G. 1981. Kinematic flow approximation of runoff on a plane: an exact analytical solution. J. Hydro. 52:171.

Peugeot C., Esteves M., Rajot J.L., Vandervaere J.P. and Galle, S. 1997. Runoff generation processes: results and analysis of field data collected at the central supersite of the Hapex-Sahel experiment. J. Hydrol. 188– 189 (1–4): 179–202.

Philip J.R. 1957. The theory of infiltration: 4. Sorptivity and algebraic infiltration equations. Soil Science, 84: 257-264.

Playan E. 1992. Two-dimensional hydrodynamic simulation of basin irrigation: analysis of shape effects on irrigation performance. Ph.D. Dissertation, Utah State University.

Pláyan E. and Martinez-cob A. 1999. Simulation of basin irrigation scheduling as a function of discharge and leveling. Invest. agr. prod. prot. veg. 14 (3).

Pláyan E. Walker W.R. and Merkley G.P. 1994. Two-dimensional simulation of basin irrigation .1.Ttheory J. Irri. and Drain. Engng. ASCE 120 (5): 837-856.

Pláyan E. Walker W.R. and Merkley G.P. 1994. Two-dimensional simulation of basin irrigation .2. Applications J. Irri. and Drain. Engng. ASCE. ASCE 120 (5)

Poesen J. 1984. The influence of slope angle on infiltration rate and Hortonian overland flow volume. Zeitschriftifür Geomorphologie 49: 117-131

Ponce M.V. and Shetty A.V. 1995. A conceptual model of catchment water balance:1 formulation and calibration. J. Hydro. 173:27-40

Ponce M.V., Li R. and Simons F. 1978. Applicability of kinematic and diffusion models. J. Hydraulic division, Proc. ASCE, Vol. 104, No. HY3.

Raymond D. J. 1976. Wave-CISK and convective mesosystems. J. Atmos. Sci. 33: 2392-2398

Reeves M. and Miller E.E. 1975. Estimating infiltration for erratic rainfall. Water Resources Res., 11: 102-110

Rockström J. and Valentin C. 1997. Hillslope dynamics of on-farm generation of surface water flows: the case of rainfed cultivation of pearl millet on sandy soil in the Sahel. Agriculture and Water Management 33:183-210.

Rodriguez-Iturbe I. and Váldes J. 1979. The geomorphologic structure of the hydrologic response- Water Resour. Res., 15(6): 1409-1420

Ross J.K. 1975. Radiative transfer in plant communities. In: J.L. Monteith (ed.), Vegetation and the atmosphere, Vol. 1. Academic Press, London. pp. 13-15.

Schmidt J., Hennrich K. and Dikau R. 2000. Scales and similarities in runoff processes with respect to geomorphometry. Hydrological Process 14:1963-1979.

Schwartz R.C., Evett S.R. and Unger P.W. 2003. Soil hydraulic properties of cropland compared with reestablished and native grassland Geoderma 116 (1-2): 47-60.

Sharman K. Singh H. and Pareek O. 1983. Rain water infiltration into a bare loamy sand. Hydrological Science J. 28:417-424

Singh V. and Bhallamudi S.M. 1998. Conjunctive surface-subsurface modeling of overland flow. Advance in Water Resou. 21: 567-579.

Singh V.P. 1989. Hydrologic system: watershed modeling Volume II. Prentice Hall, Englewood Cliff, New Jersey.

Singh V.P. 1996. Kinematic wave modeling in water resources: surface–water hydrology. John Wiley and Sons Ltd.

Smith R.E. and Hebbert R.H.B. 1983. Mathematical simulation of interdependent surface and subsurface hydrologic processes. Water Resour. Res., 19: 987-1001.

Sobieraja J.A., Elsenbeerb, H. Cameron G. (2004) Scale dependency in spatial patterns of saturated hydraulic conductivity Catena 55 pp. 49–77.

Stoker J.J. 1957. Water waves, the mathematical theory with applications. Interscience, London.

Stolte J., Ritsema C.J. Veerman G.J. and Hamminga W. 1996. Establishing temporally and spatially variable soil hydraulic data for use in a runoff simulation in a loess region of the Netherlands. Hydr. Processes 10: 1027-1034.

Strelkoff T. 1969. One-dimensional equations of open-channel flow. J. Hydraul. Div. ASCE, 95: 861–876

Tayfur G. and Singh V.P. 2004. Numerical model for sediment transport over nonplanar, nonhomogeneous surfaces. J. hydrologic Engng 9 (1): 35-41

Tayfur G., Kavvas M.L., Govindaraju R.S. and Storm D.E. 1993. Applicability of St-Venant equations for 2-dimensional overland flows over rough infiltrating surfaces J. Hydraulic Engng-ASCE 119 (1): 51-63

Taylor C., Al-Mashidani G. and Davis J.M. 1974. A finite element approach to watershed runoff. J. Hydrology 21: 231-246

Todini E. and Venutelli M. 1991. Overland flow: a two-dimensional modeling approach. In : Recenet Advances in the modeling of Hydrologic system. Kluwer Academic publishers, The Netherlands pp. 153-166

Troch P.A., Smith J.A., Wood E.F. and de Troch F.P. 1994. Hydrologic controls of large floods in a small basin: central Appalachian case study. J. Hydrology 156 (1-4) pp. 285-309

Valiani A., Caleffi V. and Zanni A. 2002. Case study: Malpasset dam-break simulation using a two-dimensional finite volume method J. Hydraulic Engng-ASCE 128 (5): 460-472.

Valiani A., Caleffi V. and Zanni A. 2003. Finite volume method for simulating extreme flood events in natural channels. J. Hydraulic Res. 41 (2): 167-177.

van de Giesen N.C., Stomph T.J. and de Ridder N. 2000. Scale effects of Hortonian overland flow and rainfall-runoff dynamics in a West African catena landscape. Hydrological Processes 14 (1): 165-175.

van Dijk A.I.J.M. and Bruijnzeel L.A. 2001. Modeling rainfall interception by vegetation of variable density using an adapted analytical model. 1. Model description. J. Hydrology 247: 230-238.

van Dijk A.I.J.M. and Bruijnzeel L.A. 2001. Modeling rainfall interception by vegetation of variable density using an adapted analytical model. 2: Model validation for a tropical upland mixed cropping system. J. Hydrology 247: 239-262.

van Genuchten M. Th. 1980. A closed form equation for predicting hydraulic conductivity in unsaturated soils. Soil Sci. Soc. Am. J., 44: 892-898.

van Heemst H.D.J. 1988. Plant data values required for simple crop growth simulation models, review and bibliography. Simulation report CABO-TT 17, Wageningen.

van Loon E.E. 2001. Overland flow: interfacing models with measurements. Ph.D. thesis Wageningen University, The Netherlands. 185 pp

van Loon E.E. Keesman K.J. 2000. Identifying scale-dependent models: The case of overland flow at the hillslope scale Water Resou. Res. 36 (1): 243-254.

Wainwright J. and Parsons A.J. 2002. The effect of temporal variations in rainfall on scale dependency in runoff coefficients. Water Resou. Res. 38 (12): 1271 10.1029/2000WR000188

Wasantha-Lal A.M. 1998. Performance comparison of overland flow algorithm. ASCE J. Hydraulic Engineering, 124(4): 342-349.

Watson D.J. 1947. Comparative physiological studies on the growth of field crops. Annals of Botany 11: 41-76

Wilcox B.P., Newman B. D., Brandes D., Davenport D. W. and Reid K. 1997. Runoff from a semiarid ponderosa pine hillslope in New Mexico. Water Resour. Res., 33: 2301– 2314.

Wood E.F., Sivapalan M. and Beven K. 1990. Similarity and scale in catchment storm response. Rev. of Geophys., 28: 1-18.

Woolhiser D.A. and Liggett J.A. 1967. Unsteady, one-dimensional flow over a plane-the rising hydrograph. Water Resour. Res., 3(3) : 753-771.

Woolhiser D.A., Smith R.E. and Giraldez J.V. 1996. Effect of spatial variability of saturated hydraulic conductivity on Hortonian overland flow. Water Resou. Res. 32(3): 671-678.

Wu C., Huang G. and Zhang Y. 1999. Theoretical solution of dam-break shock wave. J. Hydraulic Engineering, ASCE125(11): 1210-1215.

Yair A. and Kossovsky A. 2002. Climate and surface properties: hydrological response of small and and semi-arid watersheds Geomorphology 42 (1-2): 43-57.

Yair A. and Lavee H. 1976. Runoff generative process and runoff yield from arid talus antled slopes. Earth Surf. Process Landf. 1: 235–247.

Yair A. Lavee H. 1985. Runoff generation in arid and semi-arid zones. In: Anderson M.G., Burt T.P. (eds.), Hydrological Forecasting. Wiley, Chichester, pp. 183–220.

Zhang R. 1997. Determination of soil sorptivity and hydraulic conductivity from the disk infiltrometer. SSSA J. 61: 1024-1030.

Zhang W. and Cundy T.W. 1989. Modeling of two-dimensional overland flow. Water Resou. Res. 25(9): 2019-2036.

Zhao D.H., Shen H.W., Tabios G.Q. and Lai J.S. 1996. Approximate Riemann solvers in FVM for 2D hydraulic shock wave modeling. J. Hydrologic Engng. 122(12): 692-702.

Zhu J. and Mohanty B.P. 2003. Effective hydraulic parameters for steady state vertical flow in heterogeneous soils. Water Resources Res., 39(8):1029

Zoppou C. and Roberts S. 2003. Explicit schemes for dam-break simulations. J. Hydraulic Engng.-ASCE 129 (1):11-34

ACKNOWLEDGEMENTS

I thank the Almighty God, the giver of all wisdom and grace for the successful completion of this study. I would like to thank Prof. Helmut Eggers for his supervision and advice; his suggestions and constructive criticism greatly improved the quality of this work. I would also like to express my gratitude to Prof. Paul Vlek for his encouragement and immeasurable support. I sincerely appreciate the excellent guidance from my coach and tutor Dr. Nick van de Giesen, who inspire this work and provided all the necessary encouragement till the goal was accomplished. I appreciate the German government, who through the Deutscher Akademischer Austauschdienst (DAAD) provided me with scholarship for the PhD studies, and the GLOWA-Volta project that provided the funds for the research work. I thank the GLOWA project team in Ghana, Drs Marc Andreini and Matthias Fosu for all the support during the field campaign. I must not fail to mention the field staff in Ejura, Mr. Emmanuel Amoah, Kojo Moamah, Jacob Agabu. I am grateful to Mr. Kofi Campion, Dr. Jide Josiah, and Pastor & Dr. (Ms) Mark for their support in Ghana.

I appreciate the kind support of Dr. Günther Manske, Hannah Peters and the administrative staff of ZEFC, Sabine Aengenendt-Baer, Andrea Berg, Inga Haller, and Hagedorn Menasah. I thank Ms. Margaret Jend for editing and reviewing the manuscript, and for translating the short German version. Thanks to Mr. Volker Merx for providing the library support.

Special thanks to the management of the Federal University of Technology, Akure (FUTAkure), for approving my study leave for this study. I appreciate the moral support of all the academic staff of the Department of Agricultural Engineering, FUTAkure; Profs. Cornellius Ademosun, Agboola Ogunlowo, Ayorinde Olufayo; Drs Leo Agbetoye, Michael Alatise, Wale Olukunle, Manuwa, Engrs. Noah Ajayi, Johnson Fasinminrin, and Richard Falayi. I sincerely appreciate the contributions by the technical crew of the department, with particular mention of Mr. Adesina, who appreciably assisted me in the design of the runoff meter used for the study, and Mr. Jimoh who welded the runoff meters.

I sincerely appreciate the contribution of my modeling tutor and friend Dr. Babatunde Joseph and my covenant friend and inspiration, Dr. Philip Oguntunde. My thanks are extended to my friends and colleagues in the doctoral program Drs Ademola

Braimoh, Nii Codjoe, Yaw Osei-Asare, Isaac Osei Akoto, Wilson Agyare just to mention a few. I am grateful to all the members and pastorate of the Redeemed Christian Church of God, Bonn, who provided me with spiritual encouragement. I am also grateful for the moral support from, Ms. Veronica Oguntunde, Ms. Olannike Nist, Mr. and Ms. Akinbogun, Mr. and Ms. Okosun, Mr. and Ms. Adamolekun, Hon. Adeniran Ibitoye, Mr. and Ms. Komolafe, Mr. and Ms. Akinjisola Ige, Arc and Ms. Sola Aluko, Dr. and Ms. Aidi, Senator and Ms. Farukanmi, Mr. and Ms. Adejala, Mr. and Ms. Liad Tella, Mr. Yinka Tella, Mr. Steve Adedipe, Engr. and Ms. Gbenga Oyeleke Mr. Zoe Agu and Mr. and Ms. Razaq Ishola.

Thanks to my brother Mr. Gbemiga Arolasafe, who encouraged me, many years ago, to prepare well for this day and his wife Roseline, who came to my defense in Bonn. I would like to thank Mr. and Ms. Akintayo Oyedeji for their encouragement. I thank all the members of Gideon's International in Akure and Bonn, for being so supportive. I am also very grateful to the members and pastorate of the Living Faith Church, Akure. My sincere gratitude to my host family in Germany, Dr. and Ms. Heyde and to my benefactor Ms. Ayobami Oshinlu and Dr (Ms.) Schäffer, their support was immeasurable. I also appreciate the spiritual support by Bishop and Pastor (Ms.) Mike Afolabi, Bishop Thomas Aremu, Pastor (Dr.) and Ms. Oyetade, Pastor Olu Adetomiwa, Pastor and Ms. Ogbonyomi and Pastor and Ms. Olutoki.

Last, but by no means least, I would like to thank my wife, Ibidunmomi Oluwaseun, for being very supportive at all moments and enduring the sudden departure for Bonn, only days after our wedding, my daughter, Jemima Oluwafunto Gbemisola, for the indescribable encouragement, and my parents for being there for me at all times, and my in-laws for being so wonderful to me.